The advantage of Bolometric Interferometry for controlling Galactic foreground contamination in CMB primordial B-modes measurements

Elenia Manzan
University of Milan

The state-of-the-art of primordial B-modes

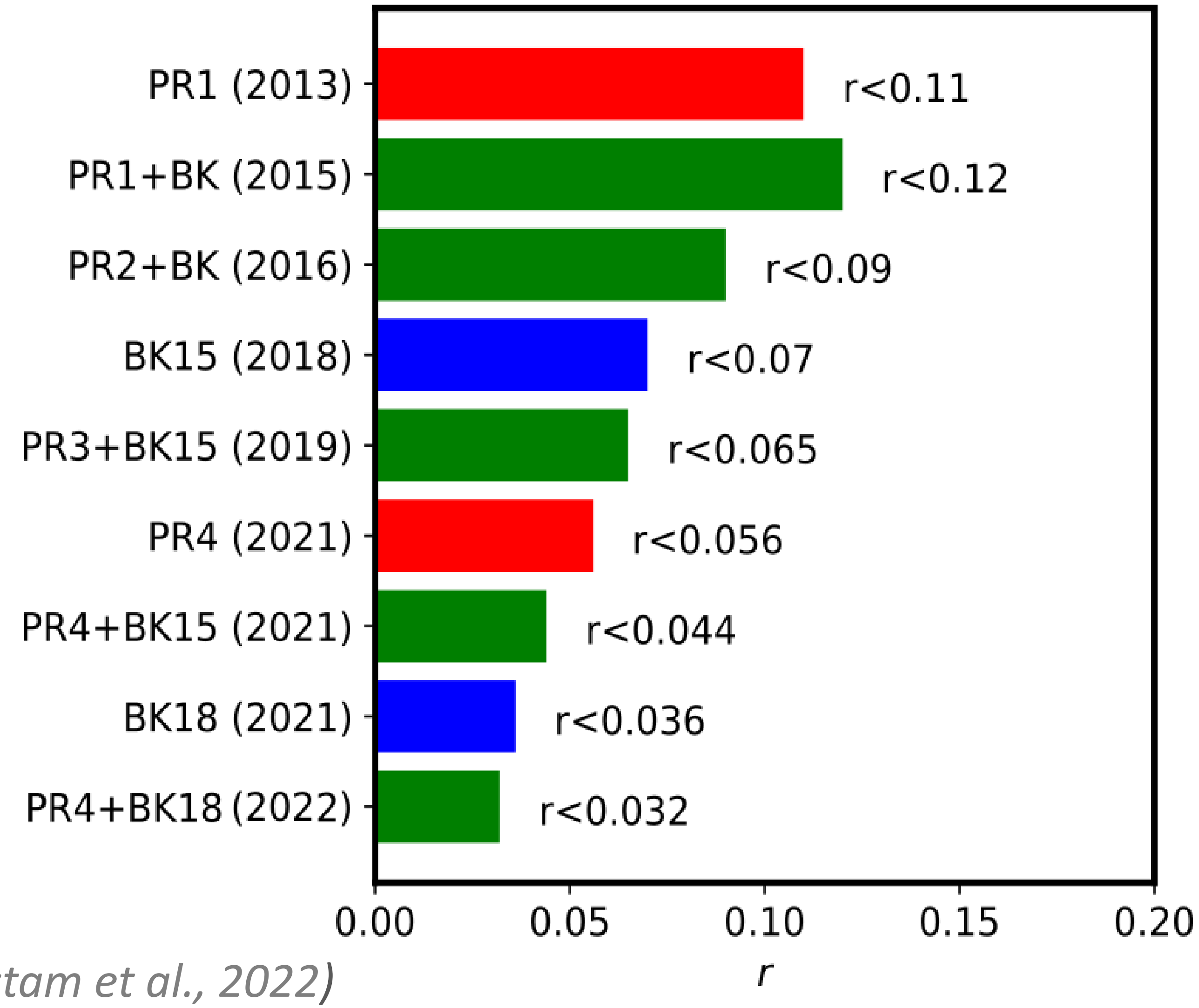

(Tristam et al., 2022)

The state-of-the-art of primordial B-modes

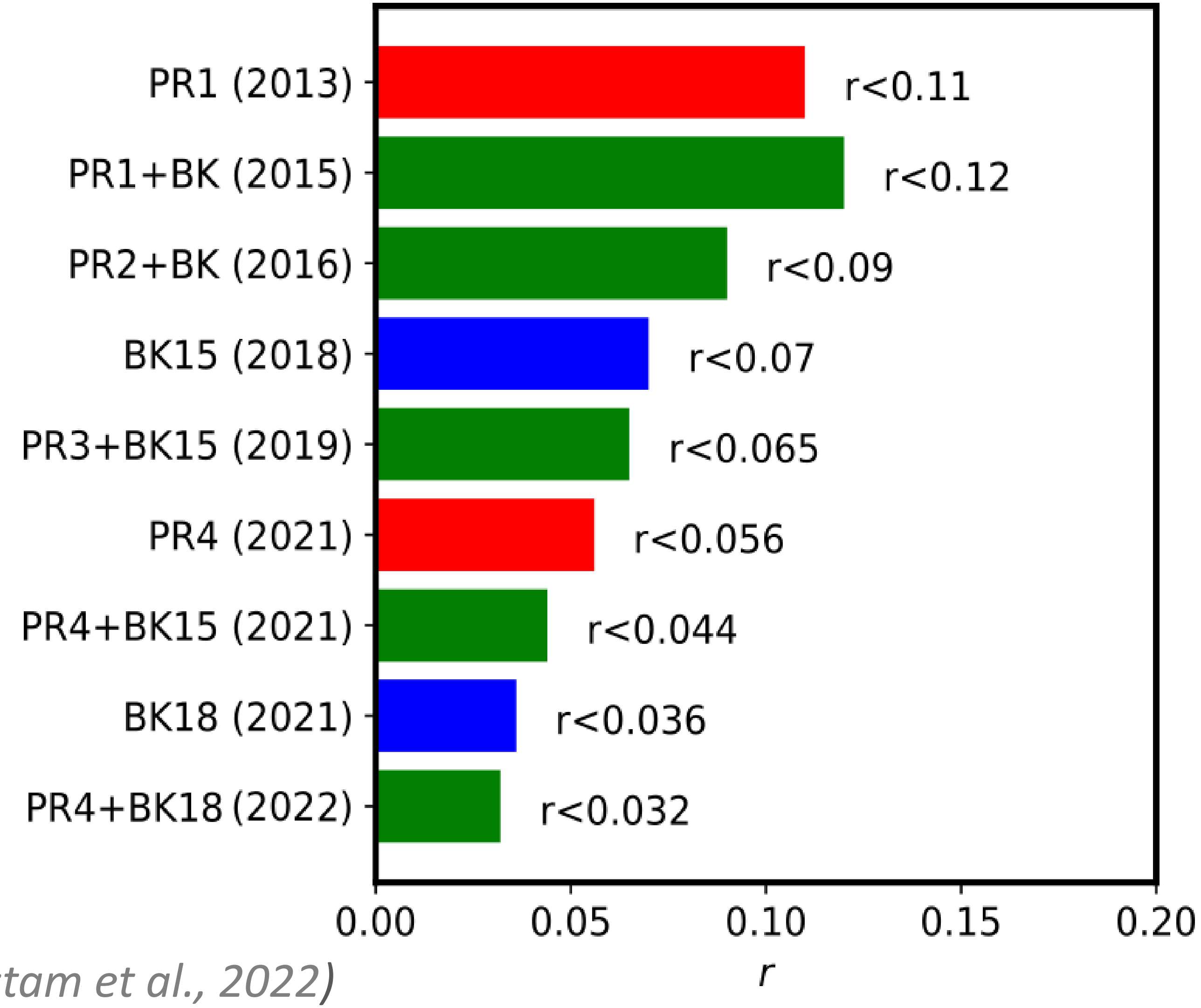

(Tristam et al., 2022)

Next target: $r < 10^{-3}$

Requirements

- Instrumental sensitivity
- Control of instrumental systematic effects
- Control of Galactic foreground contamination
  - Multifrequency observations
  - Improved foreground models

Requirements

- Instrumental sensitivity
- Control of instrumental systematic effects
- Control of Galactic foreground contamination
  - Multifrequency observations
  - Improved foreground models

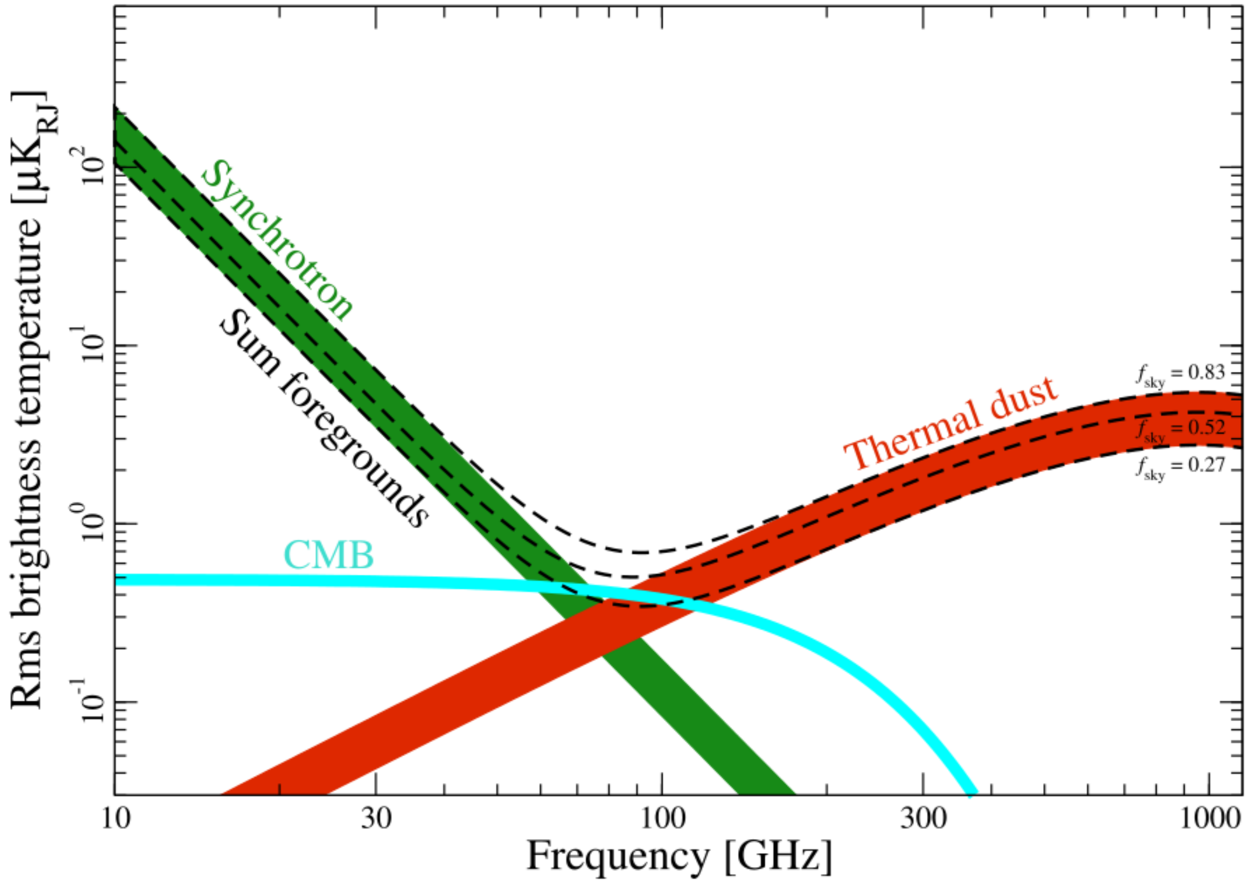

(Planck collaboration et al, 2015, A&A, 594, A10)

Our study

Are there reliable strategies to validate or invalidate a possible B-mode detection?

Bolometric Interferometry (BI) in a nutshell

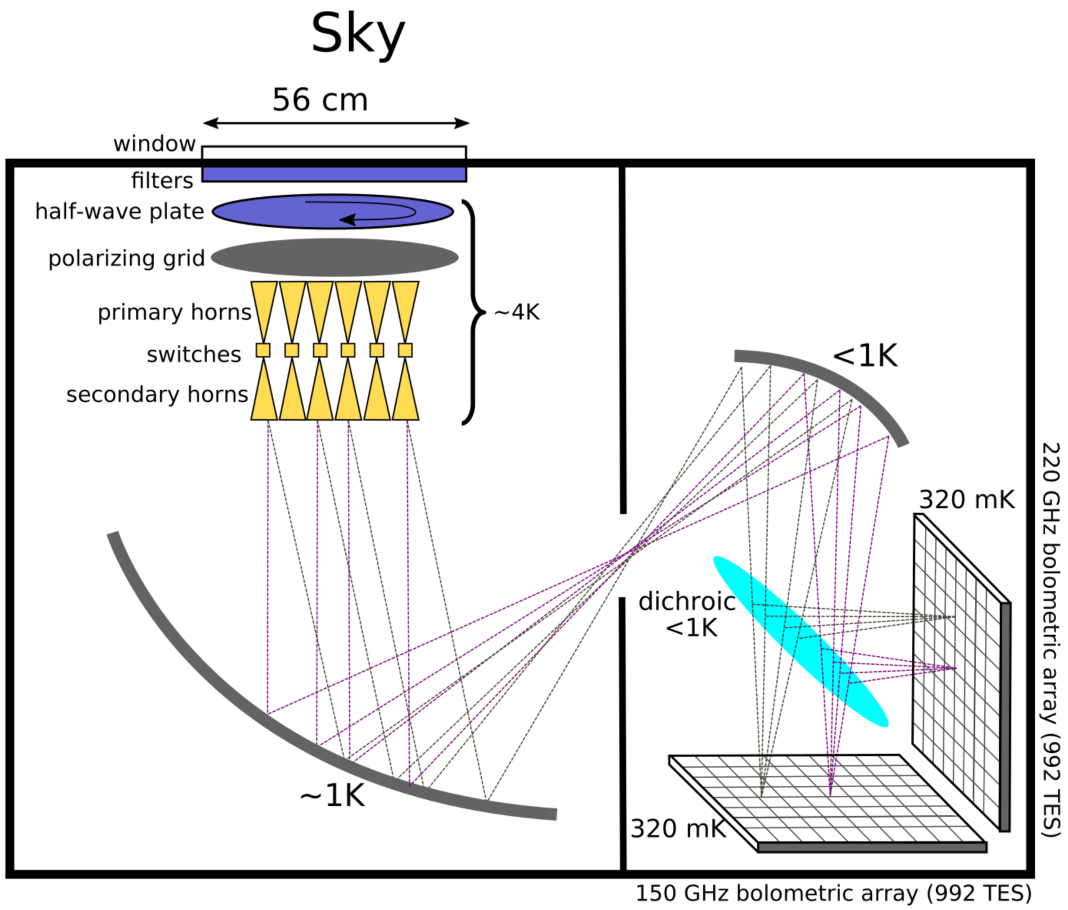

The state-of-the-art of BI: the QUBIC experiment

See D. Mennella's talk

Bolometric Interferometry (BI) in a nutshell

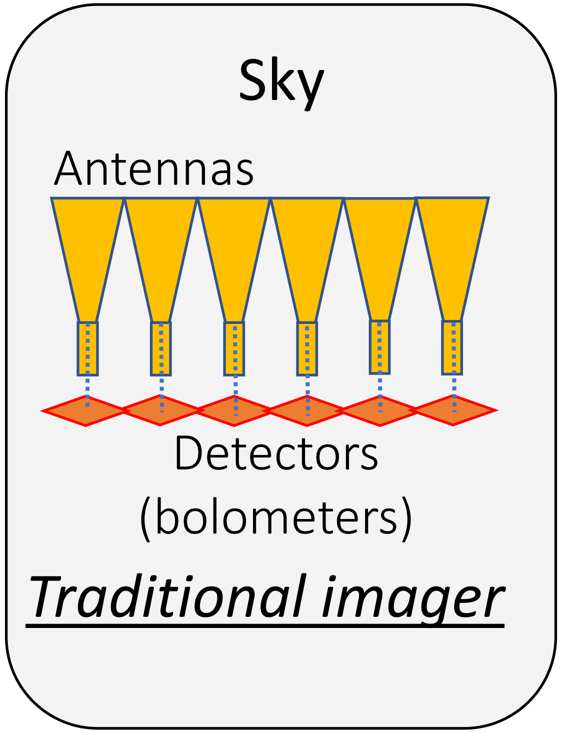

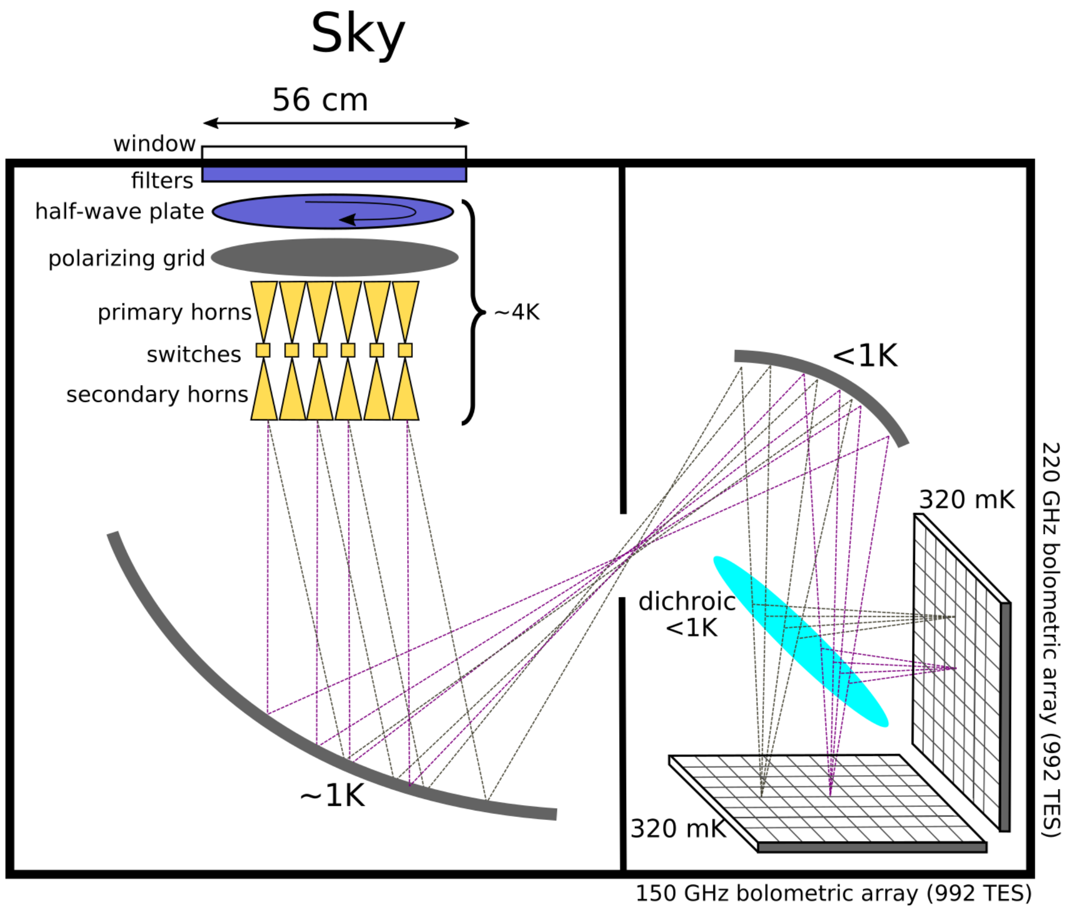

The state-of-the-art of BI: the QUBIC experiment

See D. Mennella's talk

The classical imager angular response

Signal = Sky $*$ Antenna beam pattern

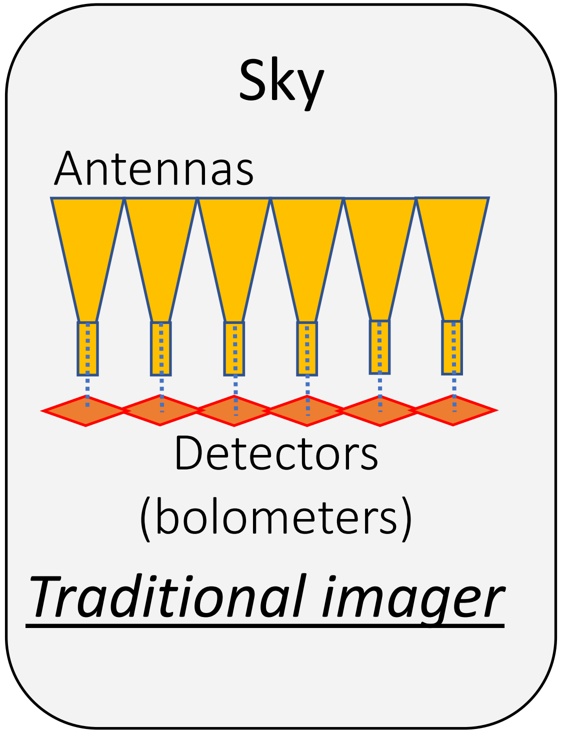

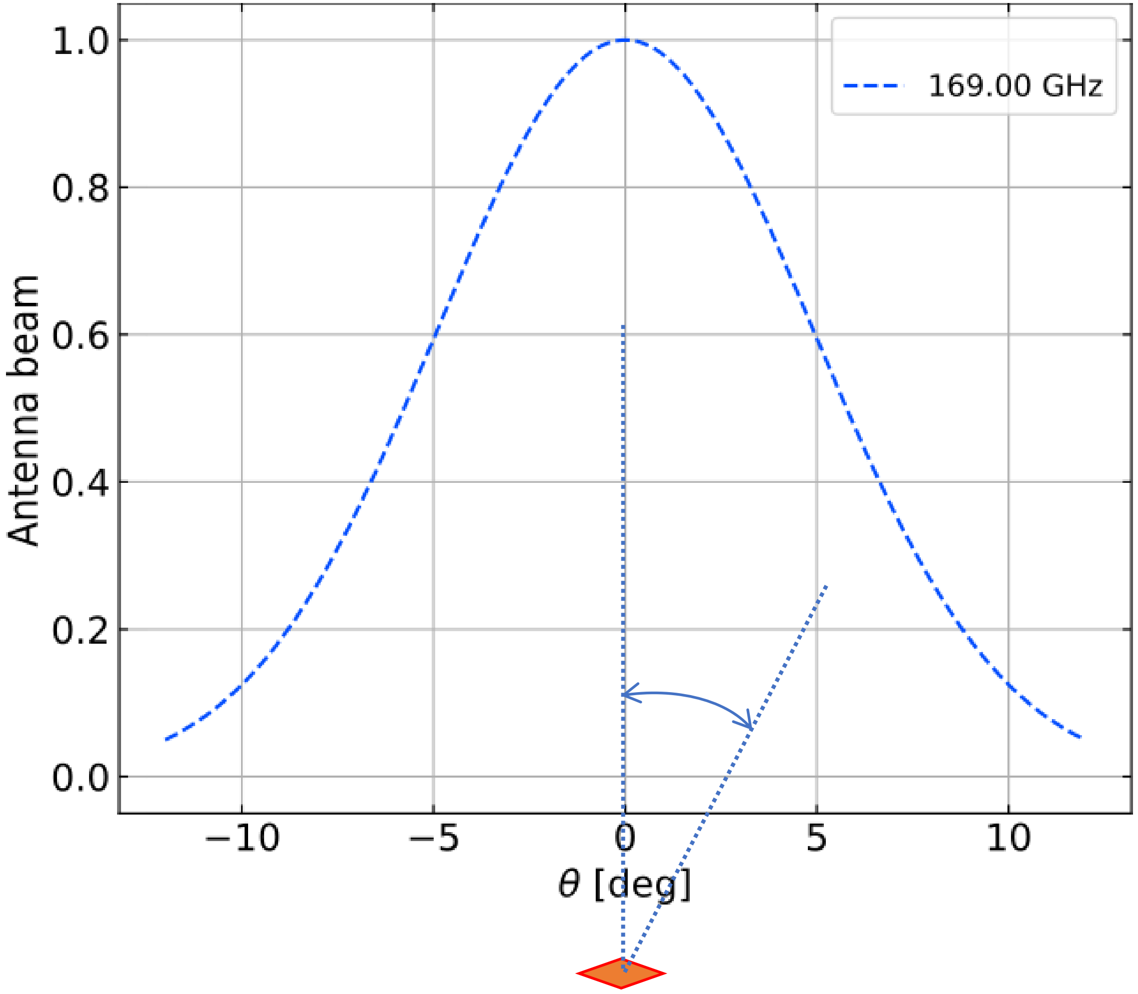

The BI angular response

Signal = Sky ∗ Synthesized beam pattern

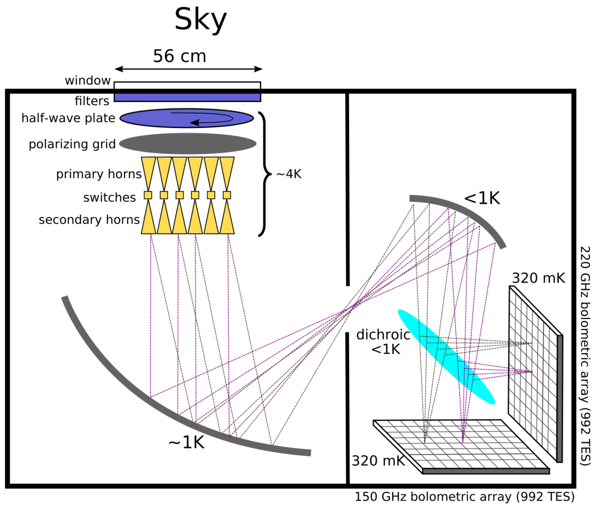

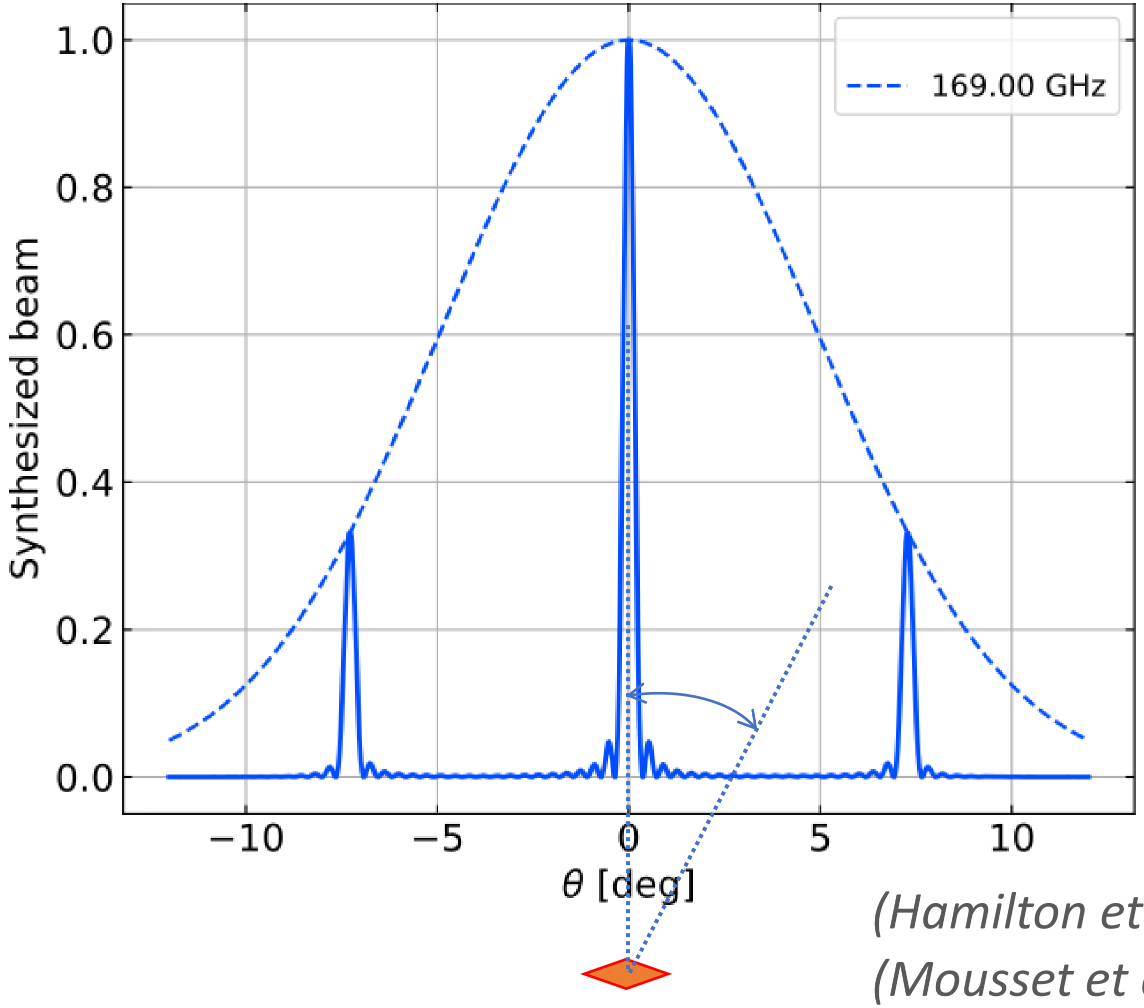

(Hamilton et al., 2021)
(Mousset et al., 2021)

The BI angular response

Signal = Sky $*$ Synthesized beam pattern

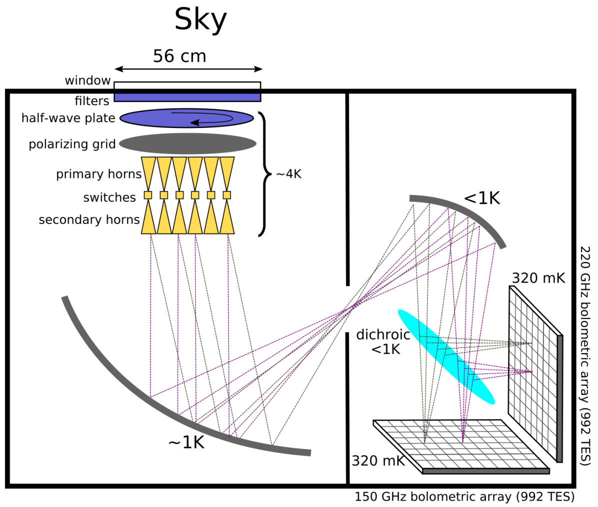

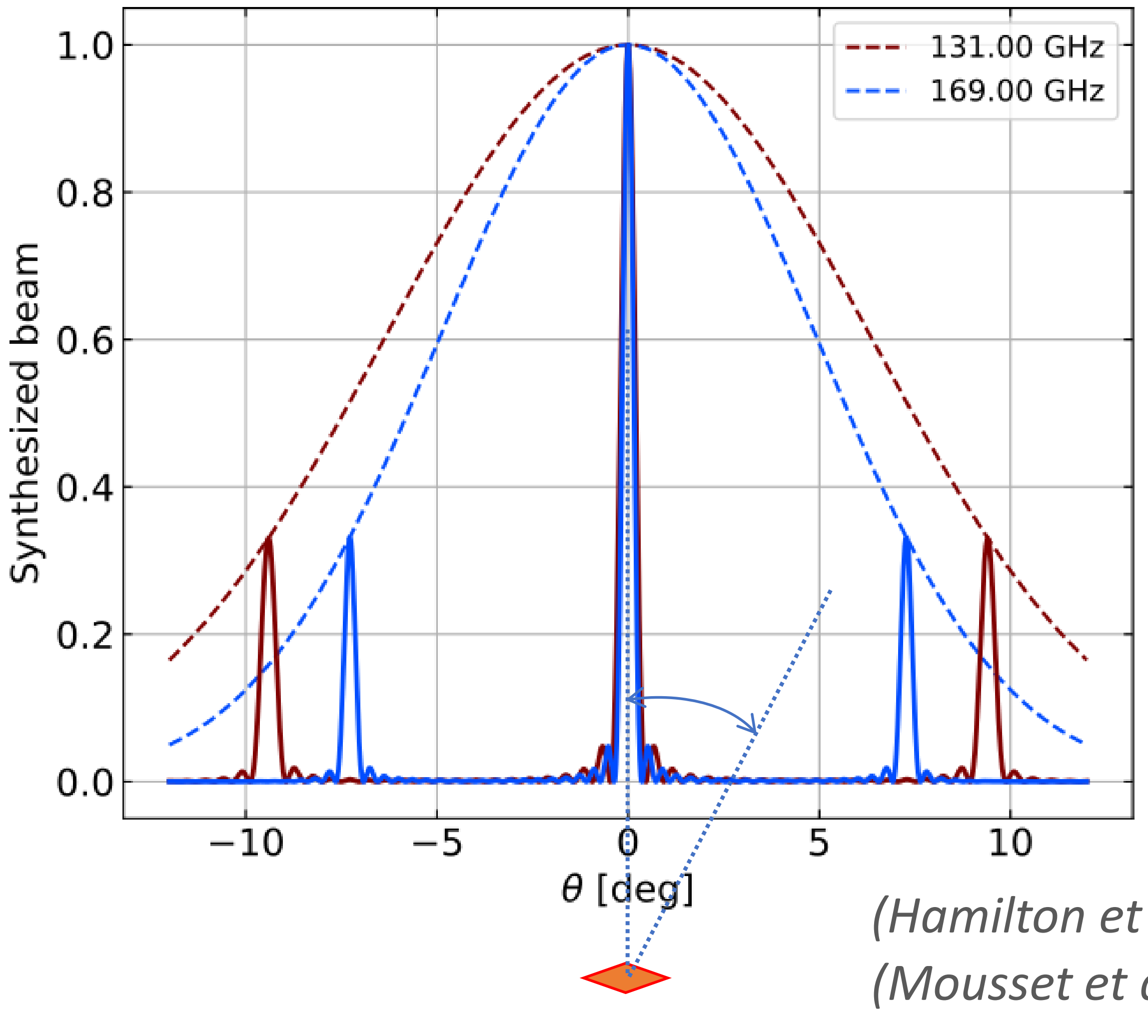

(Hamilton et al., 2021)
(Mousset et al., 2021)

Spectral Imaging

Observation **simulation** of a sky patch close to the Galactic center between 130 to 170 GHz

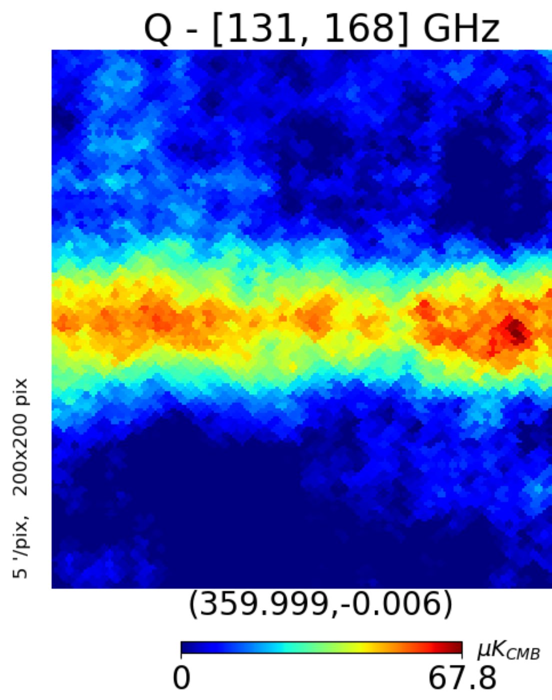

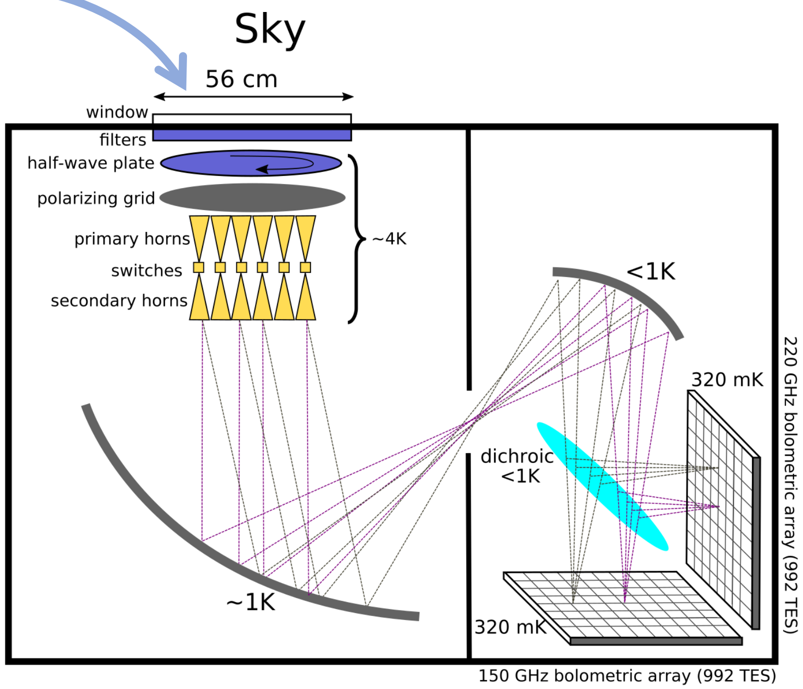

Recover sky signal in 4 sub-bands

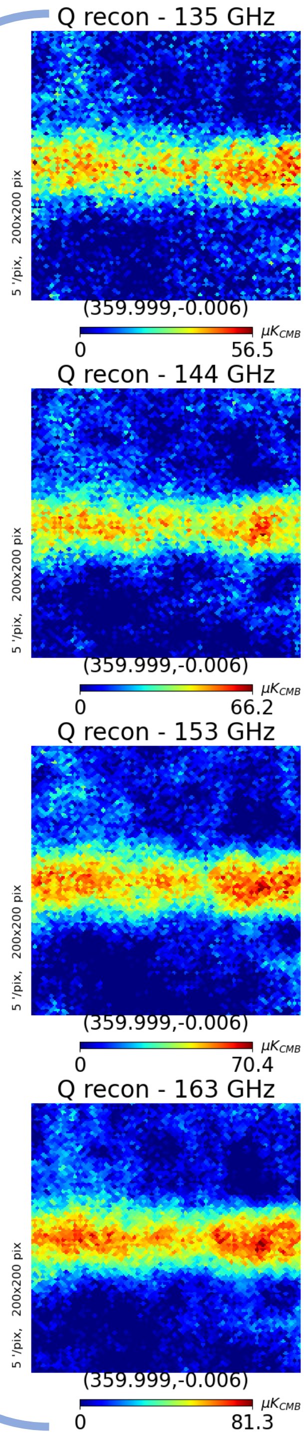

Spectral Imaging

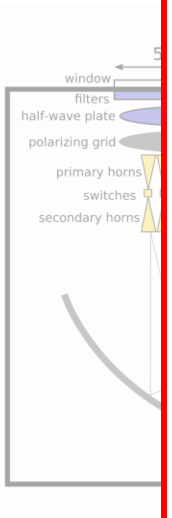

Take-home message

- Spectral imaging happens at the data analysis level

  (Mousset et al. 2022)

- It allows us to play with different spectral resolutions

- We can re-analyse data with different spectral configurations to search for biases

Galactic thermal dust emission models

Conventionally modelled as a Modified Blackbody (MBB)

$$I_d(\hat{n},\nu) = A_{d,\nu_0}(\hat{n}) \frac{e^{\frac{h\nu_0}{k_B T_d}} - 1}{e^{\frac{h\nu}{k_B T_d}} - 1} \left(\frac{\nu}{\nu_{0,d}}\right)^{\beta_d + 1}$$

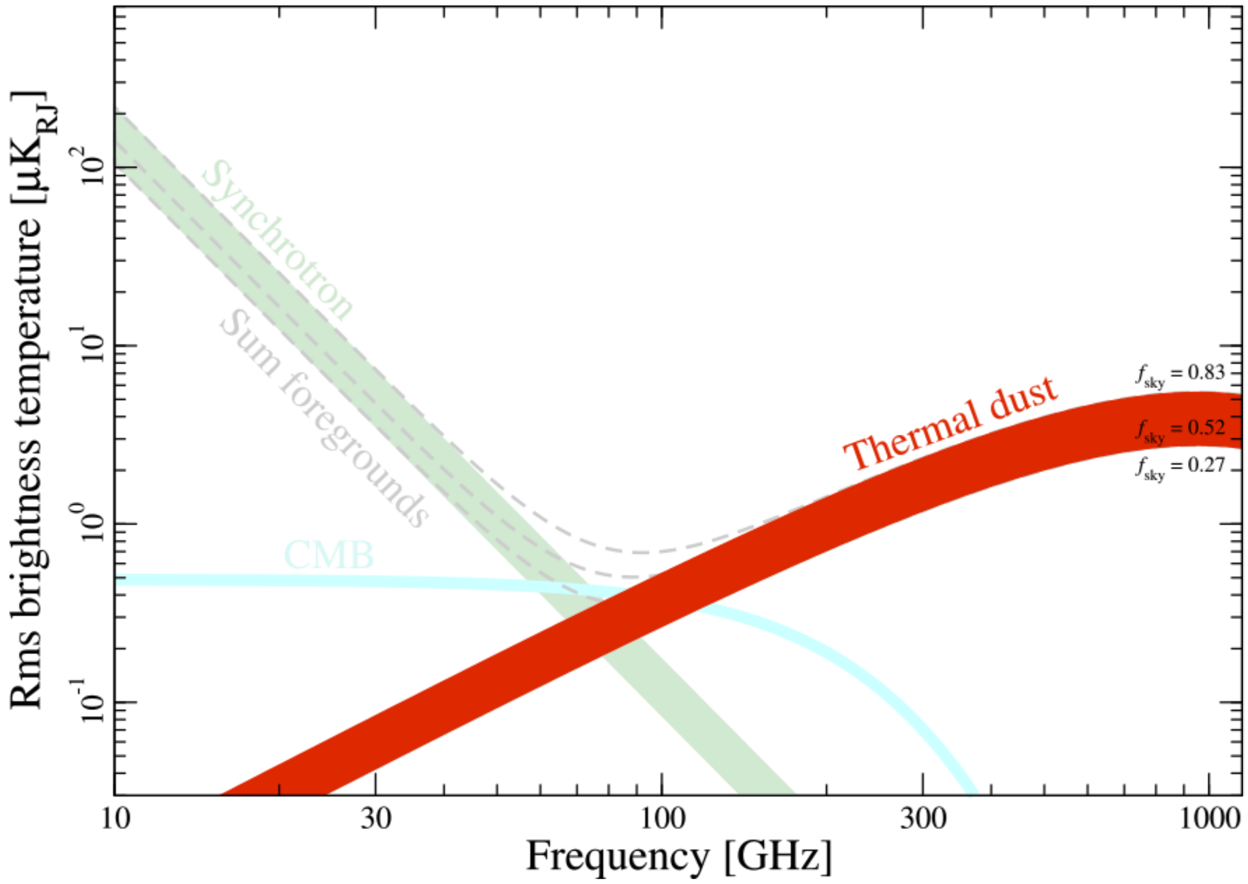

(Planck collaboration et al, 2015, A&A, 594, A10)

Galactic thermal dust emission models

Conventionally modelled as a Modified Blackbody (MBB)

$$I_d(\hat{n},\nu) = A_{d,\nu_0}(\hat{n}) \frac{e^{\frac{h\nu_0}{k_B T_d}} - 1}{e^{\frac{h\nu}{k_B T_d}} - 1} \left(\frac{\nu}{\nu_{0,d}}\right)^{\beta_d+1}$$

- PySM model **d0**: spatially constant spectral parameters $T_d, \beta_d = const$
- PySM model **d1**: spatially varying spectral parameters $T_d(\hat{n}),\ \beta_d(\hat{n})$

https://pysm3.readthedocs.io/en/latest/

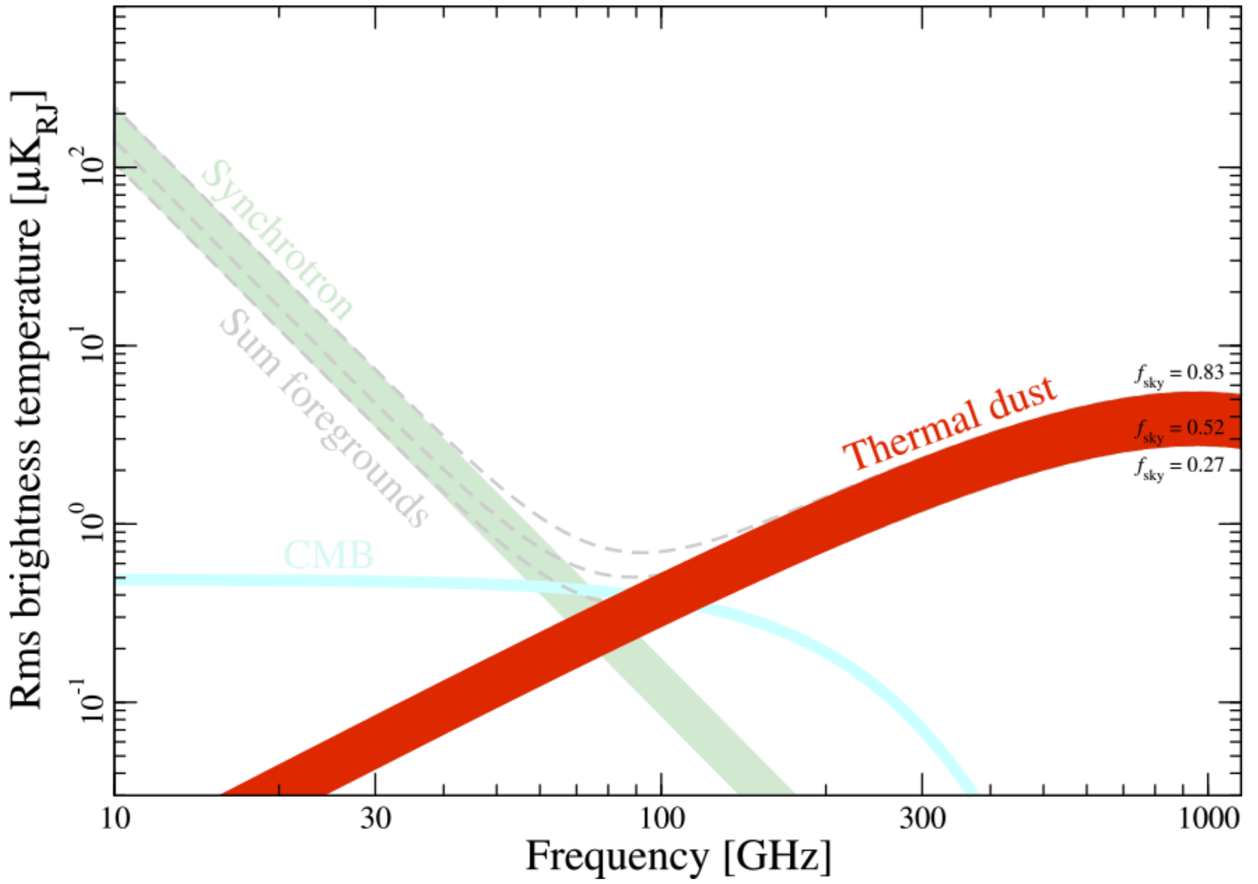

(Planck collaboration et al, 2015, A&A, 594, A10)

Galactic thermal dust emission models

PySM3

https://pysm3.readthedocs.io/en/latest/

- Modified Blackbody (MBB)
  - PySM model **d0, d1**
- Different dust grain compositions
  - PySM models **d5, d7** *(Hensley & Draine 2017)*
- Sum of single MBBs
  - PySM models **d4, d12** *(Finkbeiner et al. 1999; Martínez-Solaeche et al. 2018)*
- Dust LOS frequency decorrelations
  - PySM model **d6** *(Vansyngel et al. 2018)*

Galactic thermal dust emission models

PySM3

- Modified Blackbody (MBB)
  - PySM model **d0, d1**
- Different dust grain compositions
  - PySM models **d5, d7**
- Sum of single MBBs
  - PySM models **d4, d12**

We focused on this model

- Dust LOS frequency decorrelations
  - PySM model **d6** *(Vansyngel et al. 2018)*

Dust LOS frequency decorrelation: the PySM model

PySM3

- PySM model **d1** : Dust MBB with **spatially varying** spectral parameters

$$I_d(\hat{n},\nu) = A_{d,\nu_0}(\hat{n}) \frac{e^{\frac{h\nu_0}{k_B \boxed{T_d(\hat{n})}}} - 1}{e^{\frac{h\nu}{k_B T_d(\hat{n})}} - 1} \left(\frac{\nu}{\nu_{0,d}}\right)^{\boxed{\beta_d(\hat{n})}+1}$$

- PySM model **d6** : Dust MBB with **LOS frequency decorrelations**

$$I_d(\hat{n},\nu) = DEC(\nu,\nu_0,\ell_{corr}) \cdot A_{d,\nu_0}(\hat{n}) \frac{e^{\frac{h\nu_0}{k_B T_d(\hat{n})}} - 1}{e^{\frac{h\nu}{k_B T_d}} - 1} \left(\frac{\nu}{\nu_{0,d}}\right)^{\beta_d(\hat{n})+1}$$

(Vansyngel et al. 2018)

Dust LOS frequency decorrelation: the PySM model

PySM3

- PySM model **d1** : Dust MBB with **spatially varying** spectral parameters

$$I_d(\hat{n},\nu) = A_{d,\nu_0}(\hat{n}) \frac{e^{\frac{h\nu_0}{k_B \boxed{T_d(\hat{n})}}}-1}{e^{\frac{h\nu}{k_B T_d(\hat{n})}}-1}\left(\frac{\nu}{\nu_{0,d}}\right)^{\boxed{\beta_d(\hat{n})}+1}$$

- PySM model **d6** : Dust MBB with **LOS frequency decorrelations**

$$I_d(\hat{n},\nu) = DEC(\nu,\nu_0,\ell_{corr}) \cdot A_{d,\nu_0}(\hat{n}) \frac{e^{\frac{h\nu_0}{k_B T_d(\hat{n})}}-1}{e^{\frac{h\nu}{k_B T_d}}-1}\left(\frac{\nu}{\nu_{0,d}}\right)^{\beta_d(\hat{n})+1}$$

Decorrelation factor at the SED level (Spectral Energy Distribution)

(Vansyngel et al. 2018)

Dust LOS frequency decorrelation: the PySM model

- PySM model **d6** : Dust MBB with **LOS frequency decorrelations**

PySM3

$$I_d(\hat{n},\nu) = DEC(\nu,\nu_0,\ell_{corr}) \cdot A_{d,\nu_0}(\hat{n}) \frac{e^{\frac{h\nu_0}{k_B T_d(\hat{n})}}-1}{e^{\frac{h\nu}{k_B T_d}}-1} \left(\frac{\nu}{\nu_{0,d}}\right)^{\beta_d(\hat{n})+1}$$

Decorrelation factor is randomly sampled from a Gaussian distribution

$$DEC(\nu,\nu_0,\ell_{corr}) \leftarrow \mathcal{N}\left(\mu = 1, \sigma = \sigma(1/\ell_{corr})\right)$$

(Vansyngel et al. 2018)

Dust LOS frequency decorrelation: the PySM model

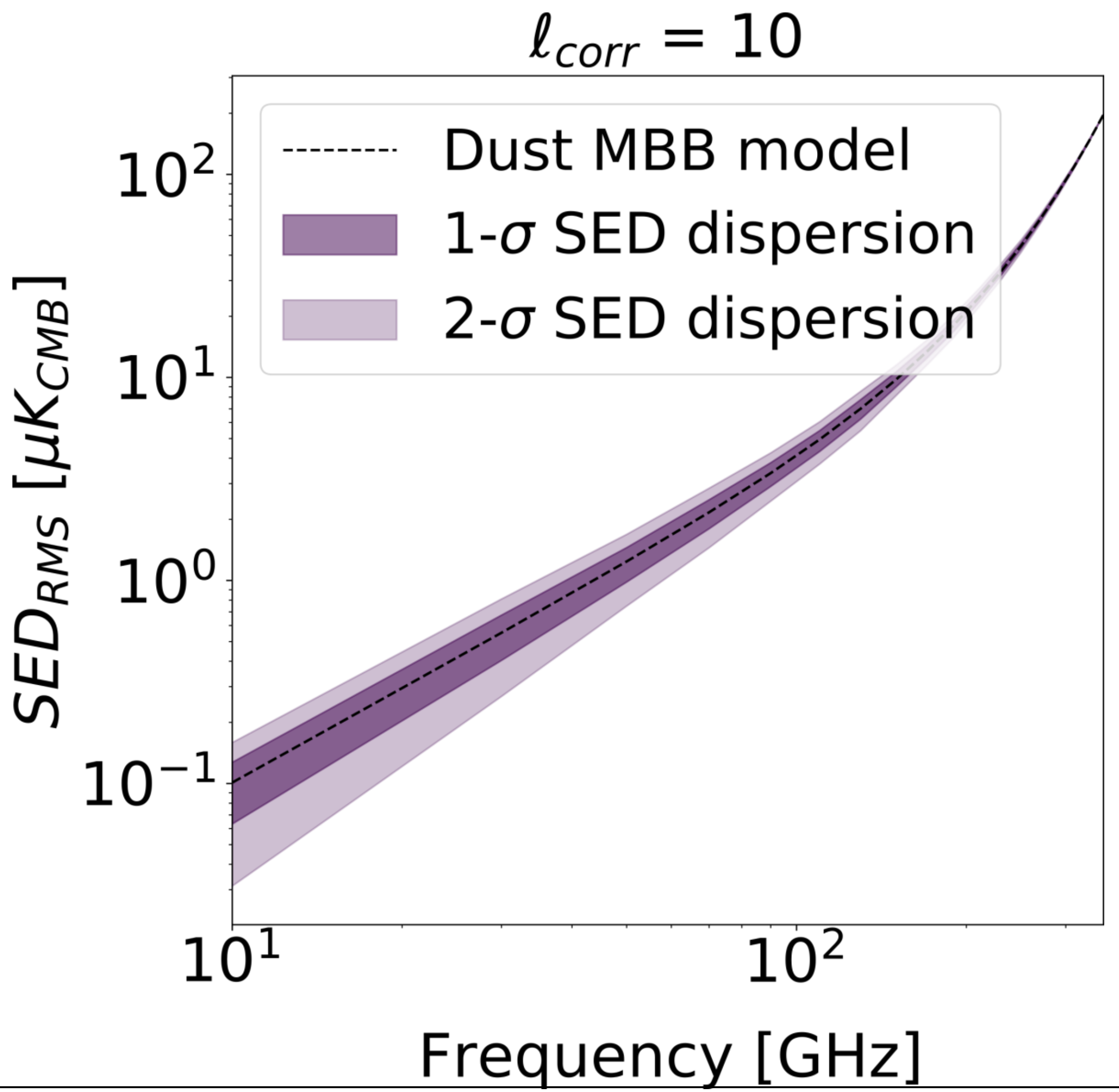

Dust LOS frequency decorrelation: the PySM model

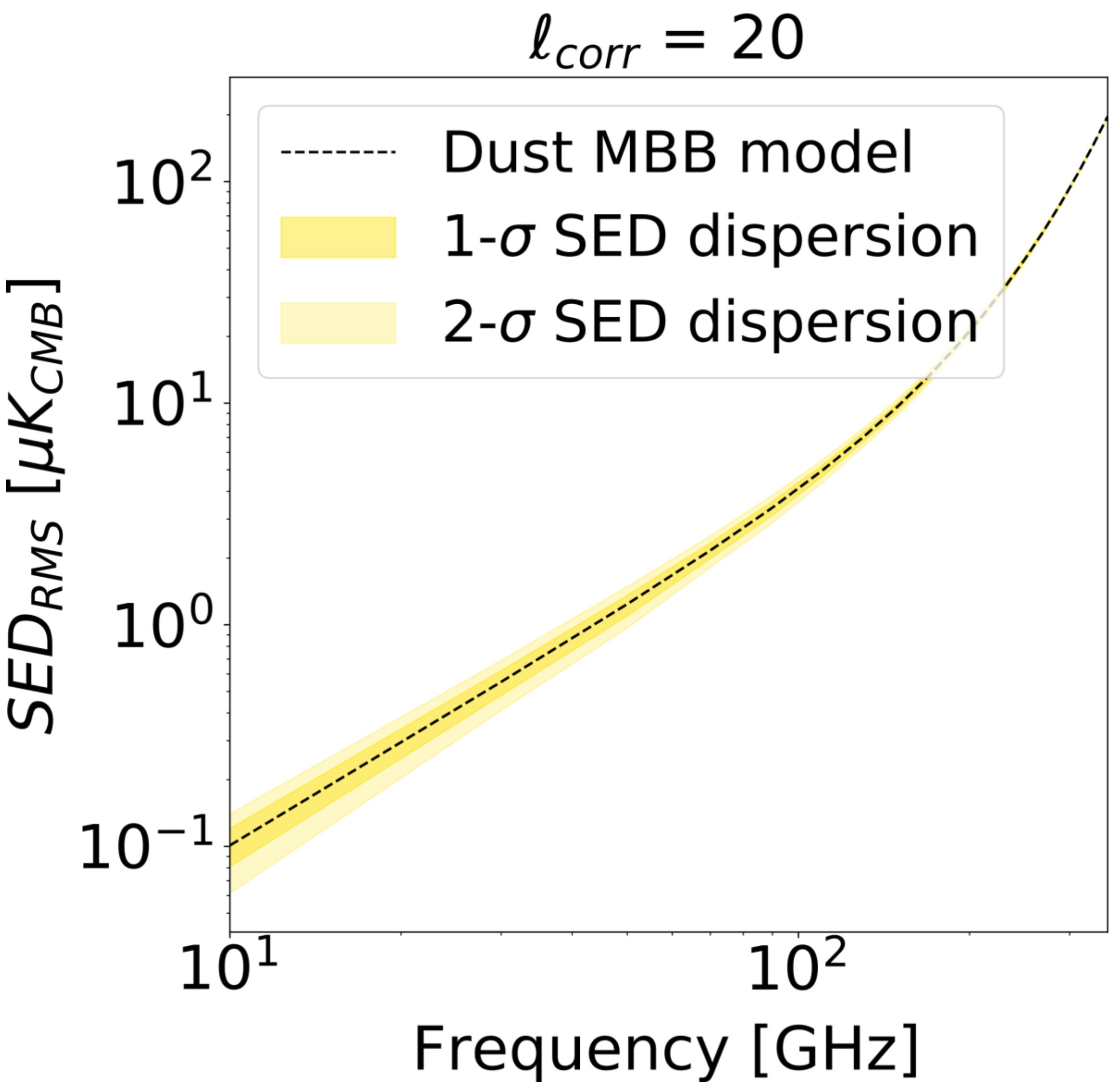

Dust LOS frequency decorrelation: the PySM model

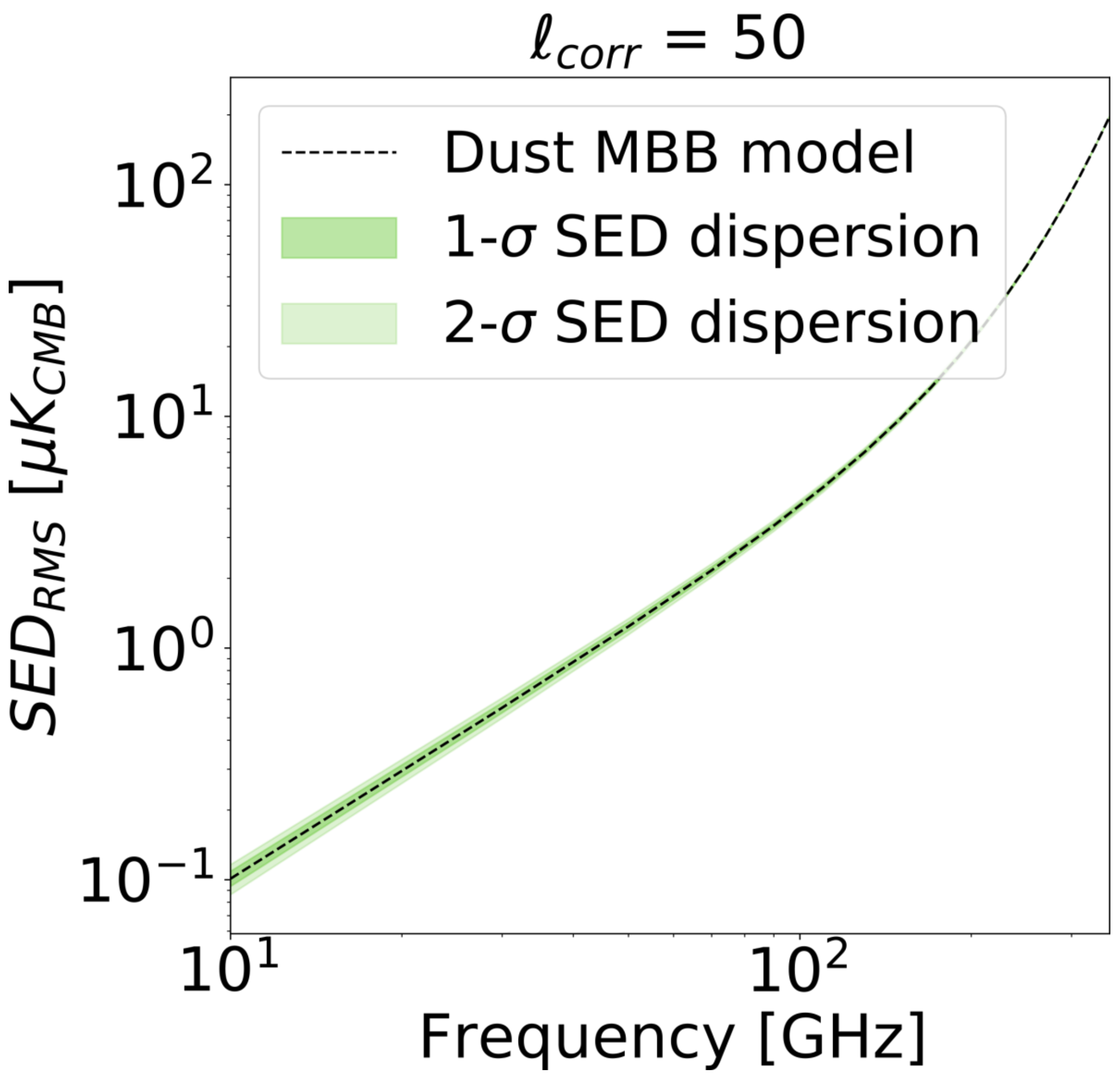

Dust LOS frequency decorrelation: the PySM model

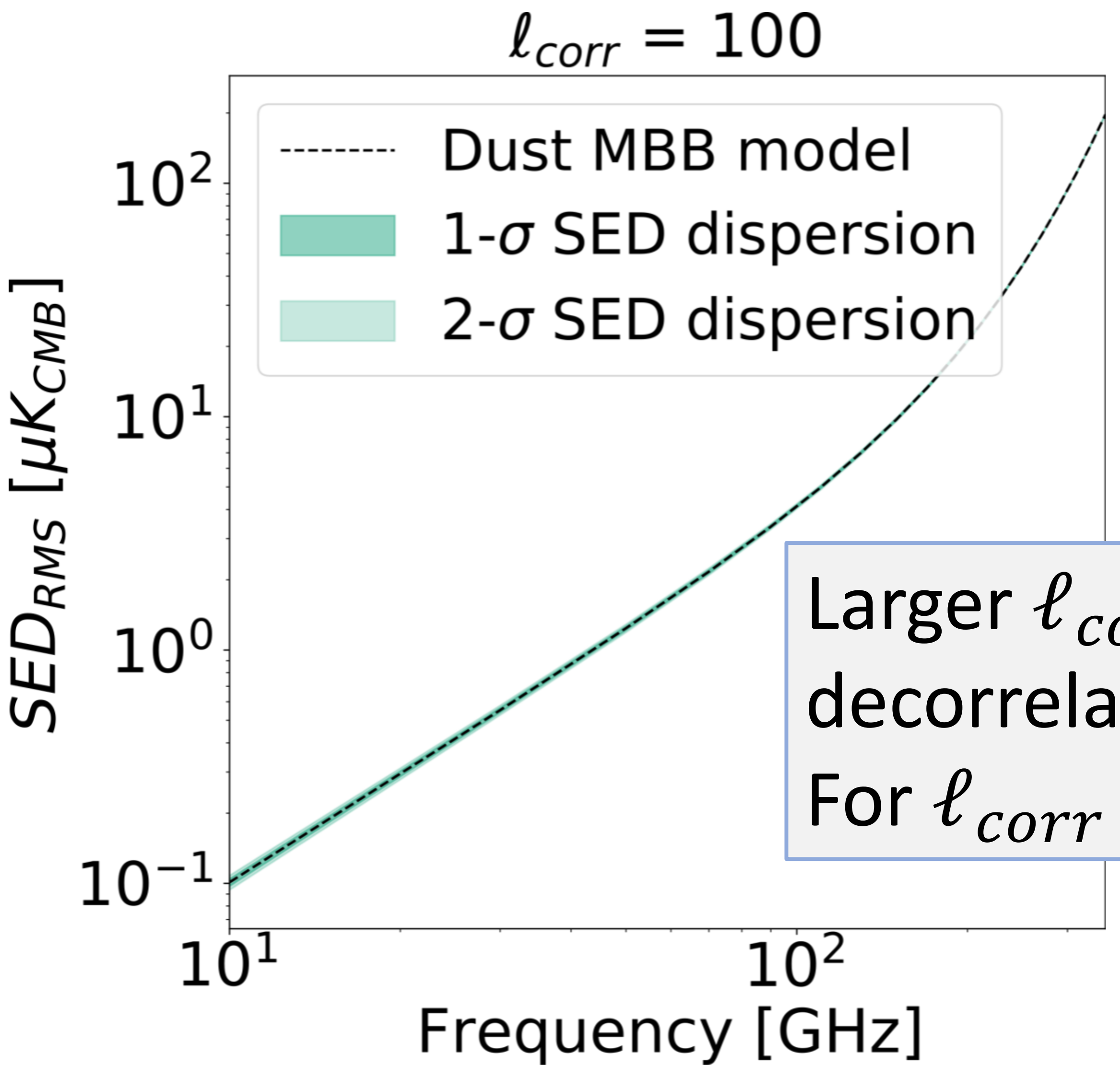

Larger ℓ_{corr} → smaller decorrelation: $R_\ell \rightarrow 1$
For $\ell_{corr} \rightarrow \infty$, SED → MBB

The pipeline: MC chain

CMB + noise + foreground

I. Model d0s0
II. Model d1s1
III. Model d6s1

→

Component separation

Dust model = MBB

FGBuster
(Stompor et al. 2008)

Commander
(Eriksen et al. 2006, 2008)

→

Clean CMB map

↓

$\mathcal{D}_\ell^{BB}$

←

$\mathcal{L}(r)$

←

Max-$\mathcal{L}(r)$

CMB-S4 & hypothetical CMB-S4/BI

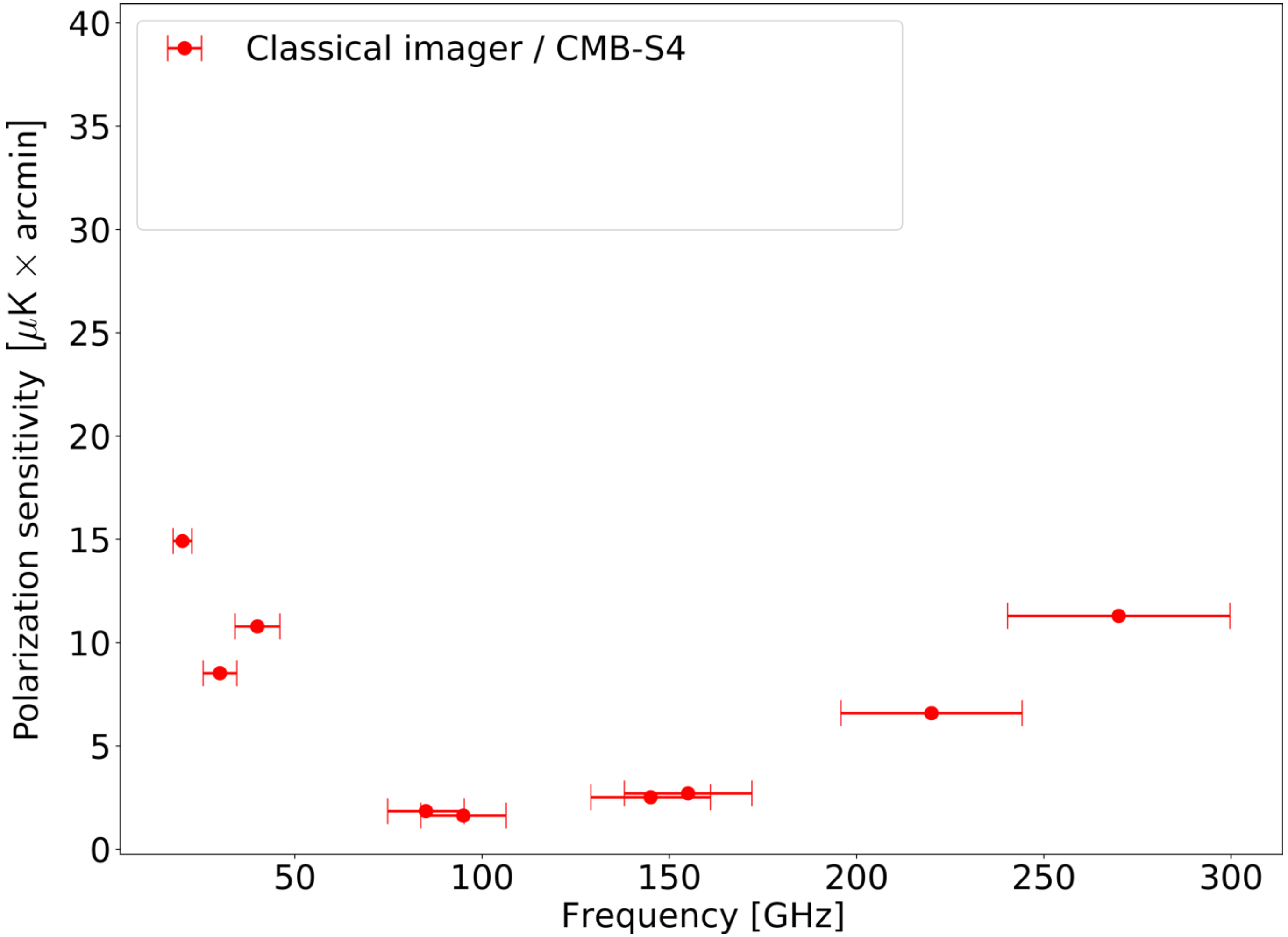

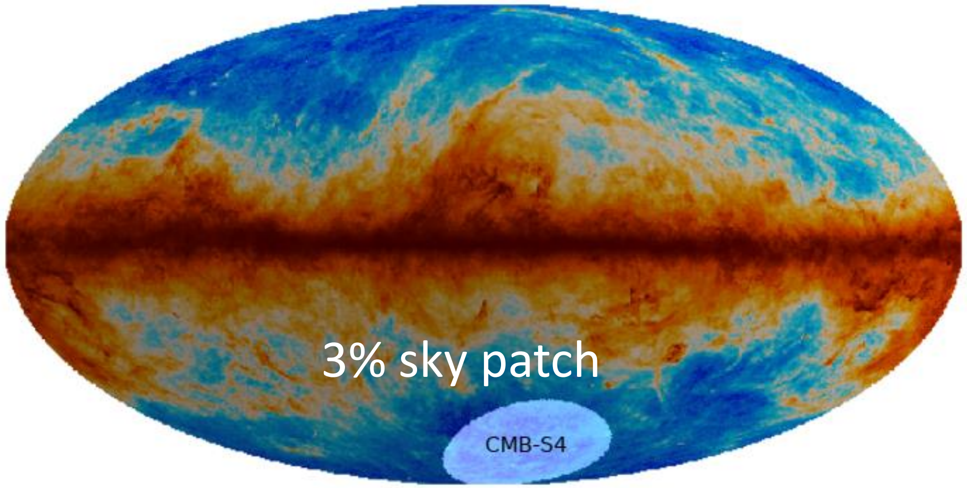

(Abazajian et al. 2022)

CMB-S4 & hypothetical CMB-S4/BI

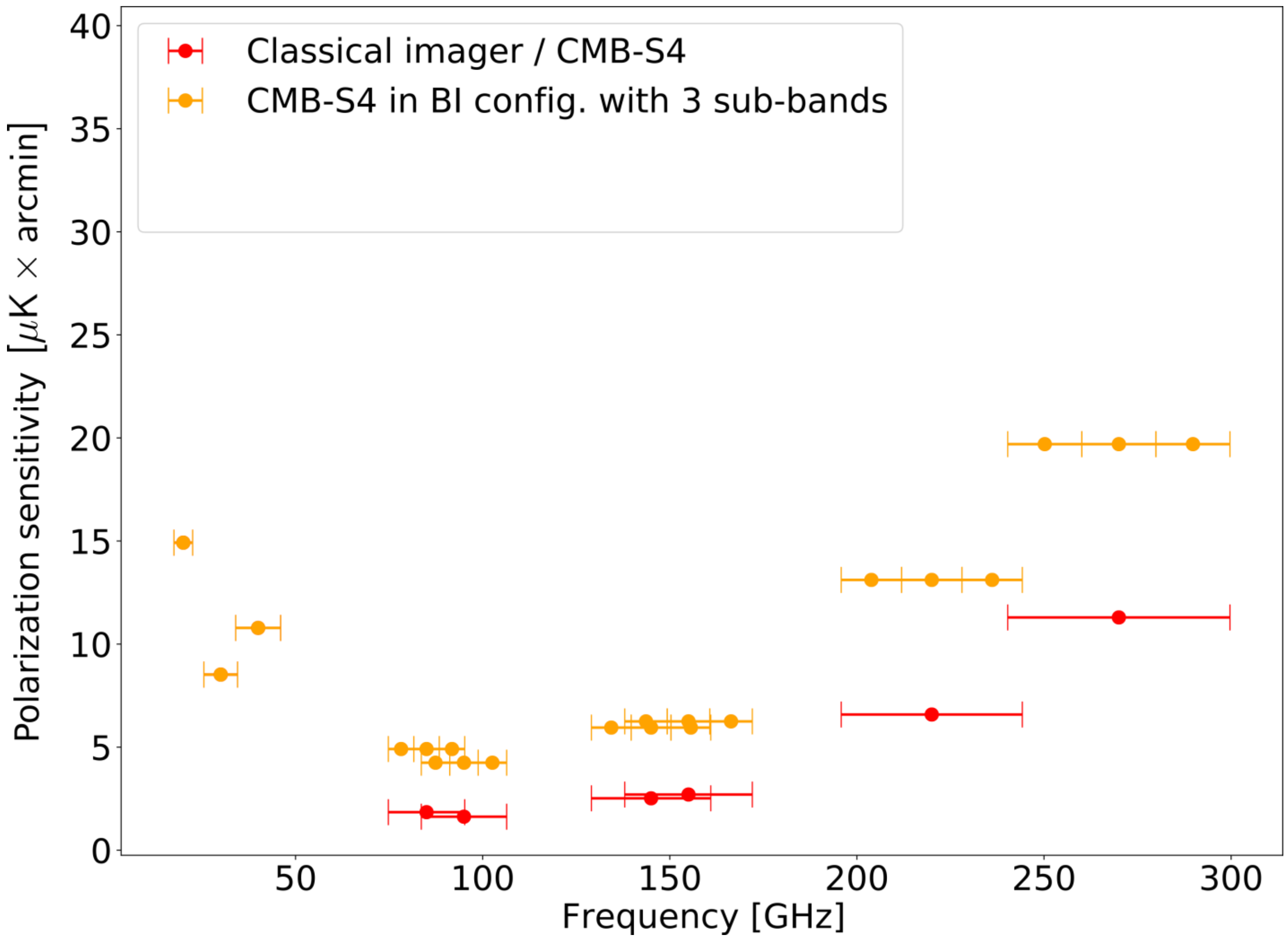

CMB-S4/BI configuration:
S4 frequency band is
subdivided into n_{sub} sub-bands

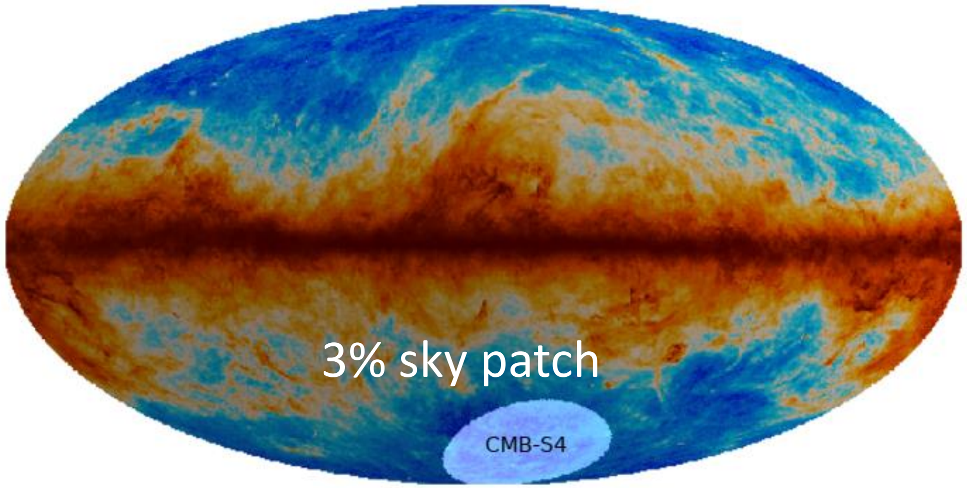

CMB-S4 & hypothetical CMB-S4/BI

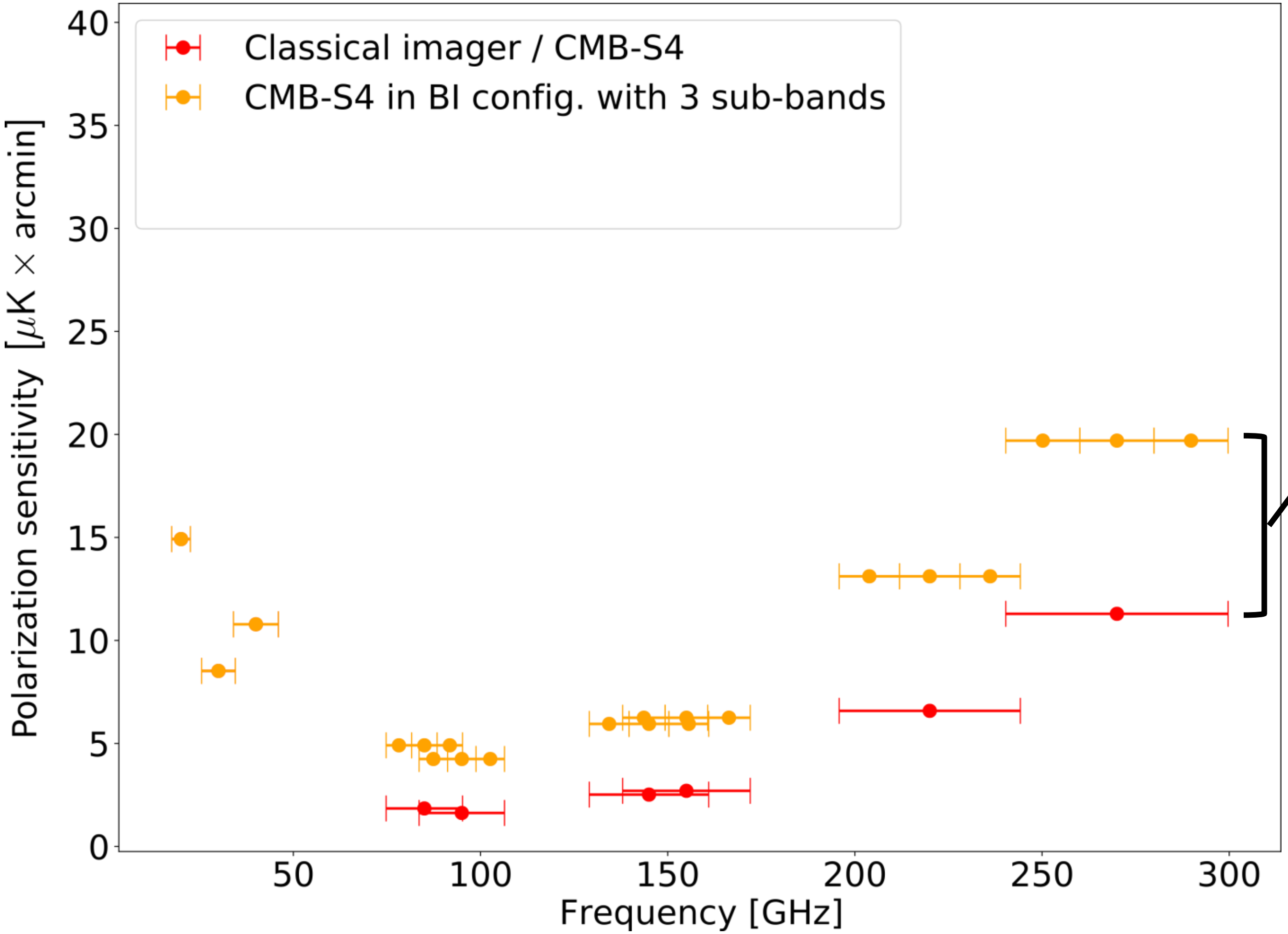

The sensitivity in each sub-band degrades as

$$\sigma_{i,j}^{\mathrm{BI}} = \sigma_i^{\mathrm{S4}} \cdot \sqrt{n_{\mathrm{sub}}} \cdot \varepsilon$$

$$i = 1, \dots, N_{\mathrm{bands,S4}}$$

$$\mathrm{j} = 1, \dots, n_{\mathrm{sub}}$$

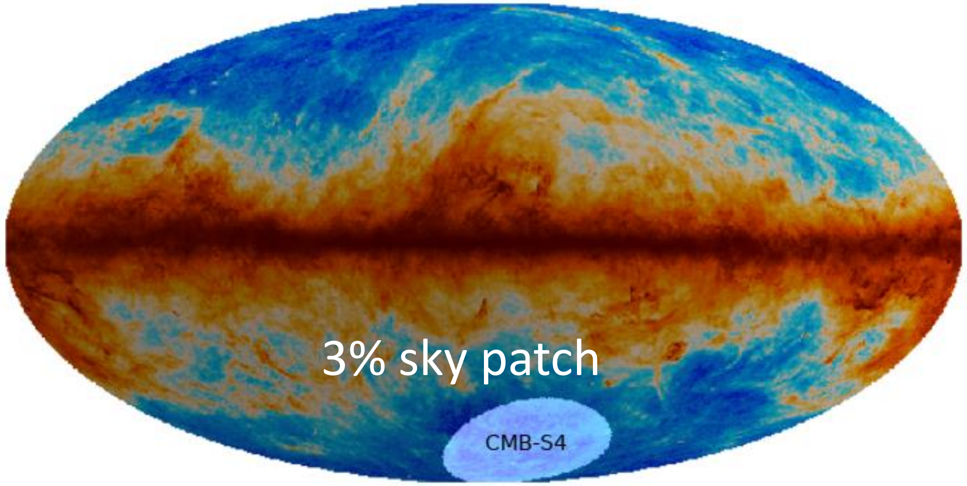

CMB-S4 & hypothetical CMB-S4/BI

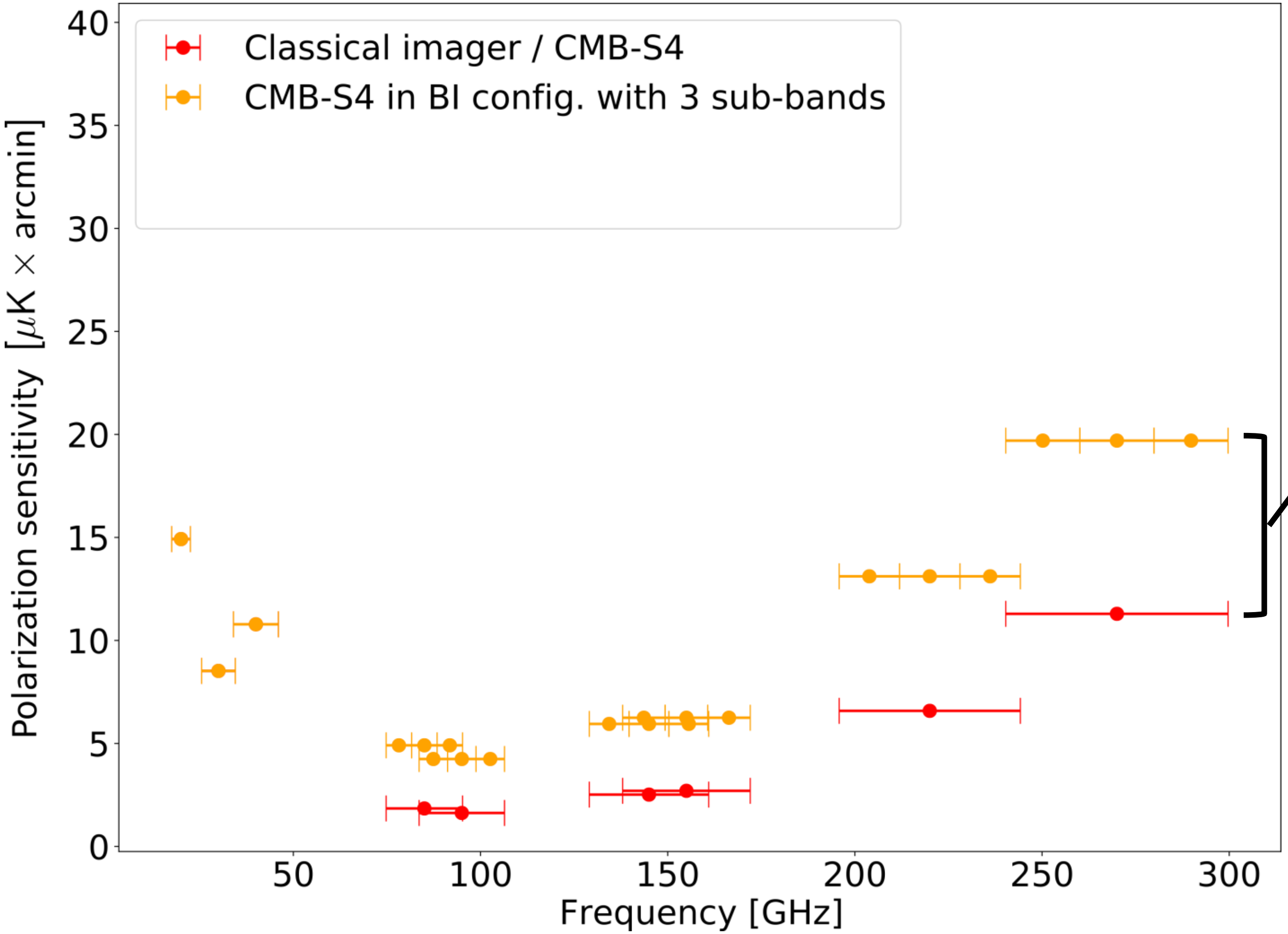

The sensitivity in each sub-band degrades as

$$\sigma_{i,j}^{\mathrm{BI}} = \sigma_i^{\mathrm{S4}} \cdot \sqrt{n_{\mathrm{sub}}} \cdot \varepsilon$$

$$i = 1, \ldots, N_{\mathrm{bands,S4}}$$

$$\mathrm{j} = 1, \ldots, n_{\mathrm{sub}}$$

Sub-optimality factor ε :
increases the white noise level to account for correlated noise (proxy)
(Mousset et al. 2022)

CMB-S4 & hypothetical CMB-S4/BI

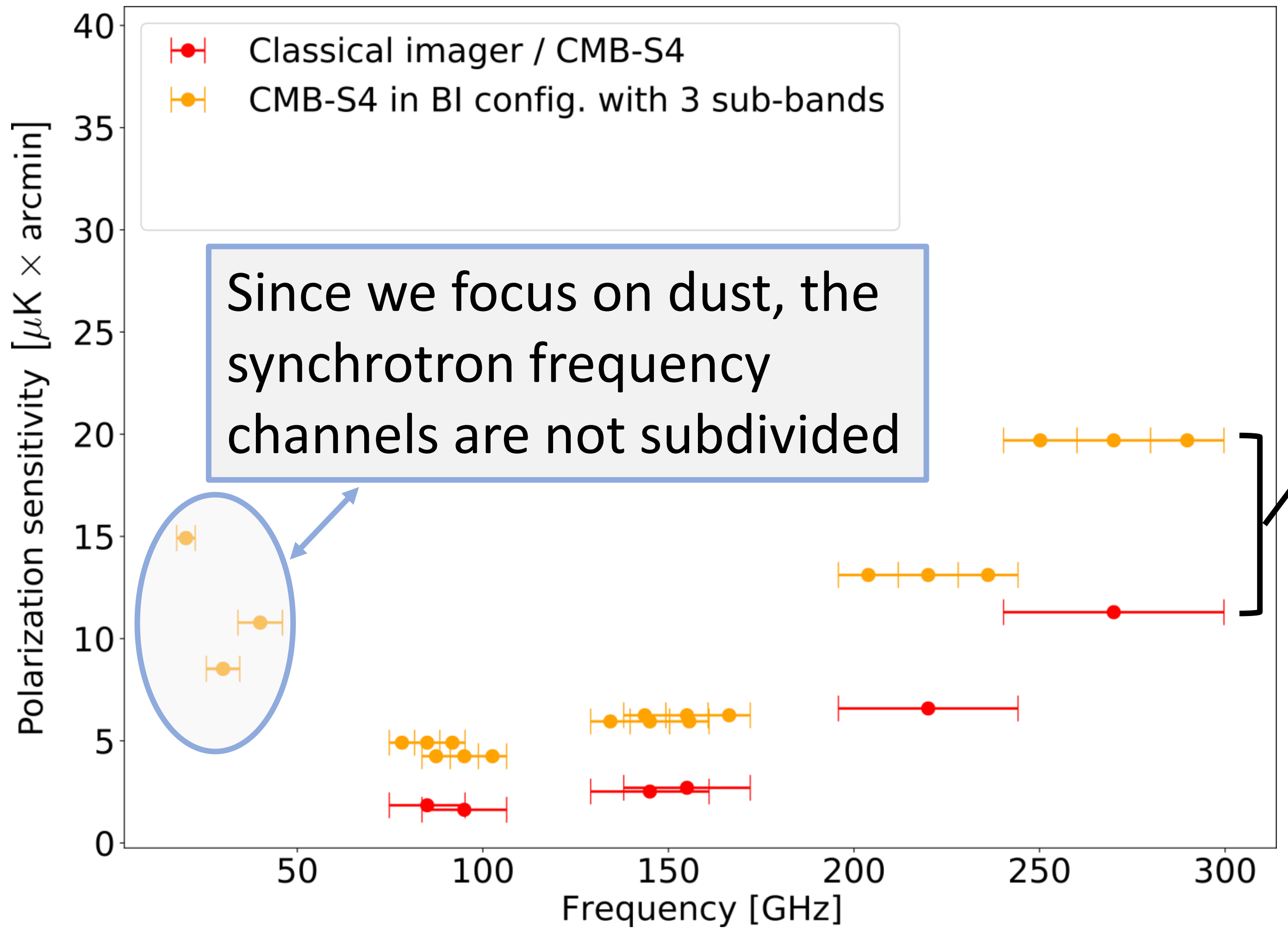

The sensitivity in each sub-band degrades as

$$\sigma_{i,j}^{\mathrm{BI}} = \sigma_i^{\mathrm{S4}} \cdot \sqrt{n_{\mathrm{sub}}} \cdot \varepsilon$$

$$i = 1, \dots, N_{\mathrm{bands,S4}}$$

$$\mathrm{j} = 1, \dots, n_{\mathrm{sub}}$$

Sub-optimality factor ε :
increases the white noise level to account for correlated noise (proxy)
(Mousset et al. 2022)

CMB-S4 & hypothetical CMB-S4/BI

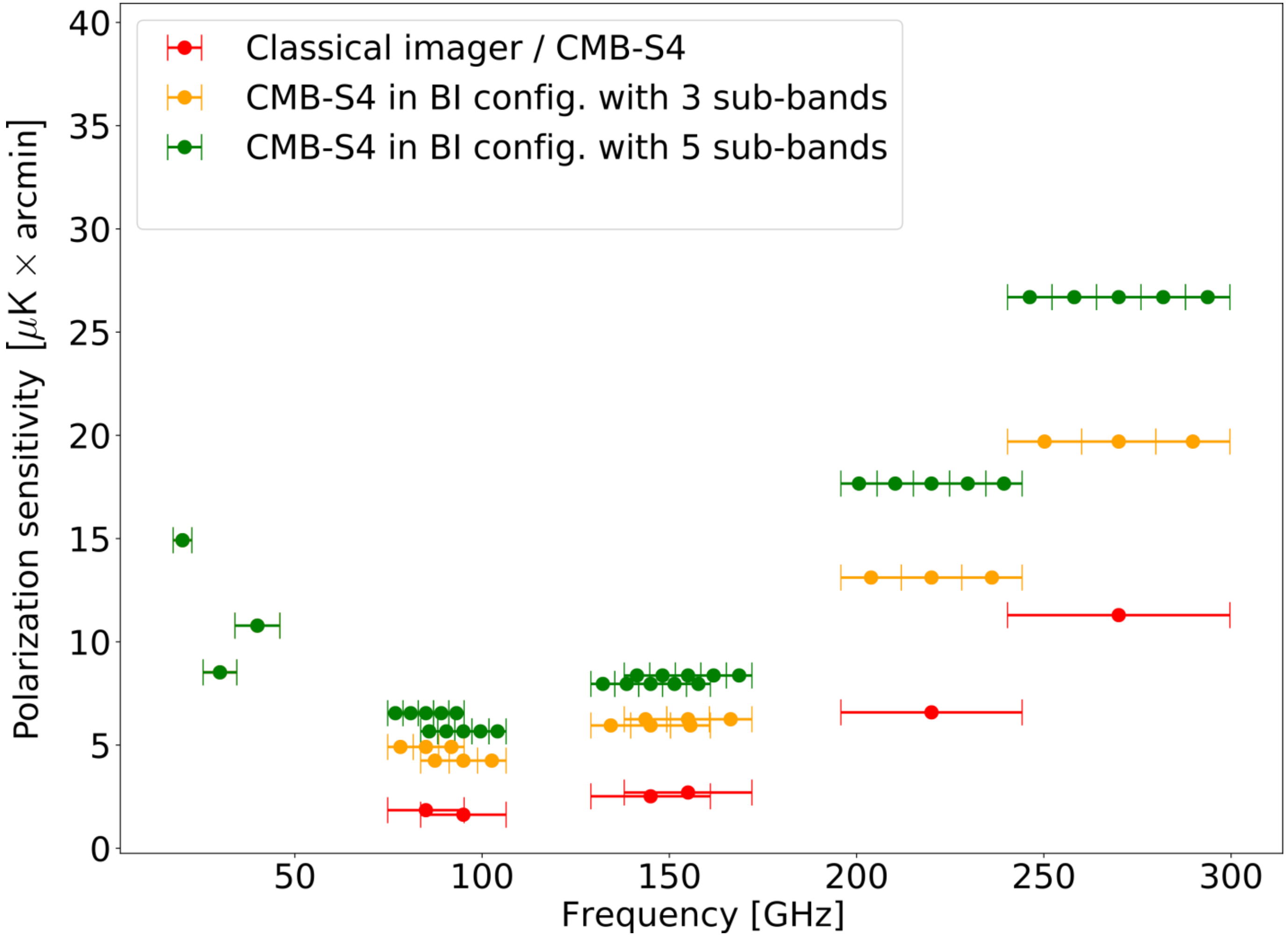

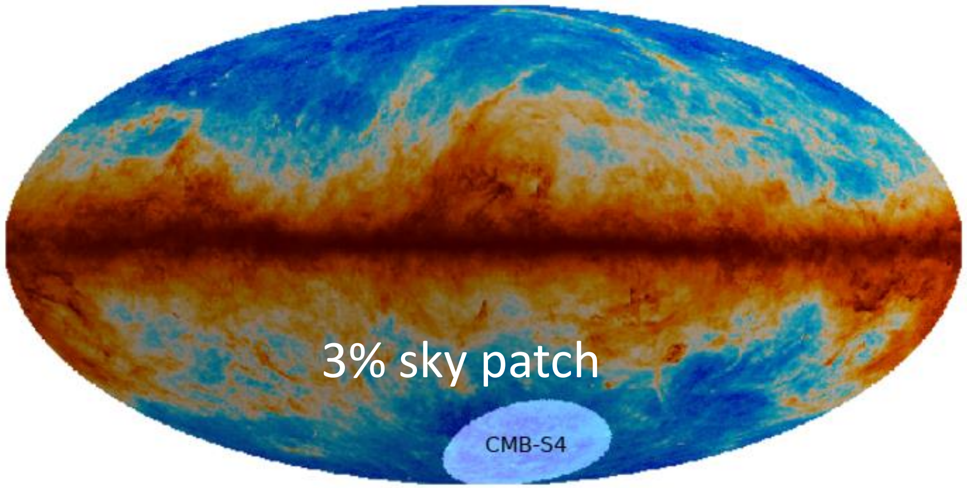

CMB-S4 & hypothetical CMB-S4/BI

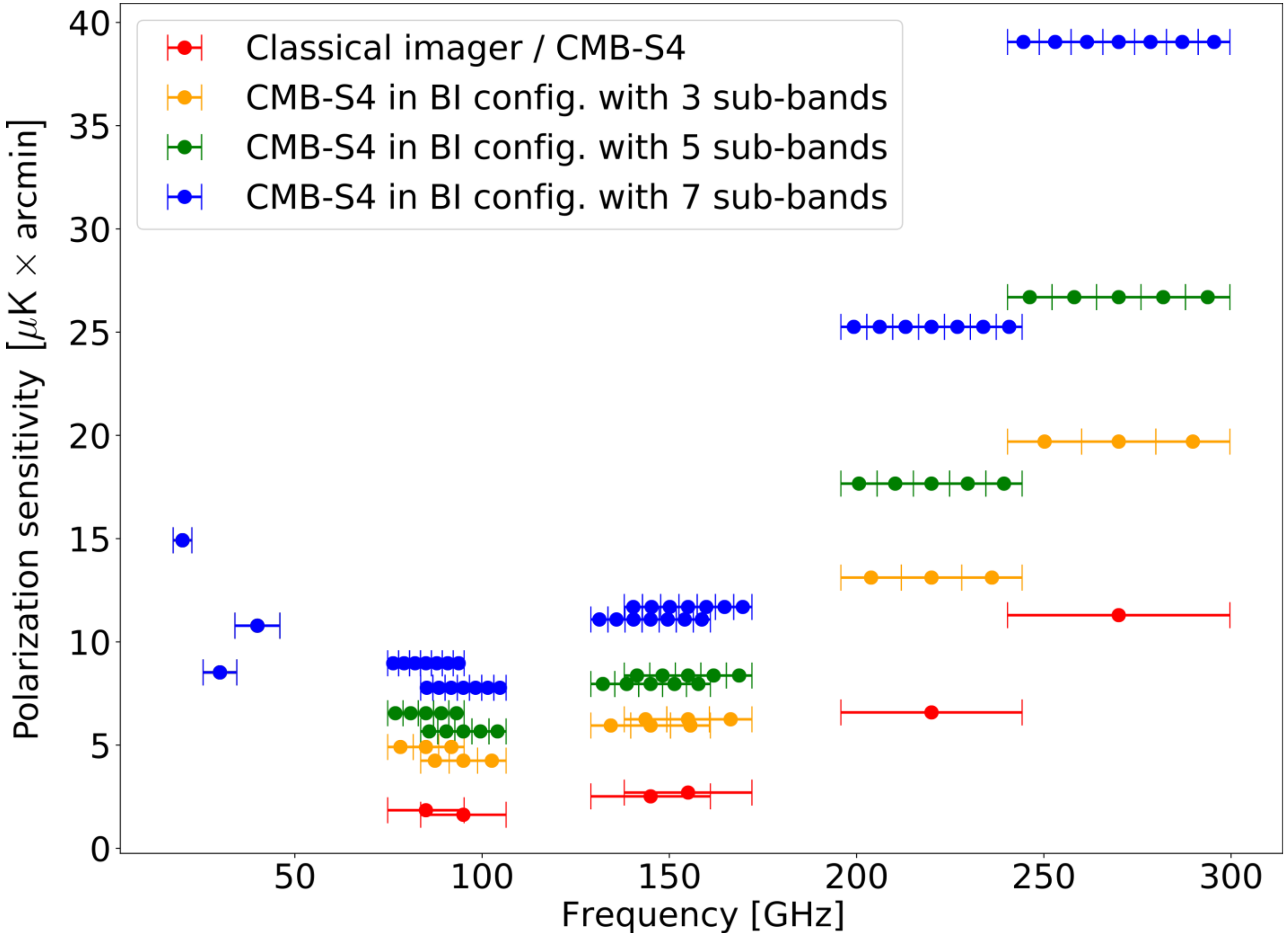

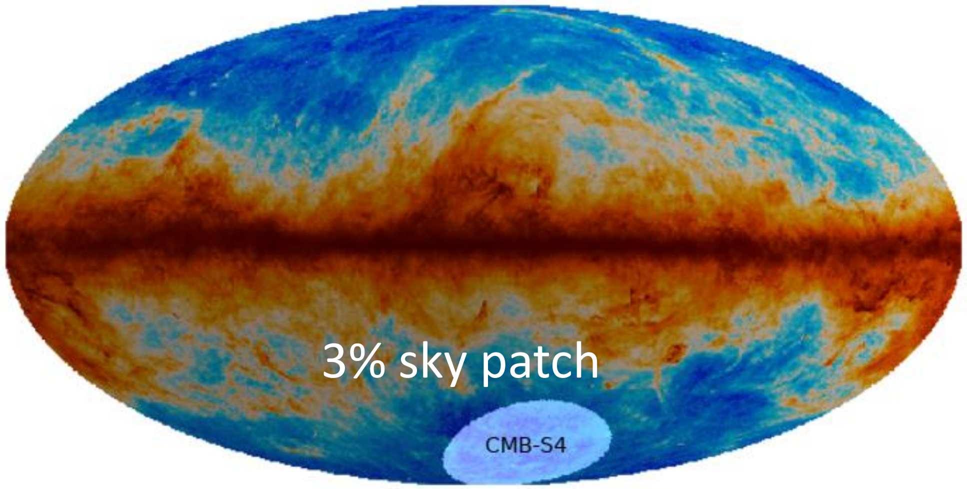

CMB-S4 & hypothetical CMB-S4/BI

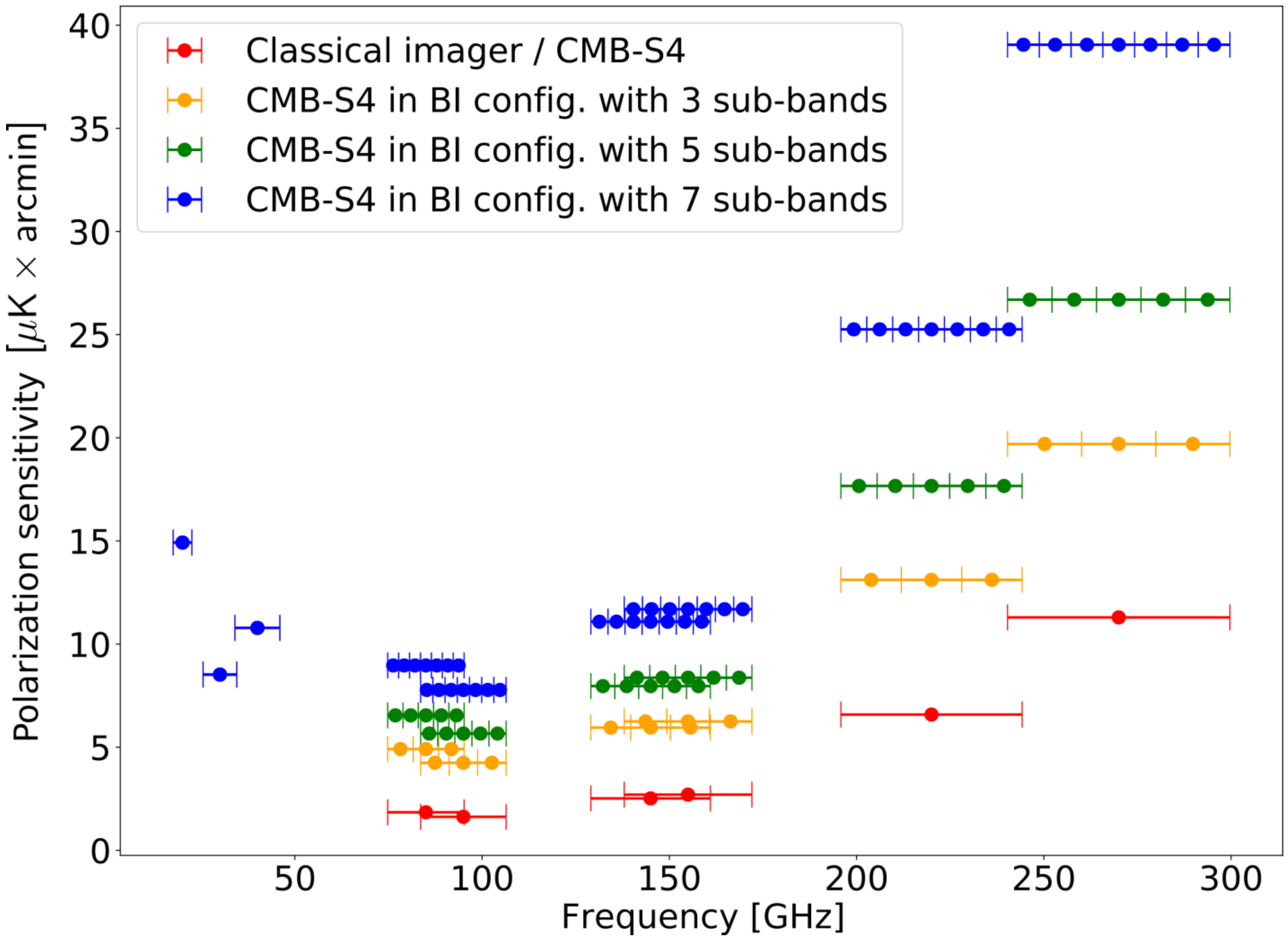

In total we considered seven CMB-S4/BI cases with n_{sub} ranging from 2 to 8

Regnier M., Manzan E. et al. 2023 to be submitted

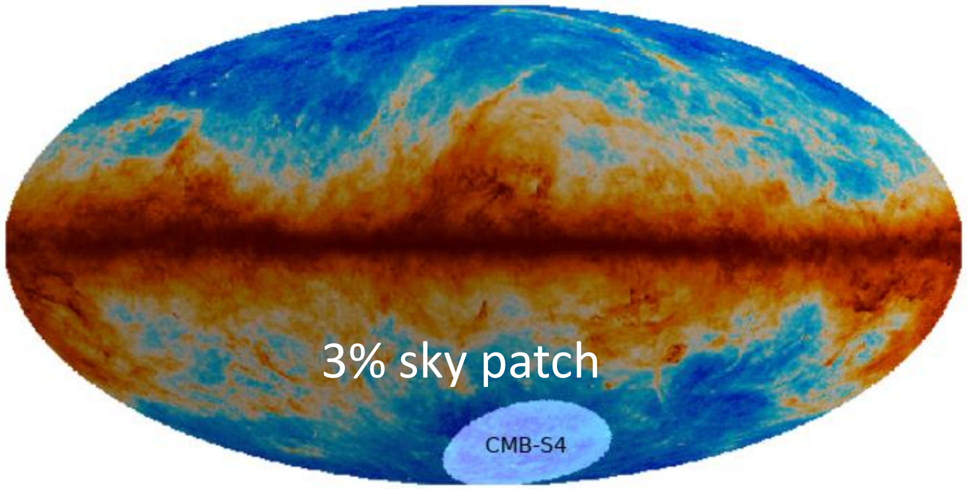

Results

Regnier M., Manzan E. et al. 2023 to be submitted

If we fit with the correct model

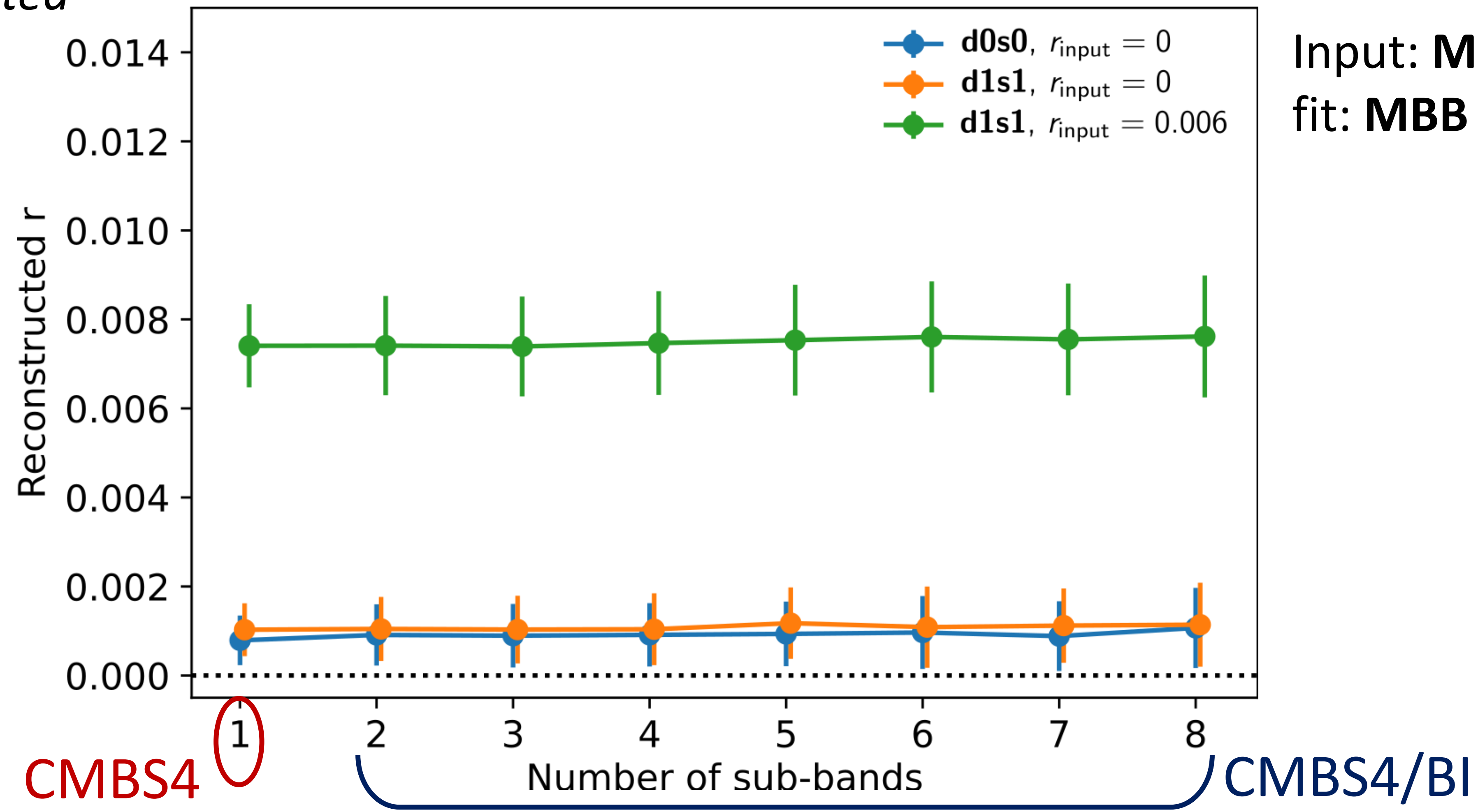

Input: **MBB**
fit: **MBB**

Results

Regnier M., Manzan E. et al. 2023 to be submitted

If we with the wrong model

A classical imager would measure $r \sim 0.008$

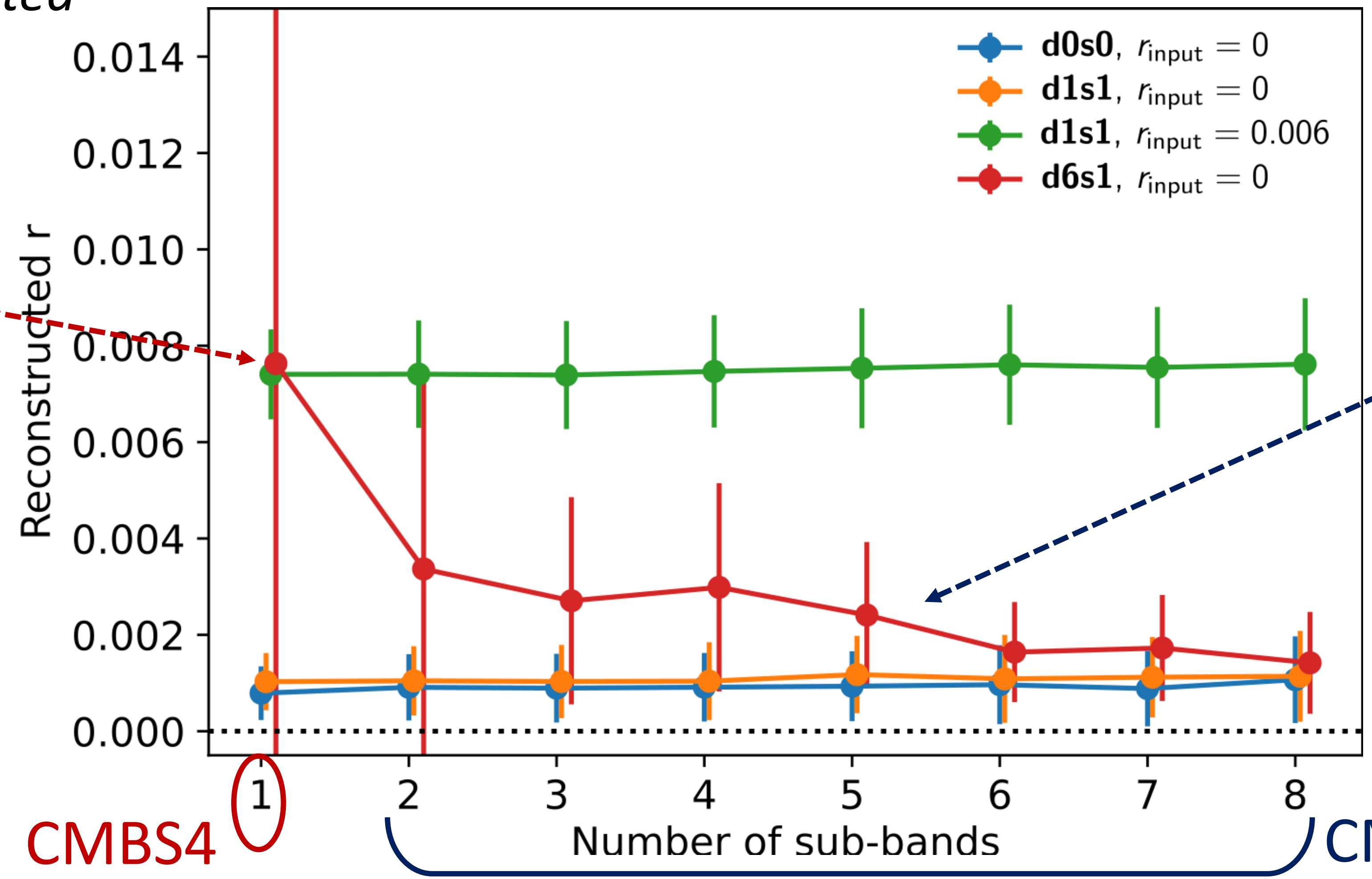

With BI the estimated ***r*** reduces with increasing $n_{\rm sub}$

Regnier M.,
Manzan E.
et al. 2023
to be submitted

Results

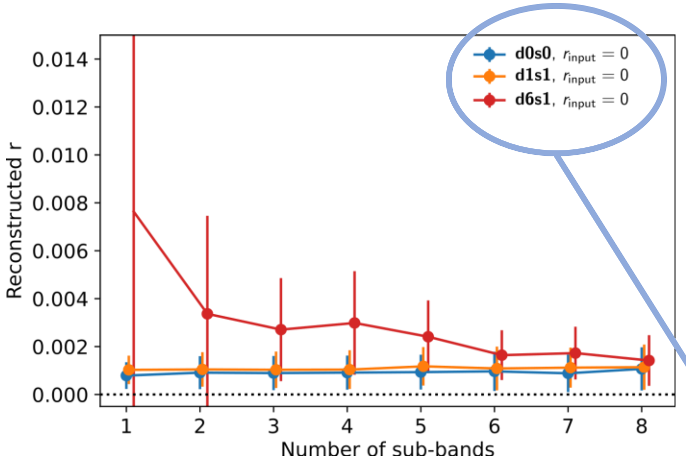

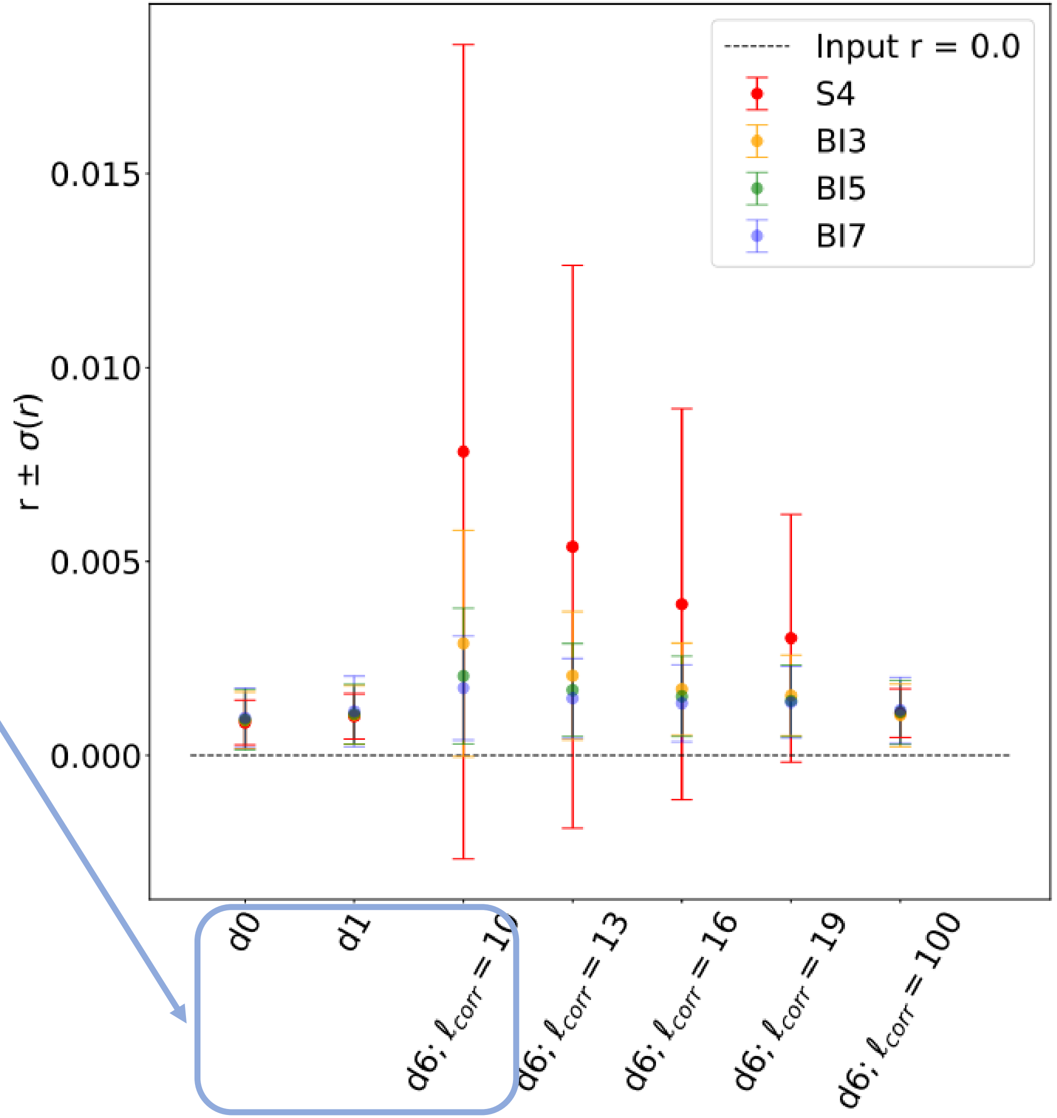

The advantage of BI in

- decreasing the bias on ***r***
- diagnosing foreground residuals

is maintained even in the case of smaller levels of dust LOS frequency decorrelation

Conclusions

- The in-band frequency resolution provided by BI and its ability to re-analyze the data allows us to detect dust LOS frequency decorrelation residuals that could bias an imager of similar performance.
- These results have been consistently obtained using FGBuster and Commander
- This opens the prospect to exploit this potential in the context of future CMB polarization experiments that will be challenged by complex foregrounds in their quest for *B*-modes detection.

Backup slides

Dust frequency decorrelation: current constraints

Correlation Ratio $R_\ell(\nu_1, \nu_2)$:

$$R_\ell(\nu_1, \nu_2) = \frac{C_\ell^{\nu_1 \times \nu_2}}{\sqrt{C_\ell^{\nu_1 \times \nu_1} \cdot C_\ell^{\nu_2 \times \nu_2}}}$$

(Planck Collaboration et al. 2017)

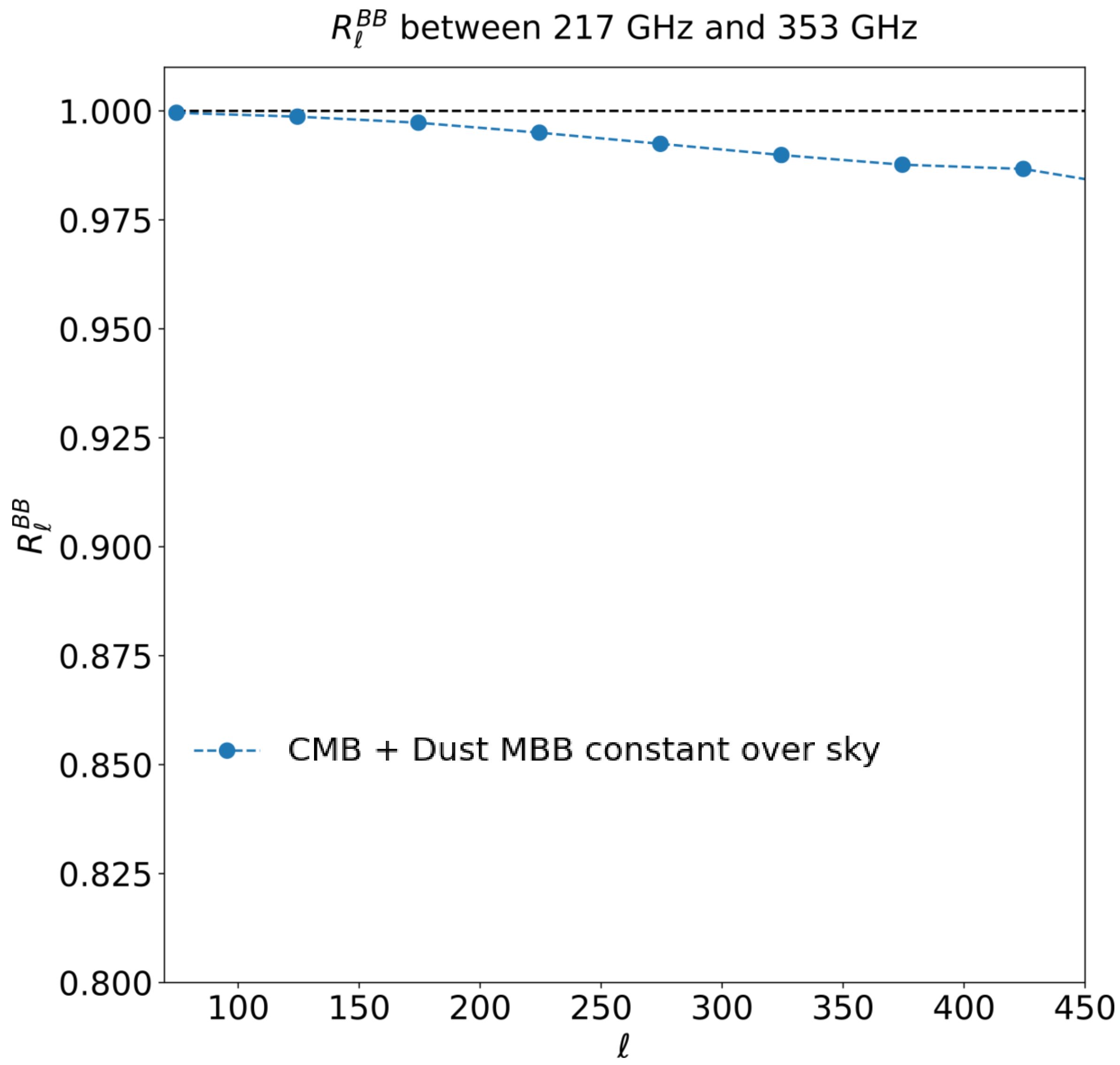

Dust frequency decorrelation: current constraints

Correlation Ratio $R_\ell(\nu_1, \nu_2)$:

$$R_\ell(\nu_1, \nu_2) = \frac{C_\ell^{\nu_1 \times \nu_2}}{\sqrt{C_\ell^{\nu_1 \times \nu_1} \cdot C_\ell^{\nu_2 \times \nu_2}}}$$

Cross-spectra between HM$_i$ at ν_1 and HM$_j$ at ν_2

Cross-spectra between HM1 and HM2 at ν_1

Cross-spectra between HM1 and HM2 at ν_2

(Planck Collaboration et al. 2017)

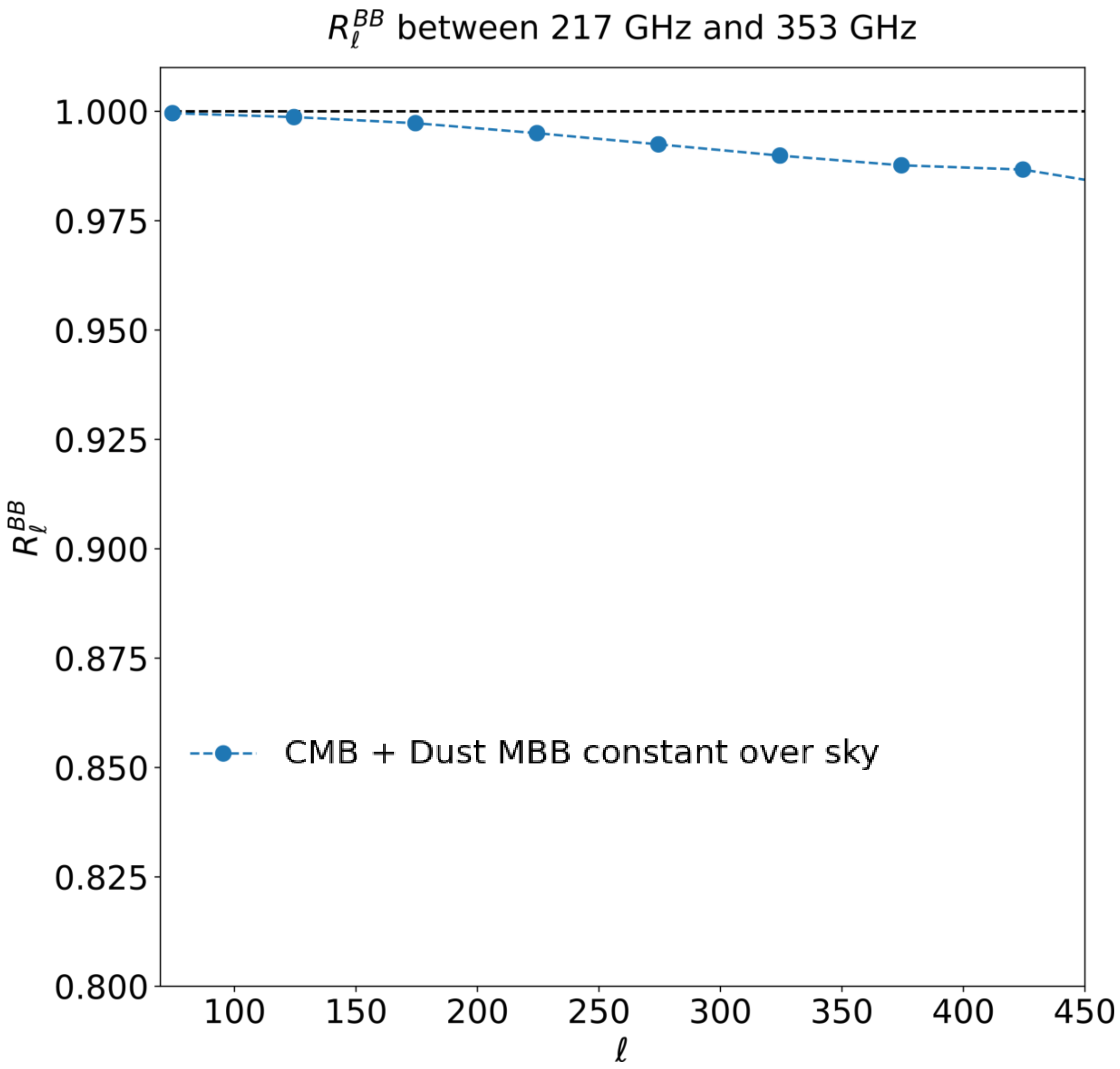

Dust frequency decorrelation: current constraints

Correlation Ratio $R_\ell(\nu_1, \nu_2)$:

$$R_\ell(\nu_1,\nu_2) = \frac{C_\ell^{\nu_1\times\nu_2}}{\sqrt{C_\ell^{\nu_1\times\nu_1}\cdot C_\ell^{\nu_2\times\nu_2}}}$$

Cross-spectra between HM$_i$ at ν_1 and HM$_j$ at ν_2

Cross-spectra between HM1 and HM2 at ν_1

Cross-spectra between HM1 and HM2 at ν_2

(Planck Collaboration et al. 2017)

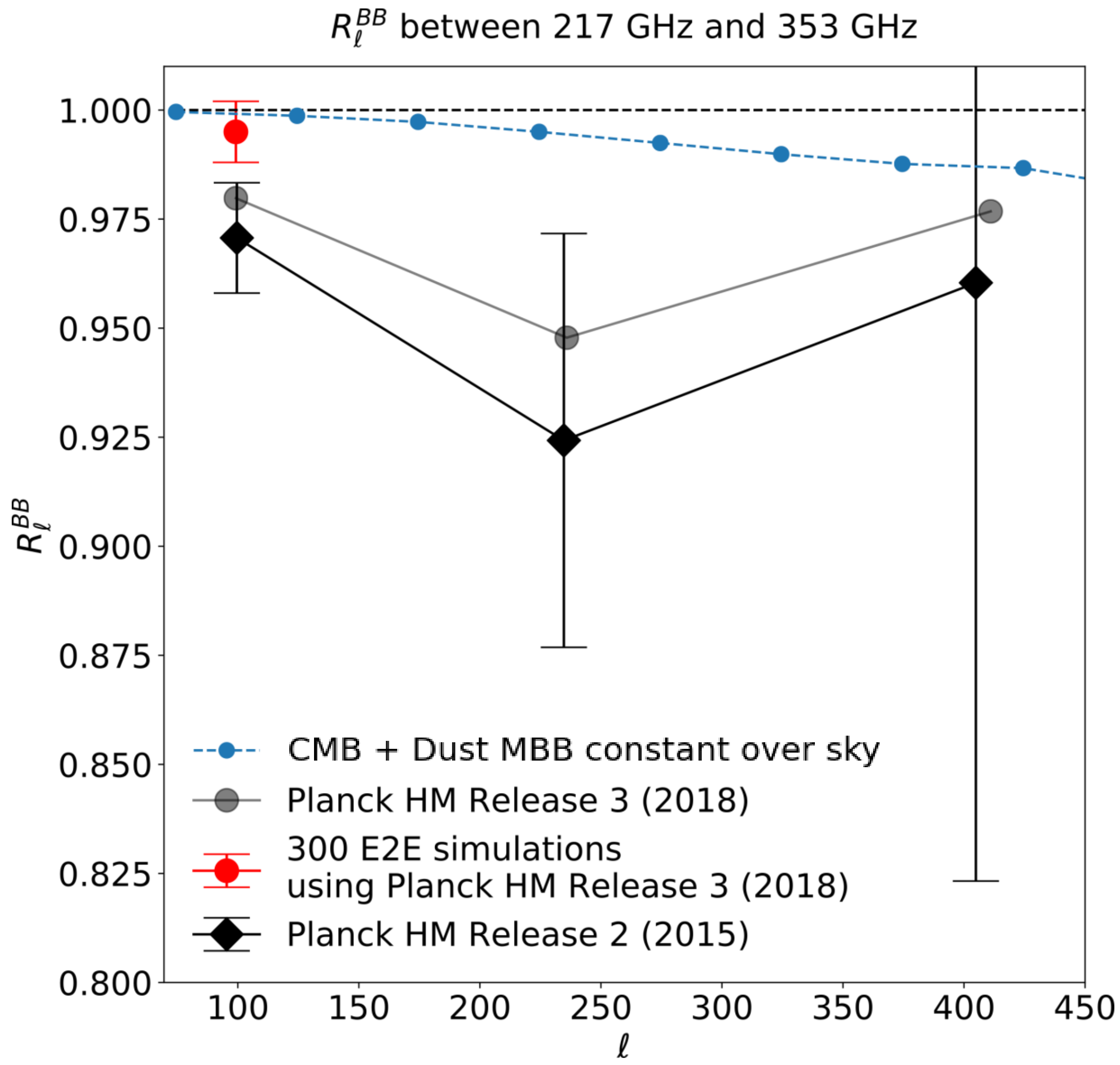

Dust frequency decorrelation: current constraints

Planck's data allows for a small level of decorrelation

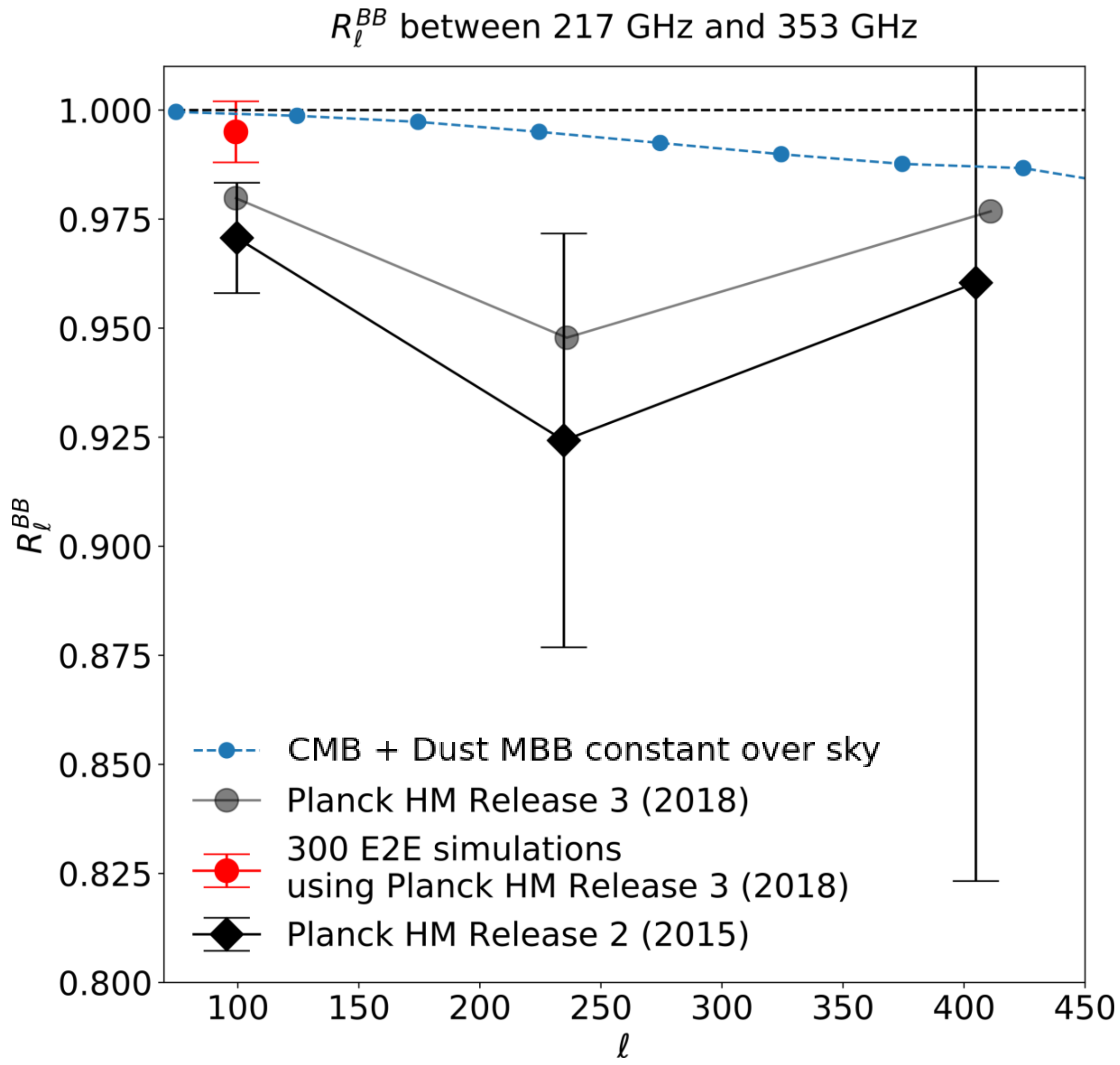

Dust LOS frequency decorrelation: the PySM model

PySM3

- PySM model **d6** : Dust MBB with **LOS frequency decorrelations**

$$I_d(\hat{n},\nu) = DEC(\nu,\nu_0,\ell_{corr}) \cdot A_{d,\nu_0}(\hat{n}) \frac{e^{\frac{h\nu_0}{k_B T_d(\hat{n})}} - 1}{e^{\frac{h\nu}{k_B T_d}} - 1} \left(\frac{\nu}{\nu_{0,d}}\right)^{\beta_d(\hat{n})+1}$$

Decorrelation factor is randomly sampled from a Gaussian distribution

$$DEC(\nu,\nu_0,\ell_{corr}) \leftarrow \mathcal{N}\left(\mu = 1, \sigma = \sigma(1/\ell_{corr})\right)$$

$$R_\ell(\nu,\nu_0) \equiv \frac{C_\ell^{\nu\times\nu_0}}{\sqrt{C_\ell^{\nu\times\nu} \cdot C_\ell^{\nu_0\times\nu_0}}} = \begin{cases} 1 & \text{for } \ell \leq 30 \\ \exp\left\{-\frac{1}{2}\cdot\left(\frac{1}{\ell_{corr}}\right)^2 \cdot \log\left(\frac{\nu}{\nu_0}\right)^2\right\} & \text{for } \ell > 30 \end{cases}$$

(Vansyngel et al. 2018)

Our level of frequency decorrelation

In our study we considered 3 types of dust emissions:

- **d0**
- **d1**
- **d6** with $\ell_{corr} \geq 10$

Regnier M., Manzan E. et al. 2023 to be submitted

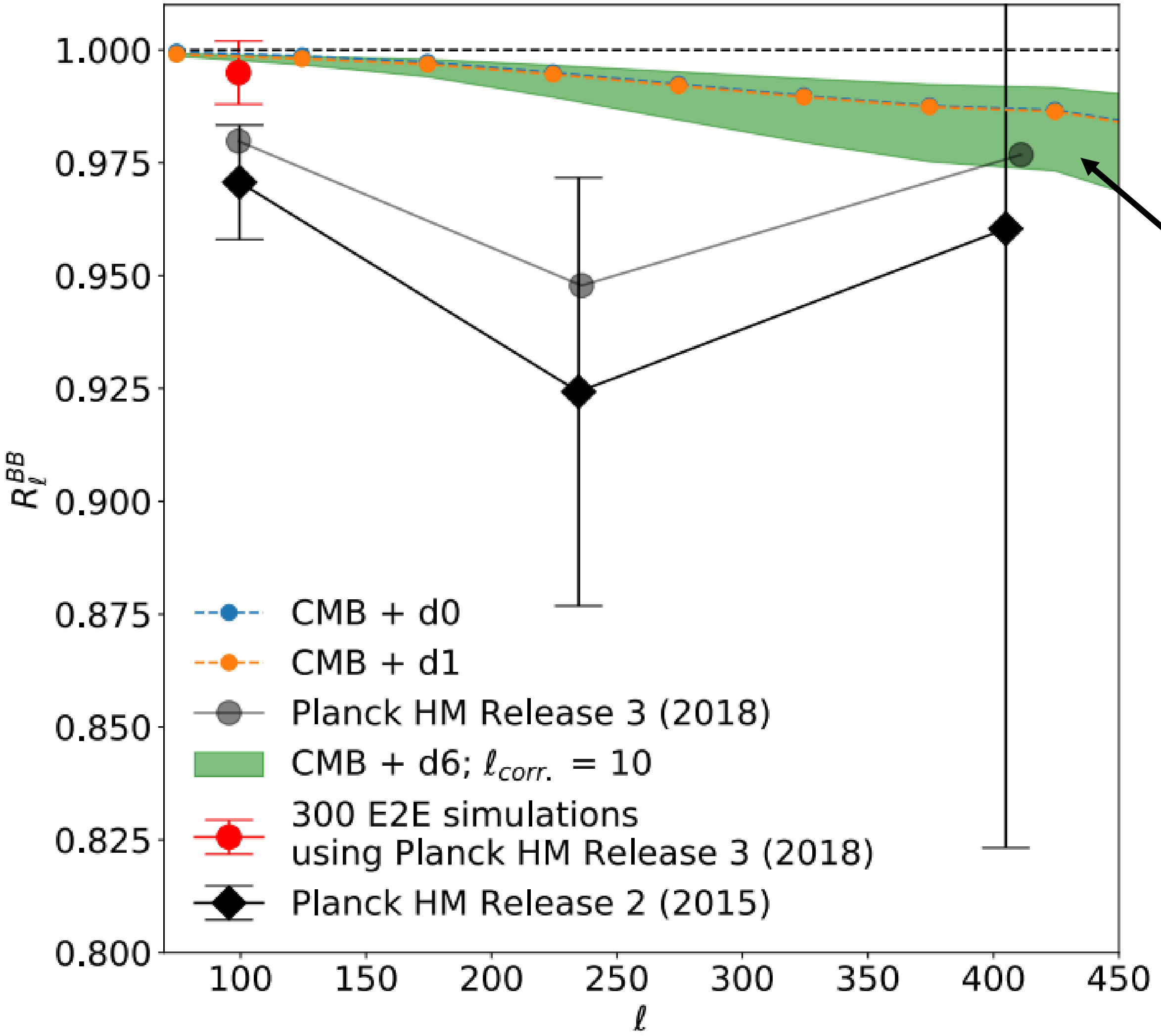

Our level of decorrelation is conservative with respect to current observations

Spectral Imaging

Signal = Sky $*$ Synthesized beam pattern

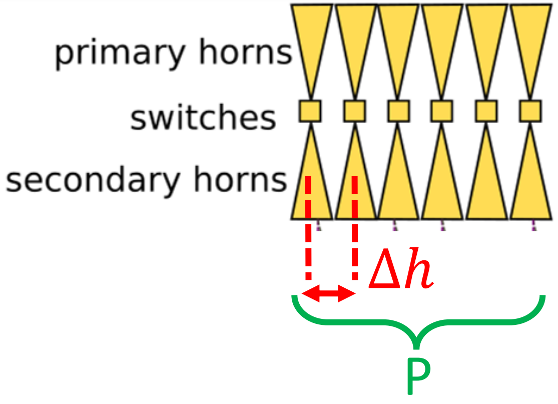

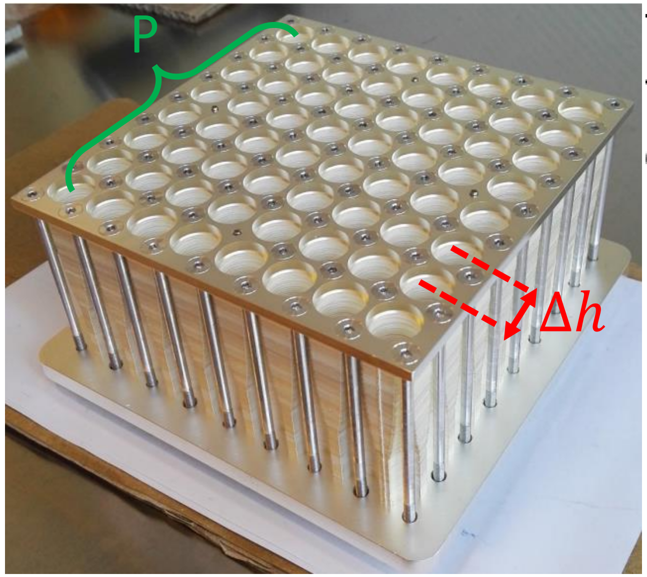

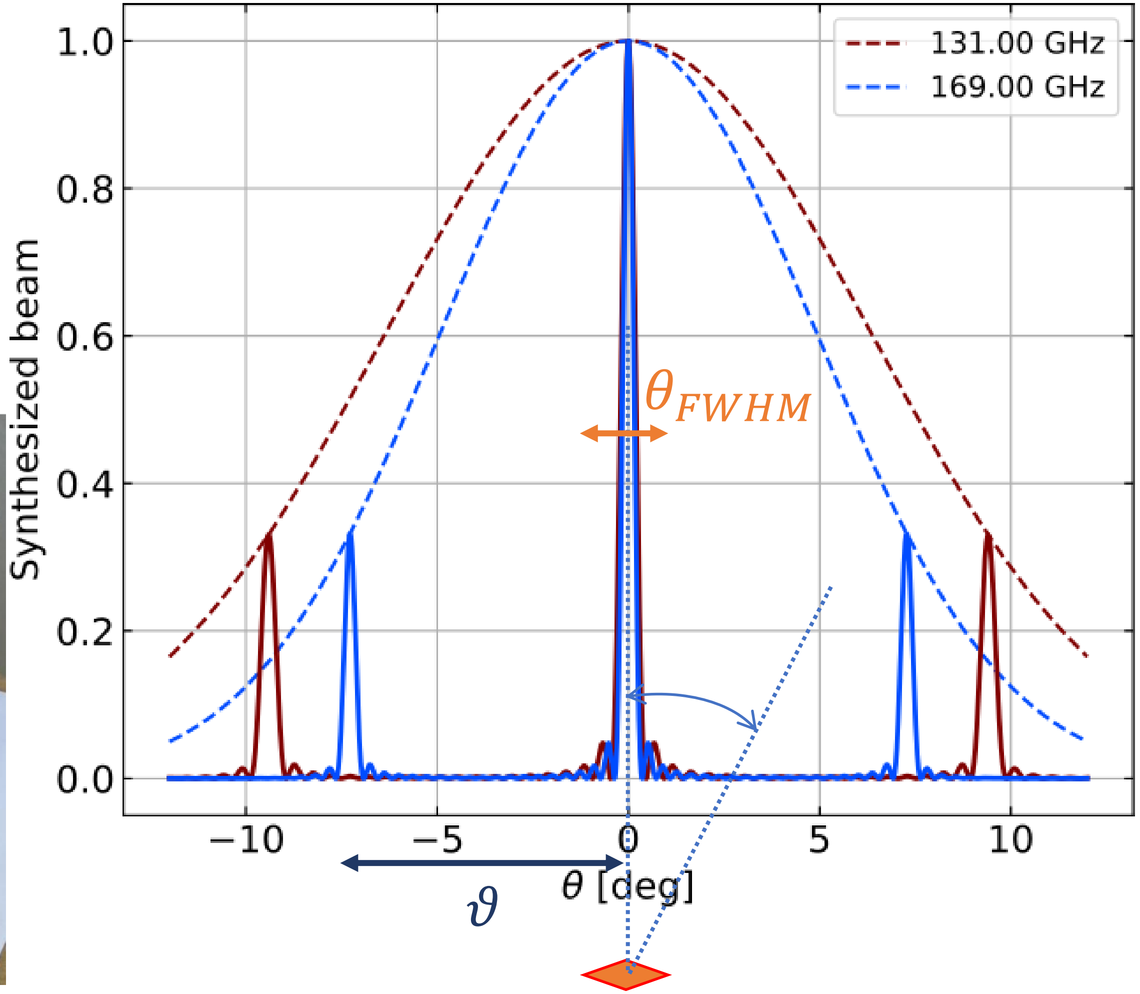

$$\theta_{FWHM} = \frac{\lambda}{(P-1)\cdot \Delta h}$$

$$\vartheta = \frac{\lambda}{\Delta h}$$

Hamilton et al., 2021

Mousset et al., 2021

Spectral Imaging

Signal = Sky ∗ Synthesized beam pattern

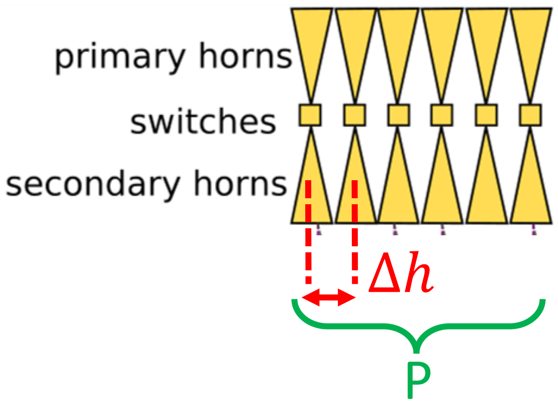

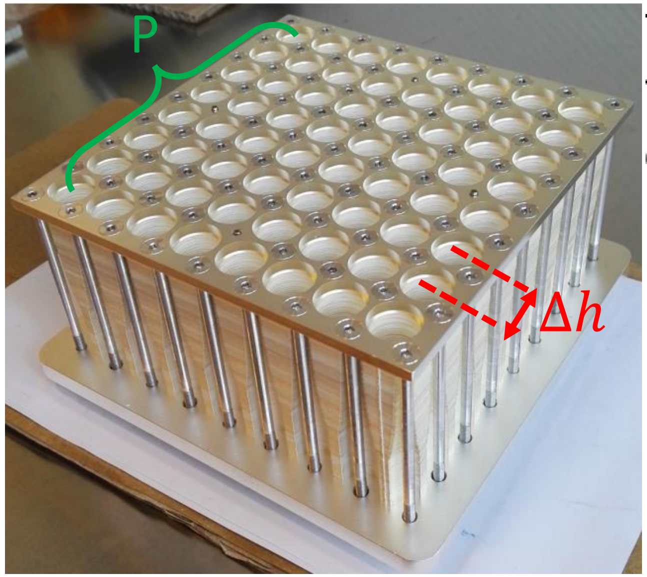

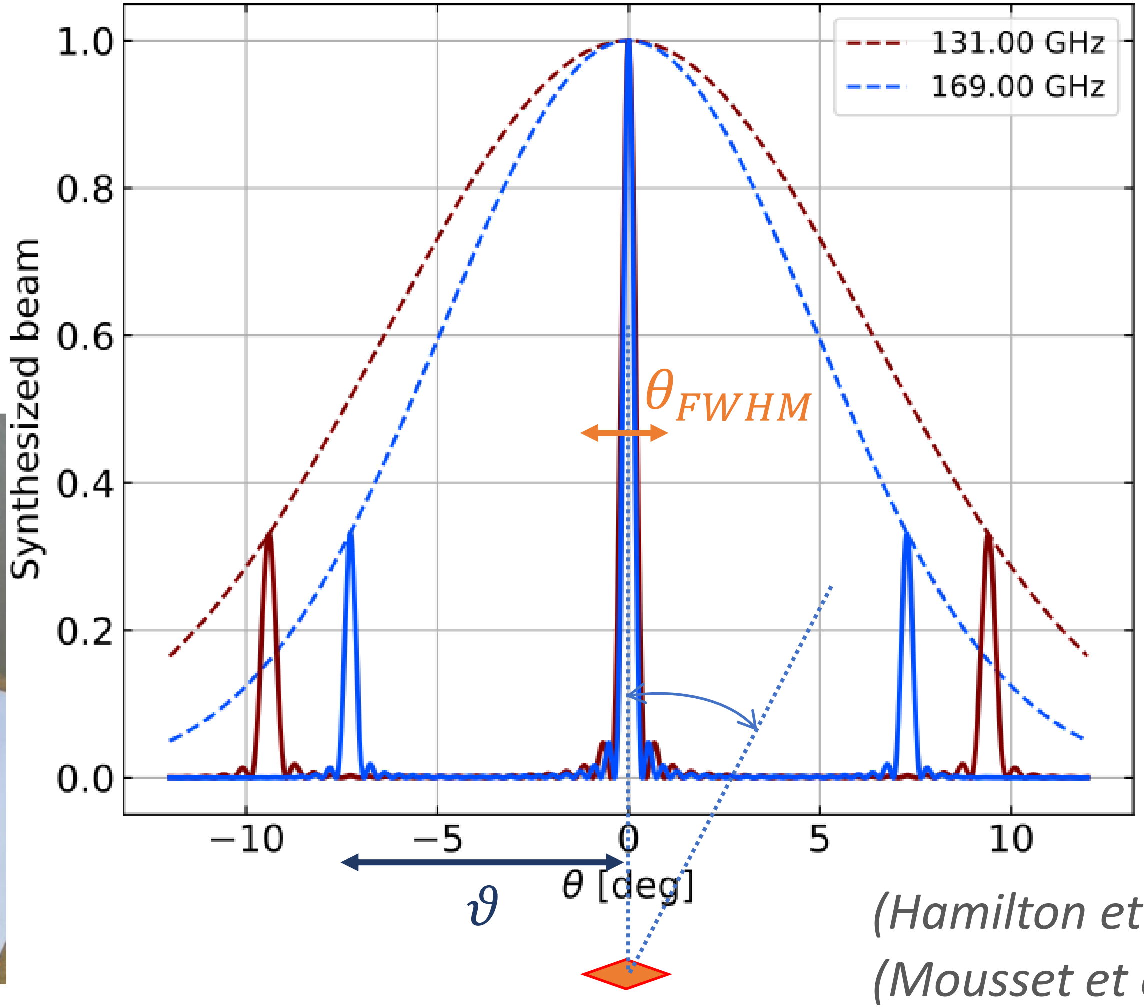

For ν_1, ν_2 such that:

$$\vartheta(\nu_2) - \vartheta(\nu_1) > \theta_{FWHM}$$

One can recover the sky signal at both ν_1 and ν_2 during data analysis. This occurs for:

$$\frac{\Delta\nu}{\nu} = \frac{1}{P-1}$$

(Hamilton et al., 2021)
(Mousset et al., 2021)

Spectral imaging in action

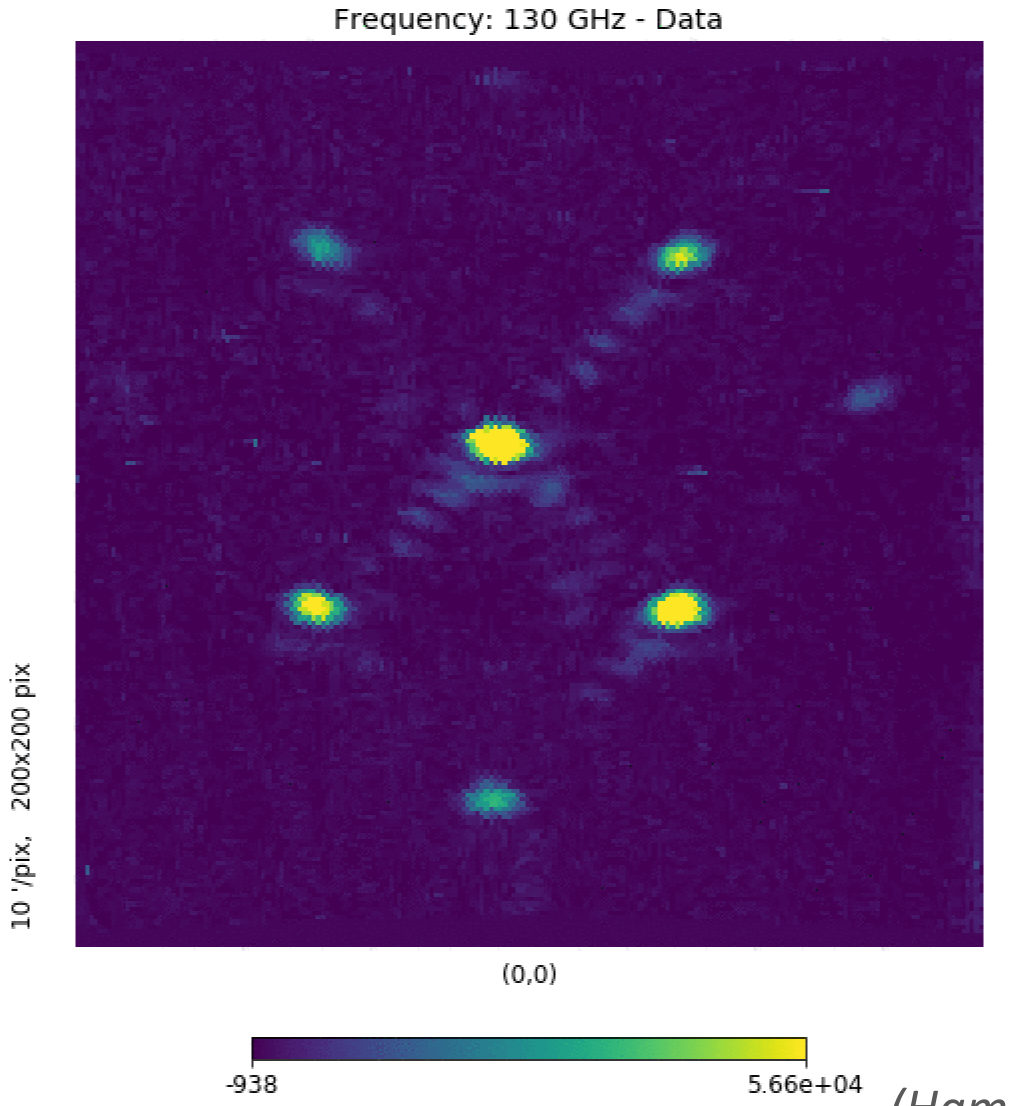

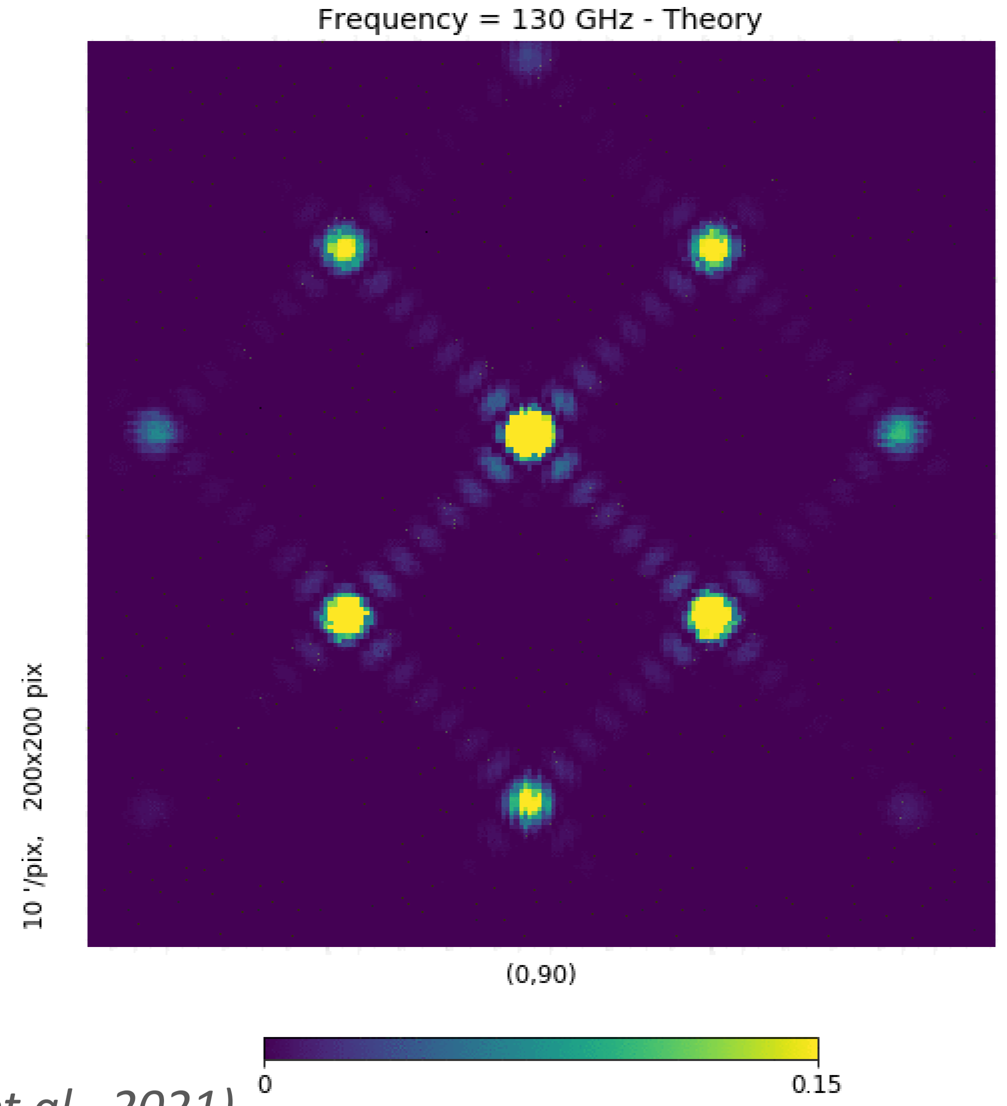

(Hamilton et al., 2021)

Spectral imaging in action

Spectral imaging **simulation** with 5 sub-bands between 192 to 247 GHz

(Mousset et al. 2022)

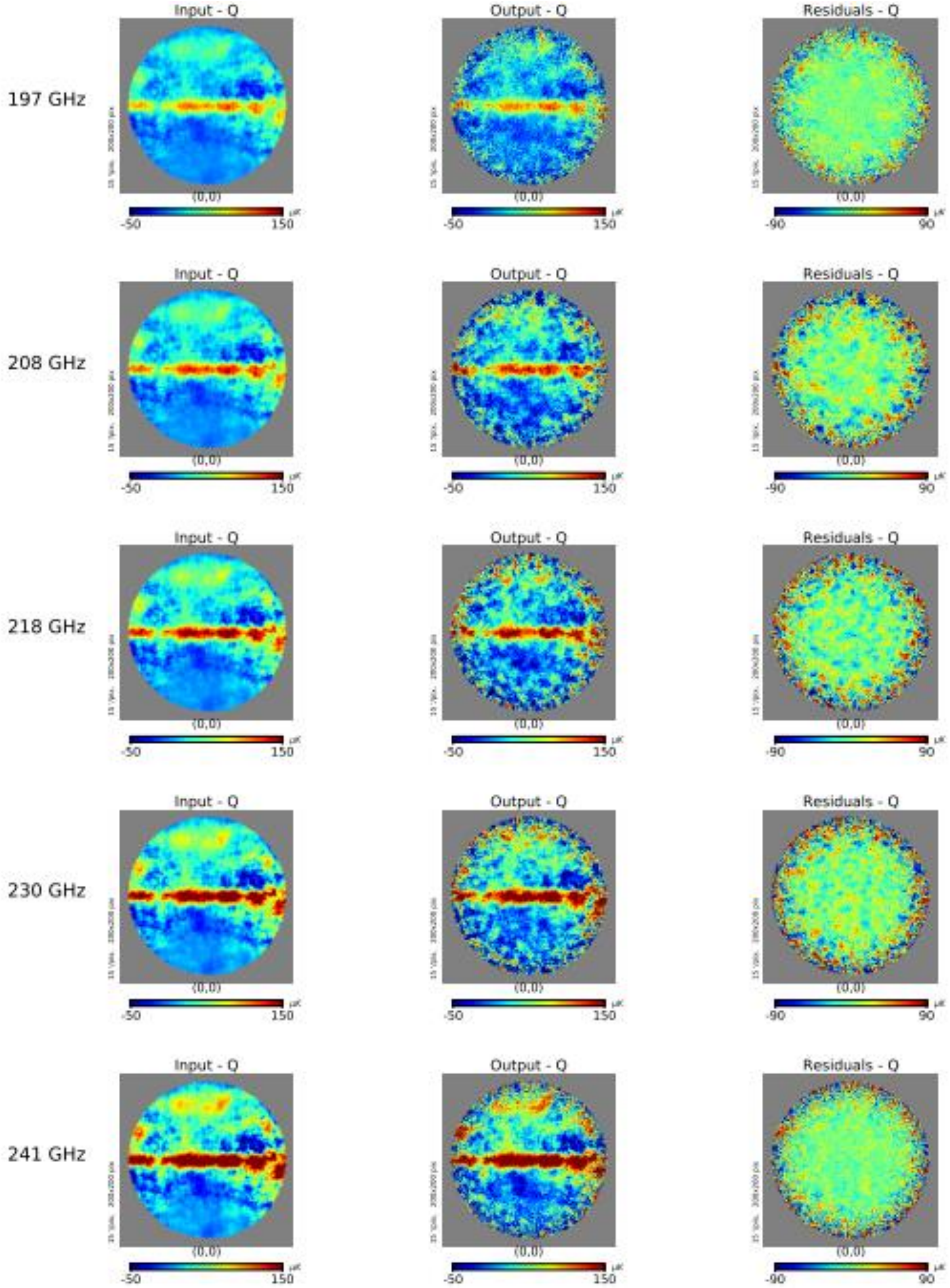

PRELIMINARY

Spectral imaging in action

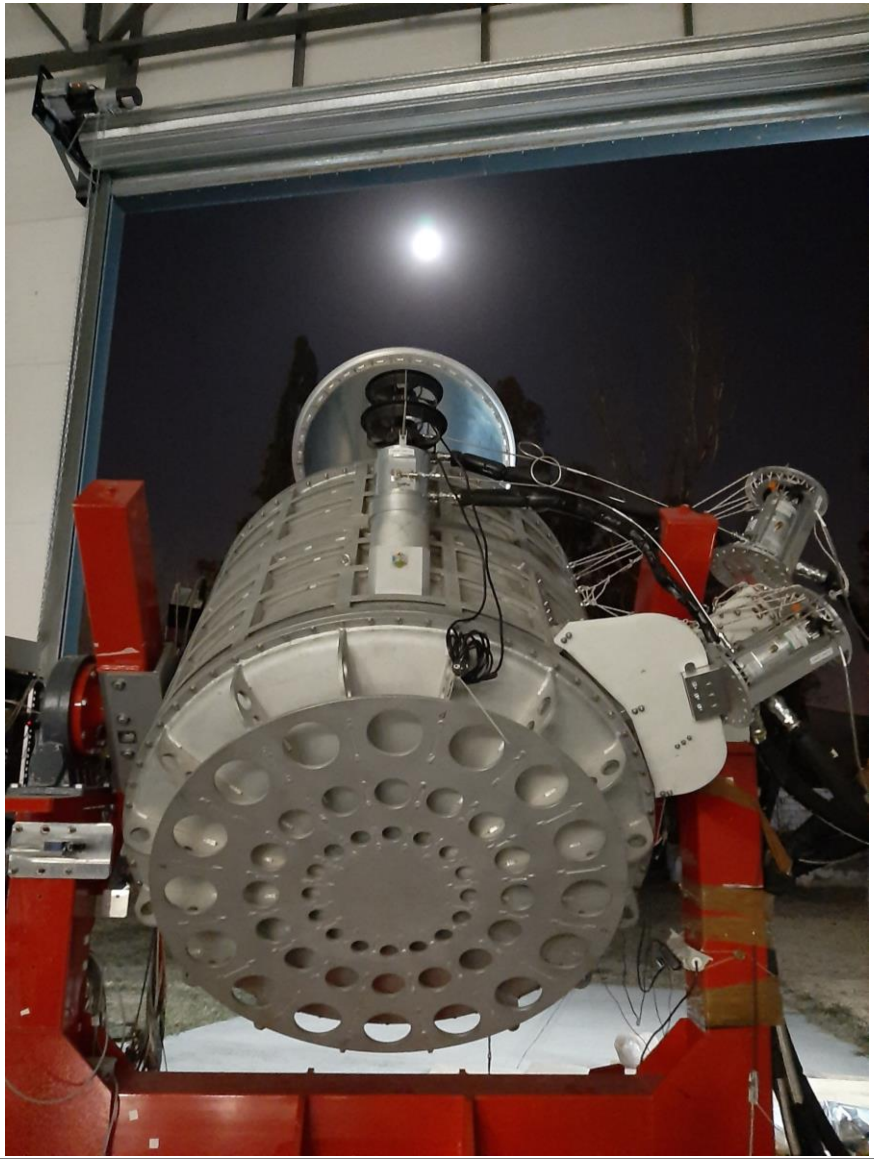

Moon Spectrum averaged from a selection of detectors

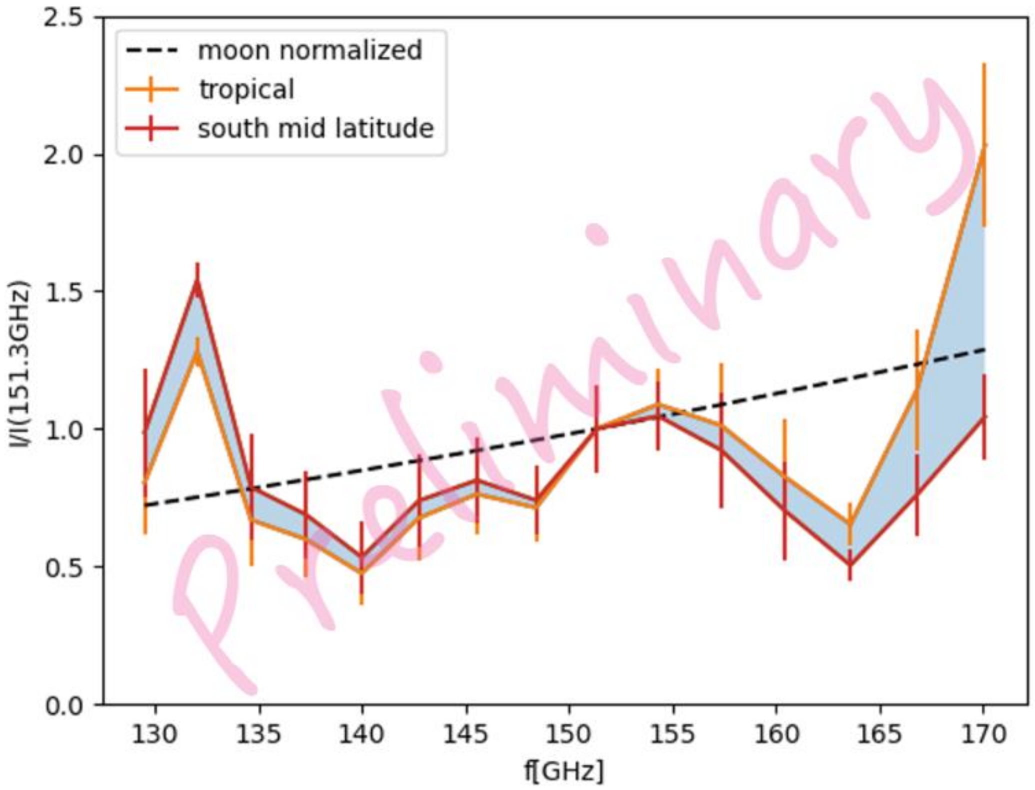

Credit: G. D'Alessandro

Sub-optimality

Frequency correlated noise is the price to pay for spectral imaging

Sup-optimality is a proxy that accounts for the increase noise at the white noise level

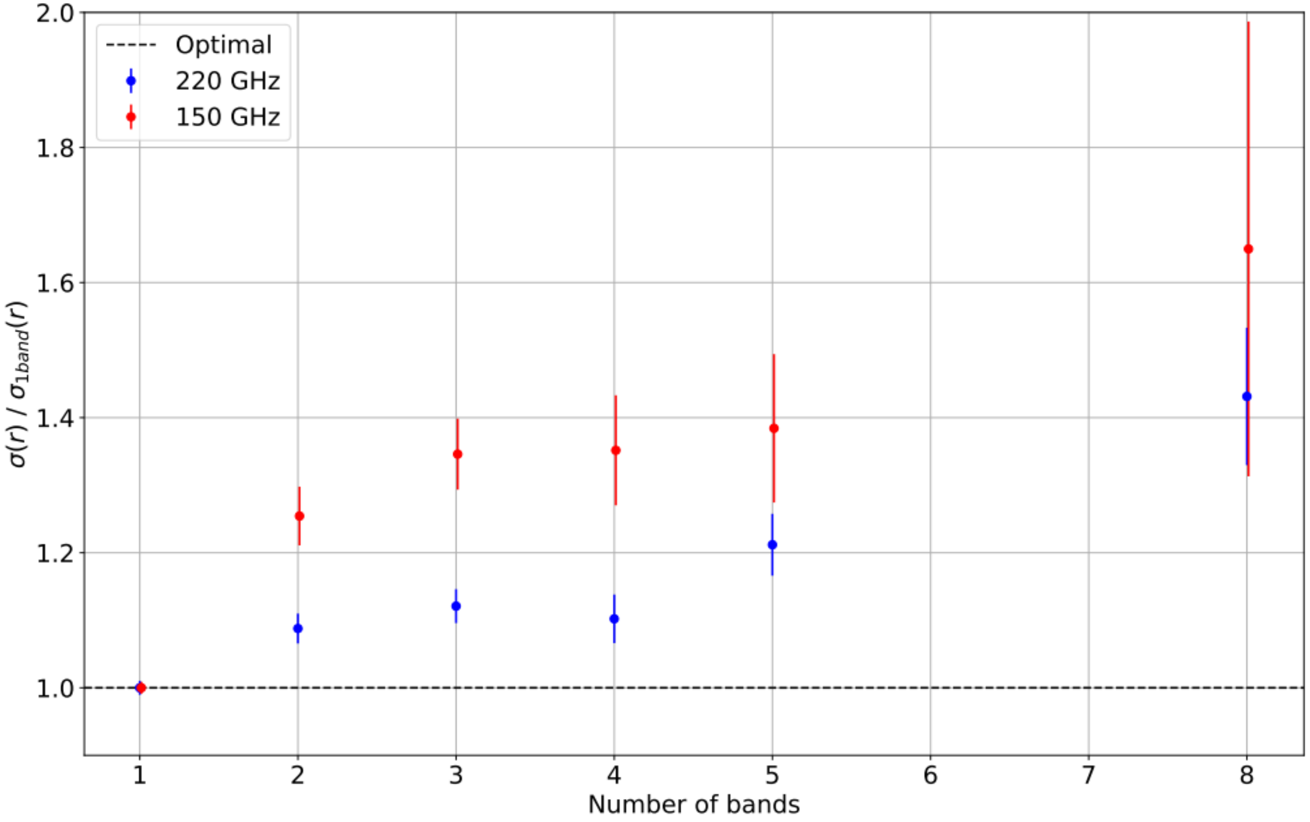

(Mousset et al. 2022)

Within the QUBIC collab we are developing a tool to properly account for BI’s noise structure in map-making and component separation: stay tuned!

The pipeline

Monte-Carlo with 500 iterations:

1. Generate a CMB realization with given $\boldsymbol{r_{input}}$
2. Generate (two) noise realization for each frequency channel for each instrument
3. Generate the foreground frequency maps in one of the following three cases:
    I. Model **d0s0**
    II. Model **d1s1**
    III. Model **d6s1**
4. Apply component separation using FGBuster or Commander. **Always assume the dust to be a MBB.**

(Stompor et al. 2008)
(Eriksen et al. 2006, 2008)

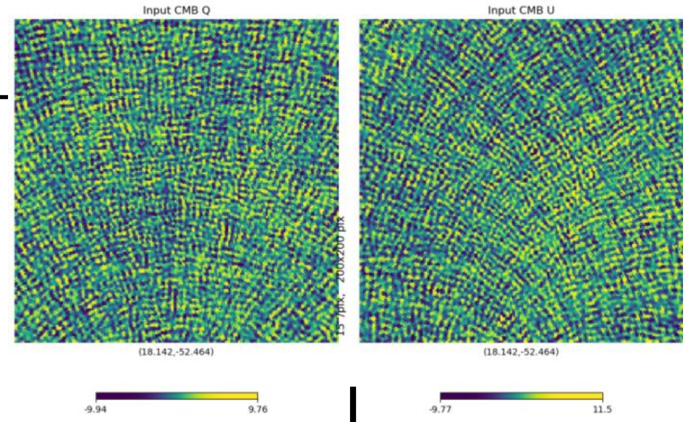

+ noise + foreground

MC Pipeline (FGBuster or Commander)

Max-L values of $\boldsymbol{r}$

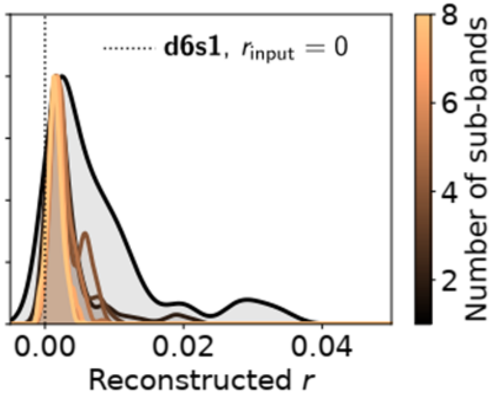

The pipeline

Monte-Carlo with 500 iterations:

1. Generate a CMB realization with given $\boldsymbol{r_{input}}$
   Generate (two) noise realization for each frequency channel for each instrument
2. Generate the foreground frequency maps in one of the following three cases:
   I. Model **d0s0**
   II. Model **d1s1**
   III. Model **d6s1**
3. Apply component separation using FGBuster or Commander. **Always assume the dust to be a MBB.**
4. Perform the (cross-)spectra of the reconstructed CMB map
5. Compute the (log -)Likelihood of $\boldsymbol{r}$. Assume a Gaussian Likelihood and a noise covariance matrix $\boldsymbol{N}$ obtained from the simulation with the **d1s1** model
6. Compute the histogram of the best fit values of $\boldsymbol{r}$

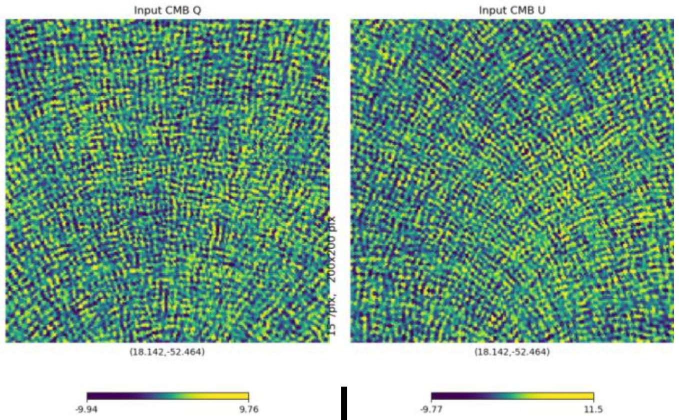

+ noise + foreground

MC Pipeline (FGBuster or Commander)

Max-L values of $\boldsymbol{r}$

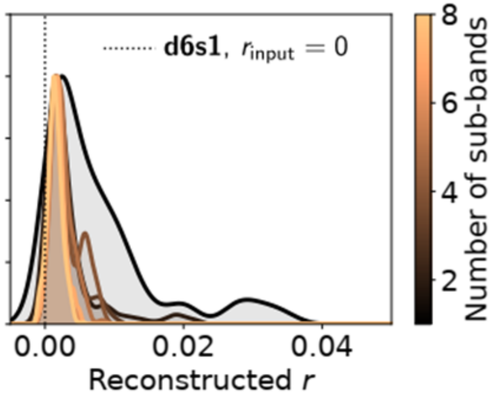

Dust frequency decorrelation: the PySM model

- Pysm model **d0 : Dust MBB with spatially constant parameters**

$$I_d(\nu) = A_{d,\nu_0}(\hat{n}) \frac{e^{\frac{h\nu_0}{k_B \boxed{T_d}}} - 1}{e^{\frac{h\nu}{k_B T_d}} - 1} \left(\frac{\nu}{\nu_{0,d}}\right)^{\boxed{\beta_d}+1}$$

- Pysm model **d1 : Dust MBB with spatially varying parameters**

$$I_d(\hat{n},\nu) = A_{d,\nu_0}(\hat{n}) \frac{e^{\frac{h\nu_0}{\boxed{k_B T_d(\hat{n})}}} - 1}{e^{\frac{h\nu}{k_B T_d(\hat{n})}} - 1} \left(\frac{\nu}{\nu_{0,d}}\right)^{\boxed{\beta_d(\hat{n})}+1}$$

- Pysm model **d6 : Dust MBB with frequency decorrelations**

$$I_d(\hat{n},\nu) = DEC(\nu,\nu_0,\ell_{corr}) \cdot A_{d,\nu_0}(\hat{n}) \frac{e^{\frac{h\nu_0}{k_B T_d(\hat{n})}} - 1}{e^{\frac{h\nu}{k_B T_d}} - 1} \left(\frac{\nu}{\nu_{0,d}}\right)^{\beta_d(\hat{n})+1}$$

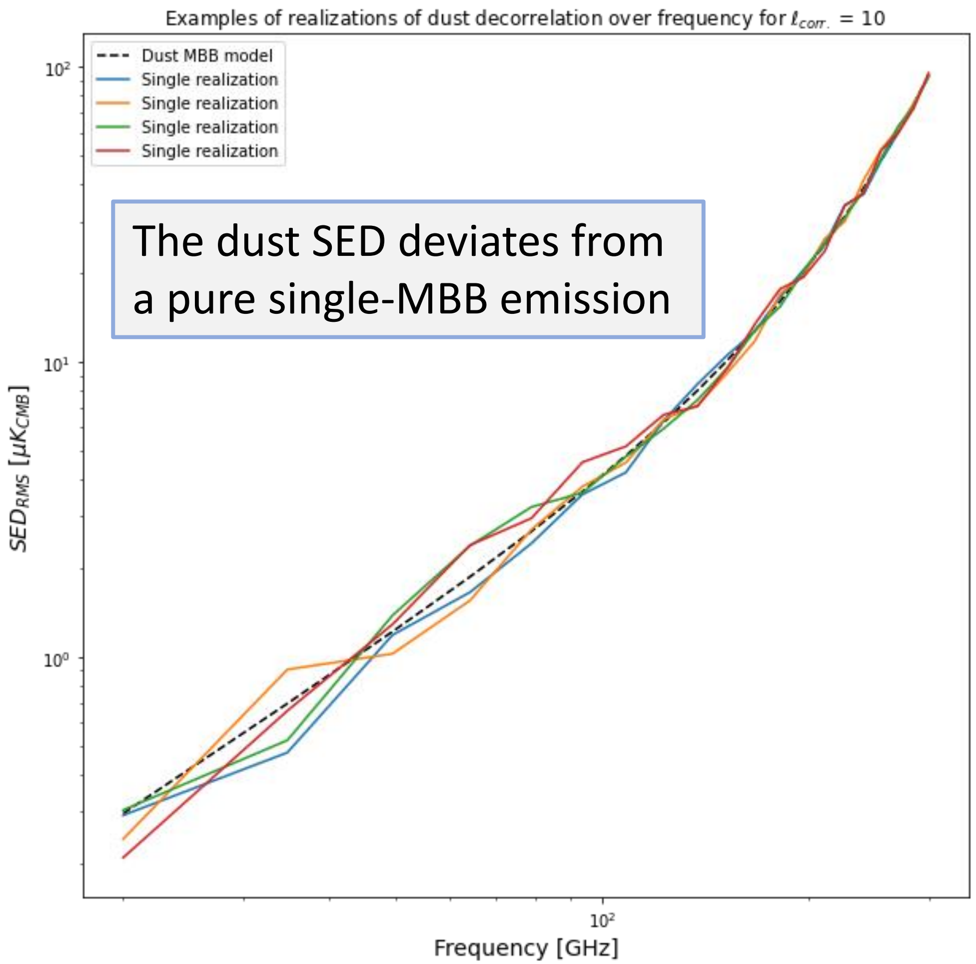

The dust SED deviates from a pure single-MBB emission

https://pysm3.readthedocs.io/en/latest/

Results

Maximum likelihood histograms for the reconstruction of $\boldsymbol{r}$ as a function of n_{sub}

Regnier M., Manzan E. et al. 2023 to be submitted

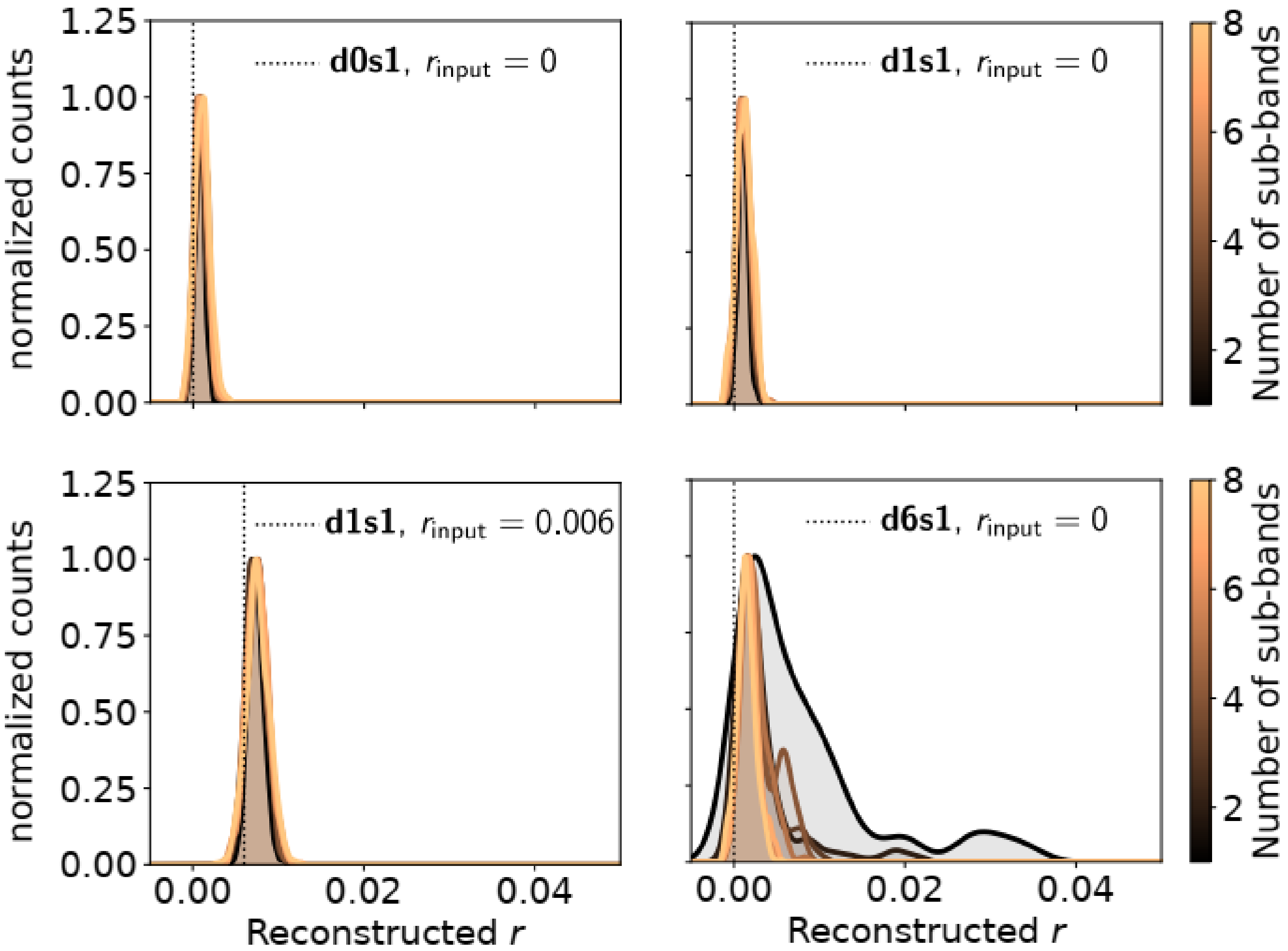

Normalized to the maximum and smoothed with a kernel density estimator (KDE)

Results

Histogram of the max-Likelihood values of ***r*** for an Imager (CMB-S4)

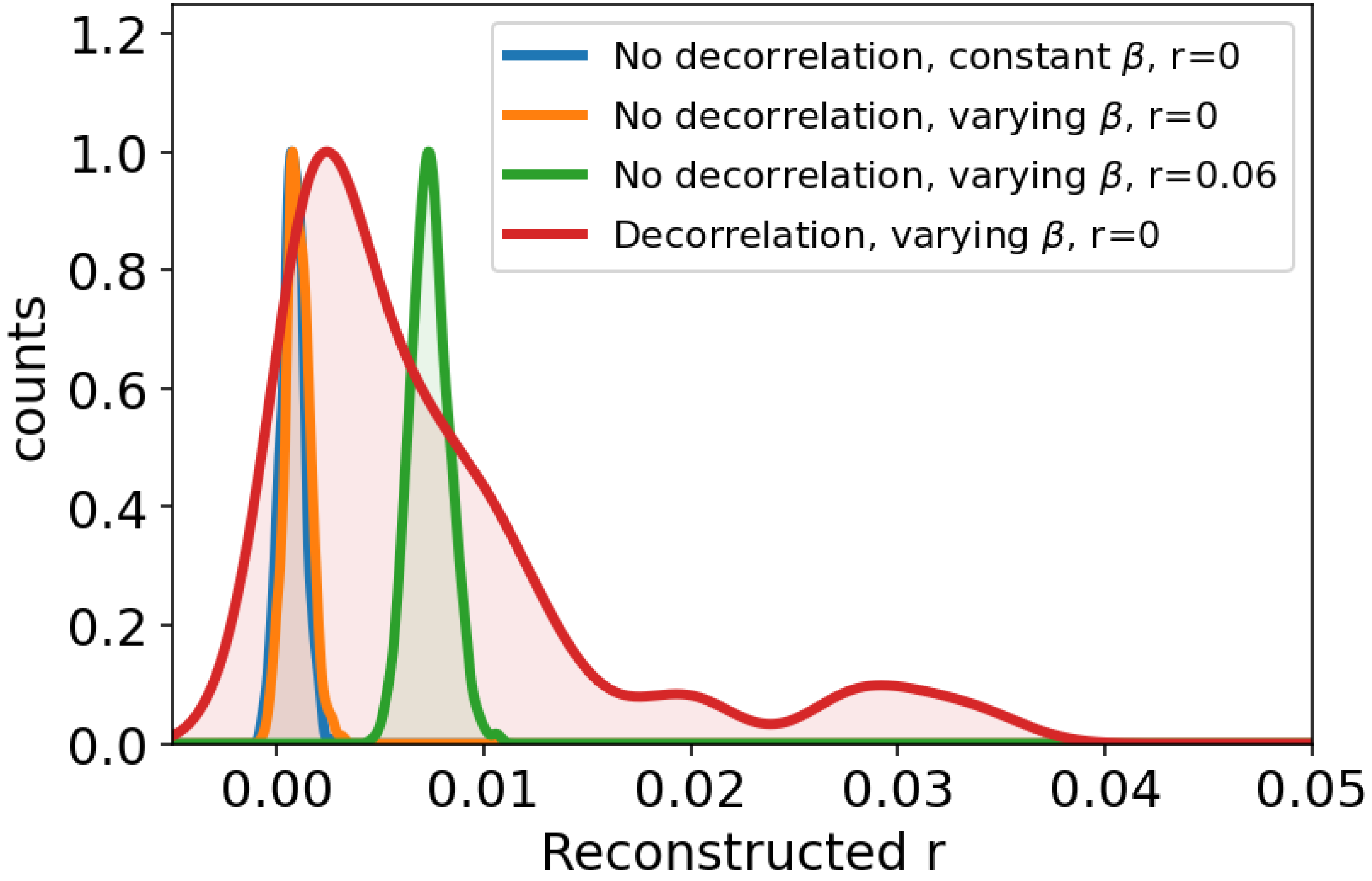

Normalized to the maximum and smoothed with a kernel density estimator (KDE)

Regnier M., Manzan E. et al. 2023
to be submitted

Results

The recovered tensor-to-scalar ratio ***r*** as a function of n_{sub}

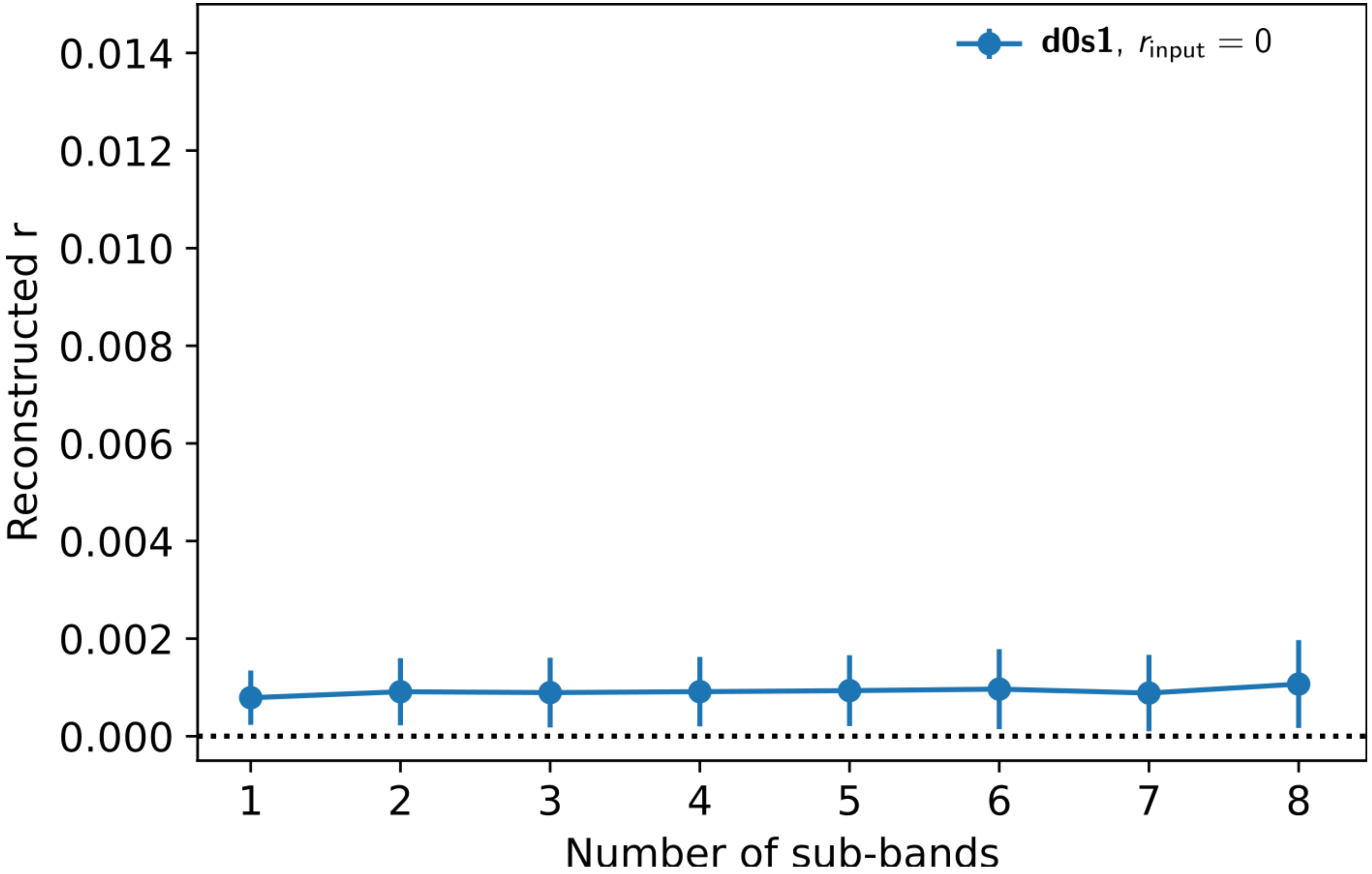

Input: **d0** - fit: **d0**

- Reconstructed ***r*** weakly depends on n_{sub} (slightly increases due to higher noise)
- Small bias: $E \rightarrow B$ leakage caused by the power spectra computation on a sky patch.
- The bias could be mitigated by increasing the mask apodization radius at the expense of a smaller effective sky fraction (< 3%), but it was outside the scope of our study

Regnier M., Manzan E. et al. 2023
to be submitted

Results

The recovered tensor-to-scalar ratio ***r*** as a function of n_{sub}

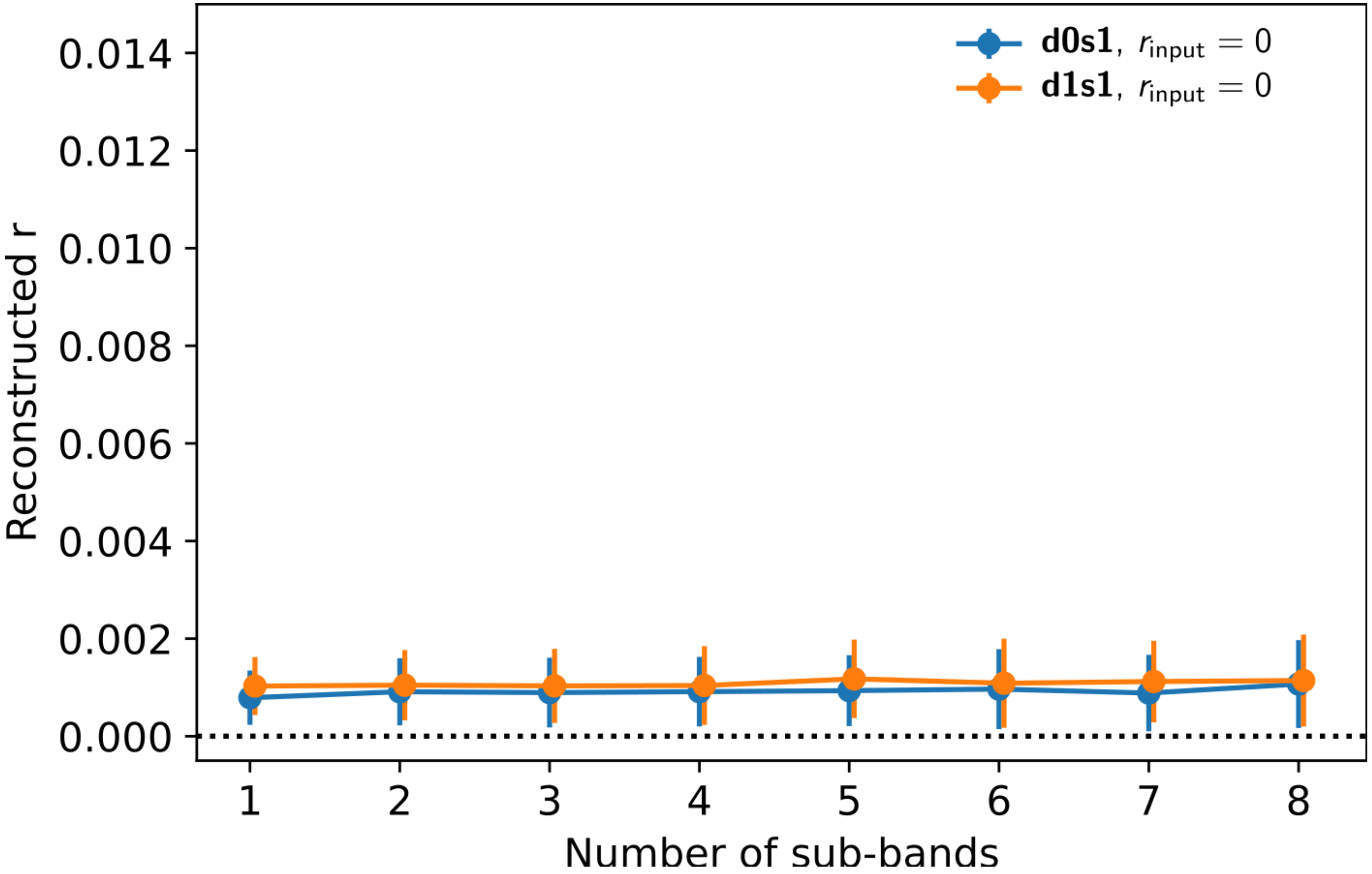

Input: **d1** - fit: **d1**

- The dust spectral index varies in the sky
- Reconstructed ***r*** weakly depends on n_{sub} (slightly increases due to higher noise)
- Bias due to the aforementioned leakage
- Bias also due to the difference in pixel size of the reconstructed maps (N_{side} = 8) compared to the input sky (N_{side} = 256)

Results

Regnier M., Manzan E. et al. 2023
to be submitted

The recovered tensor-to-scalar ratio ***r*** as a function of n_{sub}

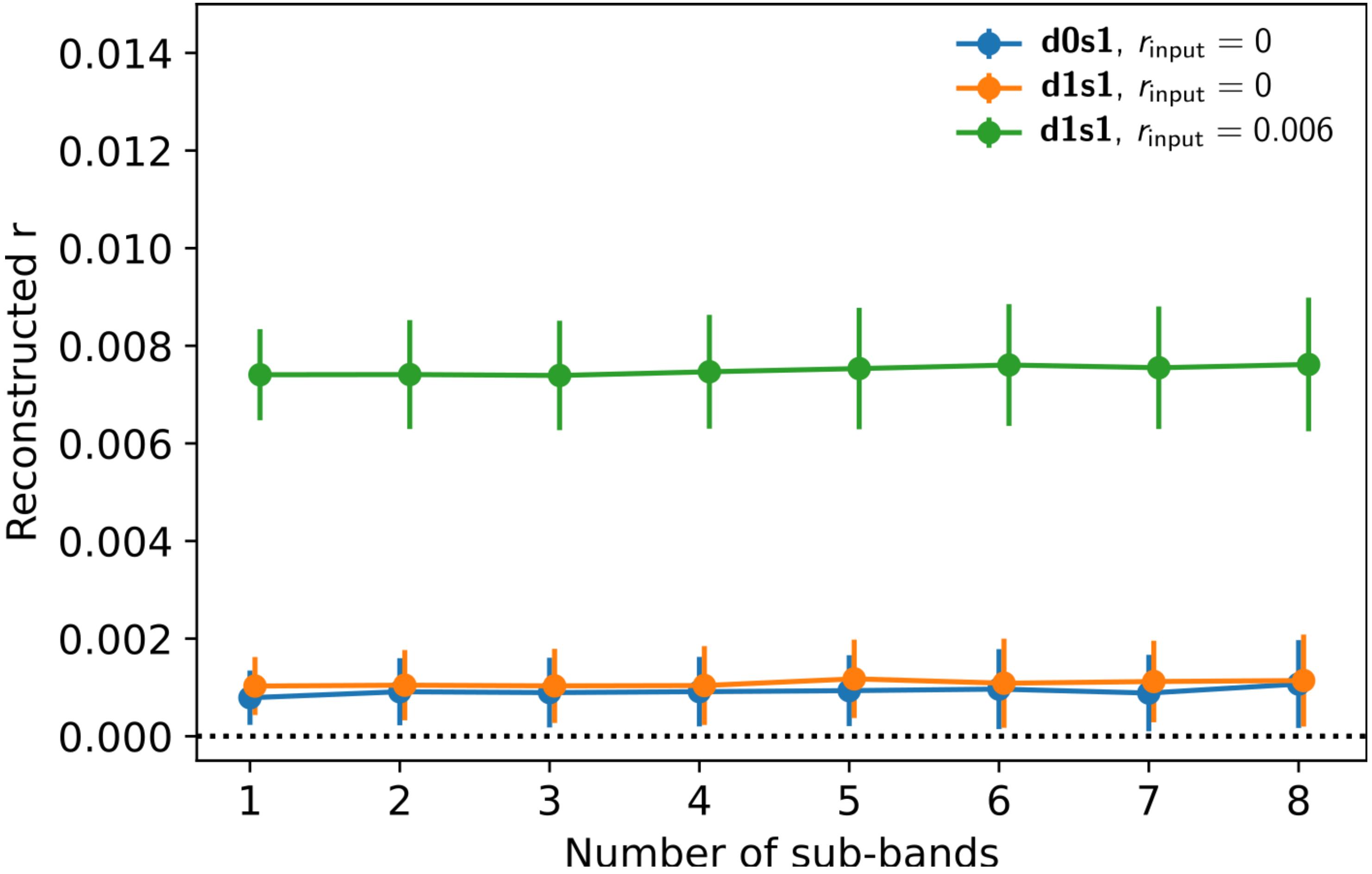

Input: **d1** - fit: **d1**

- Same as before, just different r_{input}: r_{input} = 0.006 instead of r_{input}=0

Results with Machine Learning

Regnier M., Manzan E. et al. 2023
to be submitted

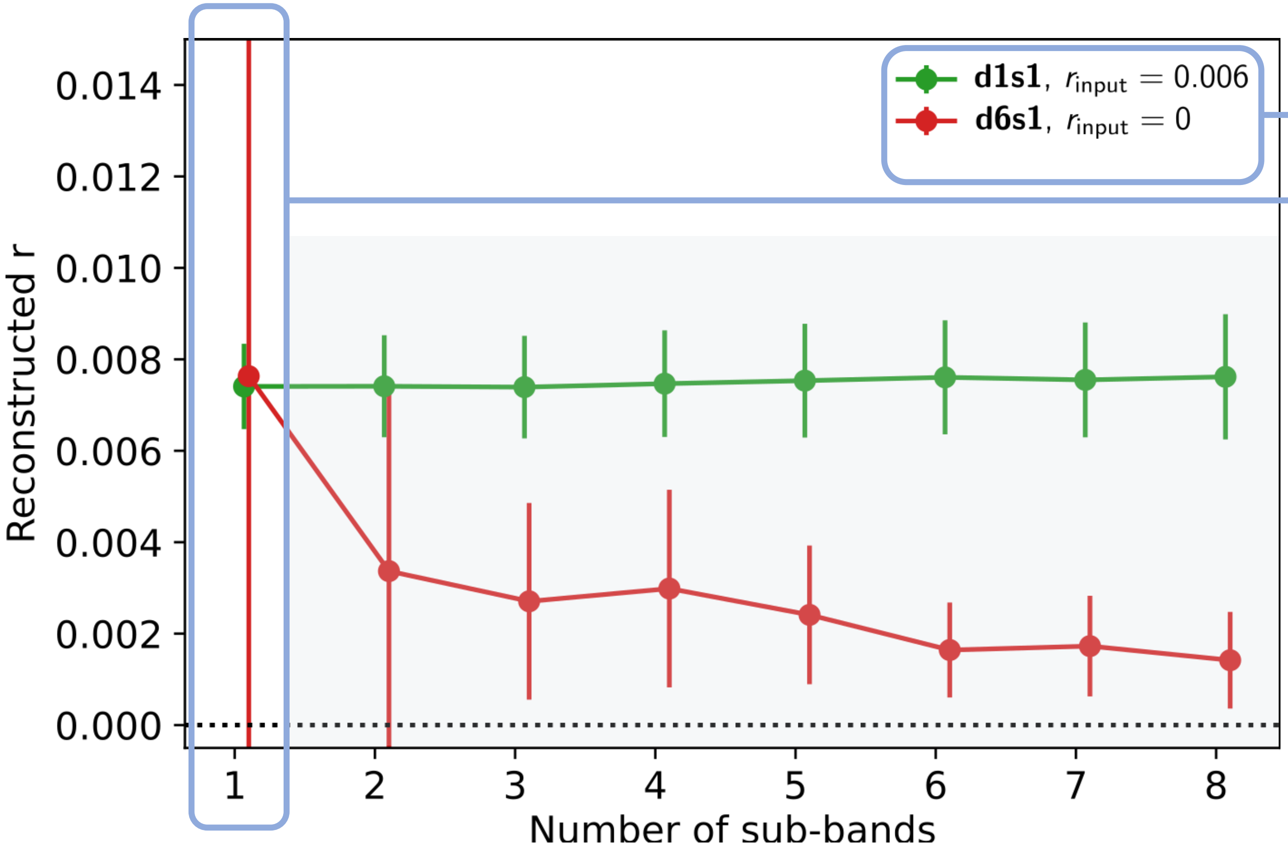

The reconstructed ***r*** would be the same for an imager

Decision Tree: are we fitting for the wrong model?

This allow us to compare CMBS4 and CMBS4/BI on a single realization (measurement)

Regnier M., Manzan E. et al. 2023 to be submitted

Results with Machine Learning

- GradientBoostingClassifier
- 500 realizations of both models:
  I. d6 with $r_{input} = 0$
  II. d1 with $r_{input} = 0.006$
- Split in half : training + testing
- Compute $\rho(n_{sub}) = \frac{r(n_{sub})}{r(n_{sub}=1)}$
- If $\rho(n_{sub}) \neq 1$: it's likely that we are fitting for the wrong model

Confusion matrix

Pure MBB

MBB with decorrelations

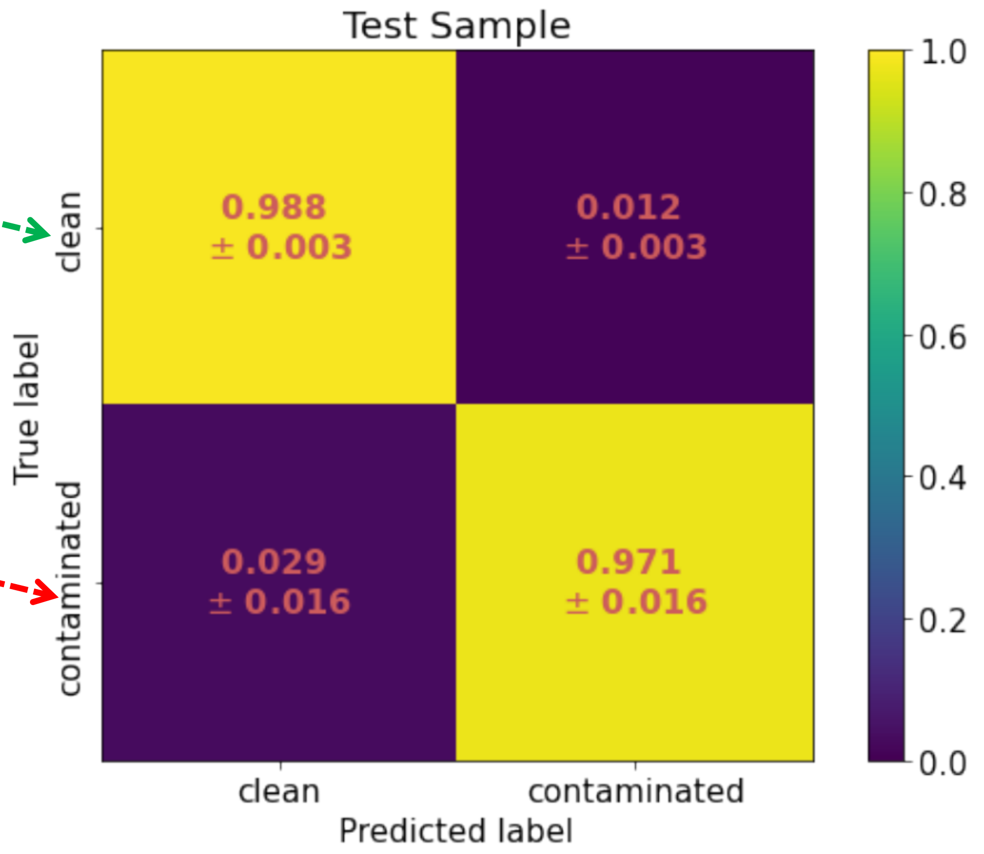

Results on the spectral index

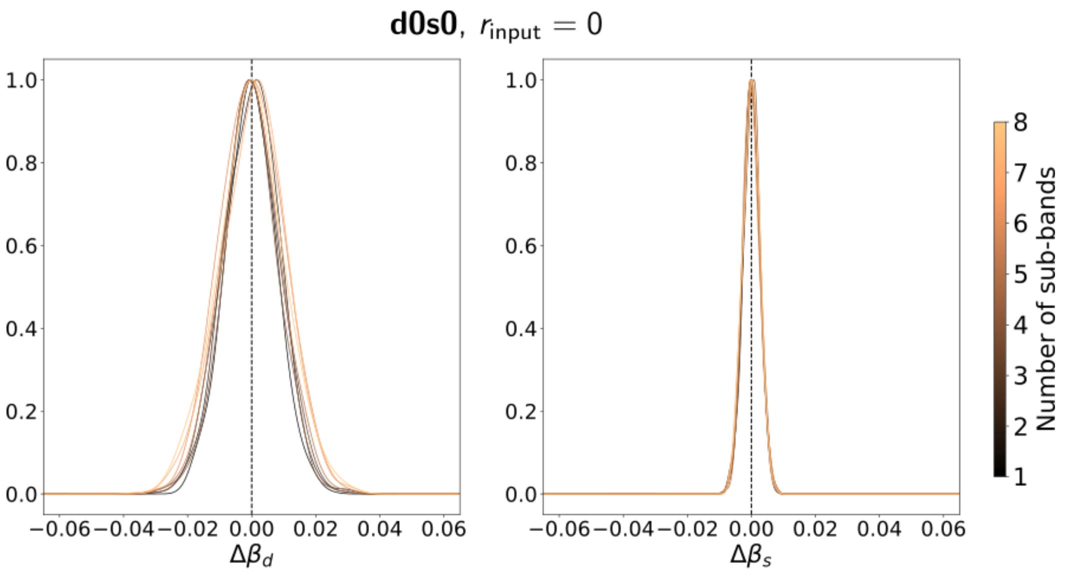

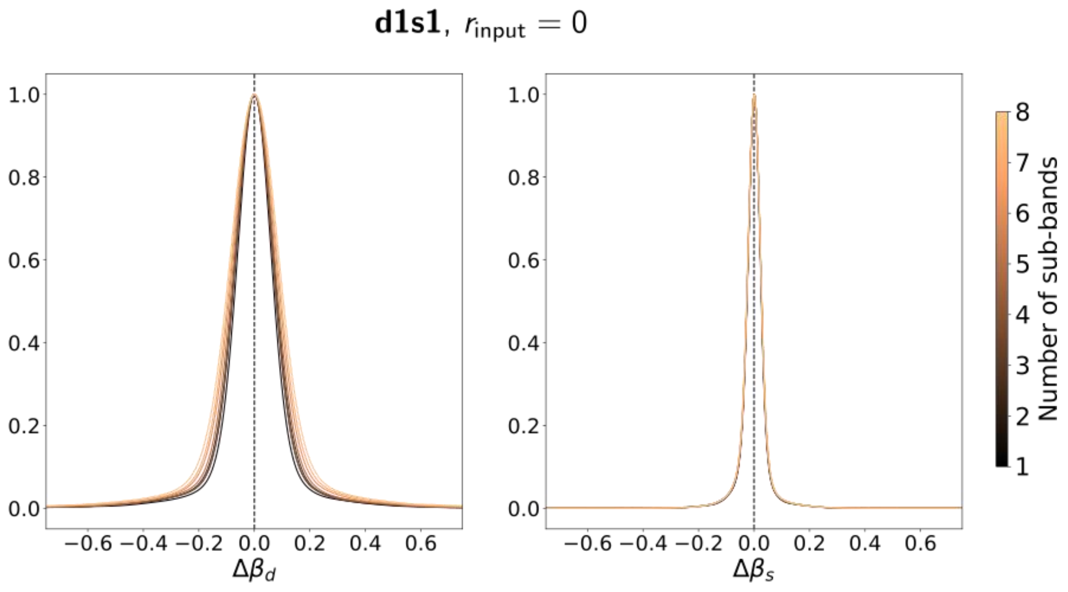

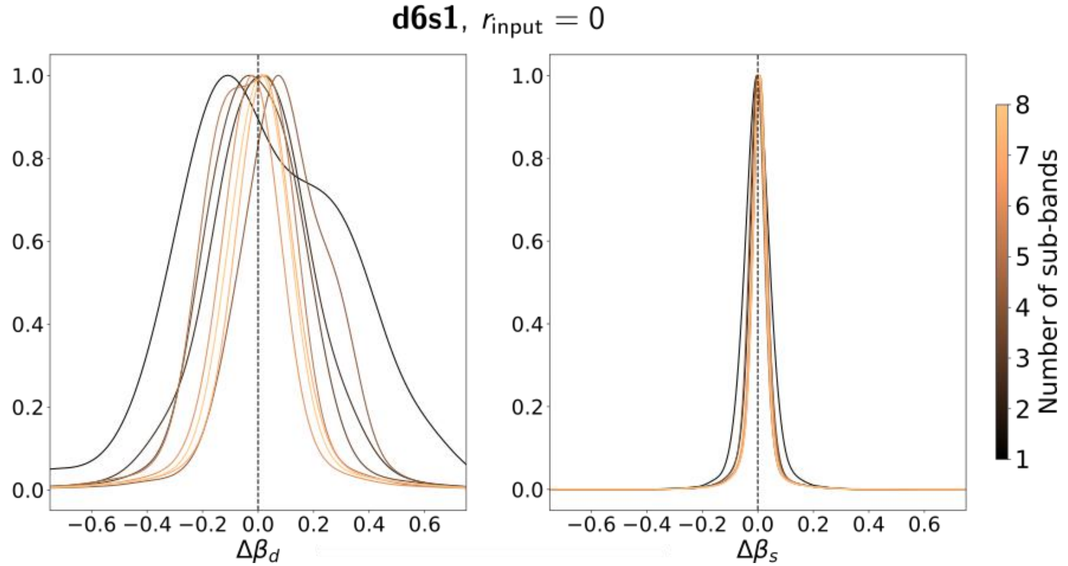

Regnier M., Manzan E. et al. 2023
to be submitted

Commander results

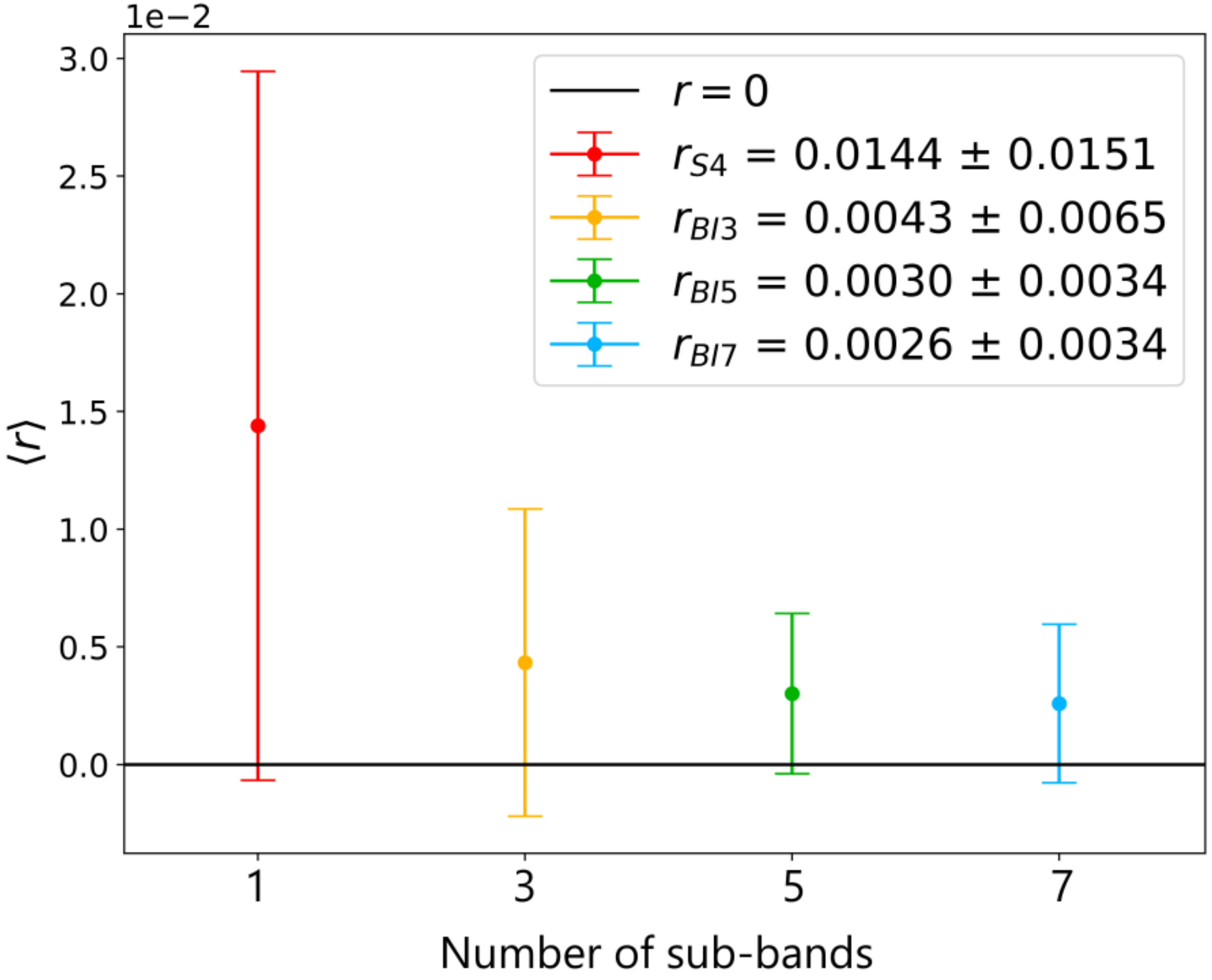

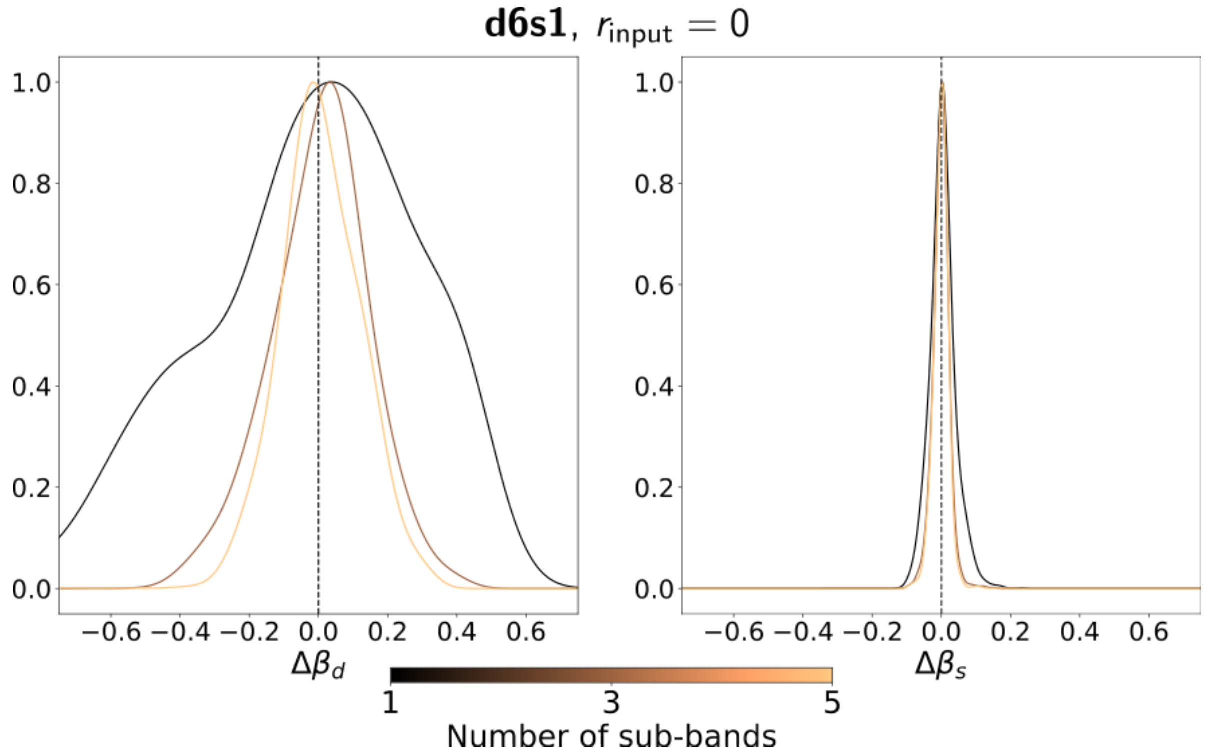

Parametric component separation

Solve $\vec{d} = A \cdot \vec{s} + \vec{n}$ $\forall \nu$, $\forall$ pixel

$\vec{s} = [a_{CMB}, a_d, a_s]$ $A = A(\vec{\omega})$ $\vec{\omega} = [\beta_d, \beta_s, T_d]$

Inverse problem: find $\vec{s}$ given $\vec{d}$

Bayes Approach: $$P(\vec{\theta}|\vec{d}) = \frac{P(\vec{d}\,|\vec{\theta})P(\vec{\omega})}{P(\vec{d})} \propto L(\vec{\theta})$$

Find $L(\vec{\theta}) \rightarrow$ find $P(\vec{\theta}|\,\vec{d})$

Gaussian Likelihood Hypothesis: $\vec{d} - A \cdot \vec{s} = \vec{n} \propto \mathcal{N}(0, \sigma^2)$

$$-2 \ln L(\vec{\omega}, \vec{s}) \propto \left(A(\vec{\omega}) \cdot \vec{s} - \vec{d}\right)^T N^{-1}\left(A(\vec{\omega}) \cdot \vec{s} - \vec{d}\right)$$

Parametric component separation: FGBuster

Maximum likelihood approach: find maximum of *spectral likelihood*

$$\vec{\omega} = [\beta_d, \beta_s, T_d]$$

$$\vec{s} = [a_{CMB}, a_d, a_s]$$

$$\partial_{\vec{\omega}}(-2 \ln L(\vec{\omega}, \vec{s})) = 0 \;\rightarrow\; \left(A_{,\vec{\omega}} \cdot \vec{s}\,\right)^T N^{-1} \left(A \cdot \vec{s} - \vec{d}\right) = 0$$

$$\partial_{\vec{s}}(-2 \ln L(\vec{\omega}, \vec{s})) = 0 \;\rightarrow\; \vec{s} = (A(\vec{\omega})^T N^{-1} A(\vec{\omega}))^{-1} A(\vec{\omega})^T N^{-1} \vec{d}$$

(Stompor et al. 2008)

Parametric component separation: FGBuster

Maximum likelihood approach: find maximum of *spectral likelihood*

$$\vec{\omega} = [\beta_d, \beta_s, T_d]$$

$$-2\ln L_{spec}(\vec{\omega}) \propto -\left(A^T N^{-1}\vec{d}\right)^T (A^T N^{-1} A)^{-1} A^T N^{-1}\vec{d}$$

Max-L of $\vec{\omega}$ (e.g. with CG starting from an initial guess)

A($\vec{\omega}$)

(Stompor et al. 2008)

$$\vec{s} = (A(\vec{\omega})^T N^{-1} A(\vec{\omega}))^{-1} A(\vec{\omega})^T N^{-1}\vec{d}$$

Parametric component separation: Commander

Samples the parameter space $\{\vec{s}, \vec{\omega}\}$

Recovers $P(\vec{\theta}|\vec{d})$ from $L(\vec{\theta})$ using *Gibbs Sampling,* i.e.

$\vec{\omega} = [\beta_d, \beta_s, T_d]$

$\vec{s} = [a_{CMB}, a_d, a_s]$

Gibbs Chain:

$$\omega_{1,i+1} \leftarrow P(\omega_1 | \vec{d}, \omega_{2,i}, \omega_{3,i}, \dots, \omega_{n,i})$$
$$\omega_{2,i+1} \leftarrow P(\omega_2 | \vec{d}, \omega_{1,i+1}, \omega_{3,i}, \dots, \omega_{n,i})$$
$$\omega_{3,i+1} \leftarrow P(\omega_3 | \vec{d}, \omega_{1,i+1}, \omega_{2,i+1}, \omega_{4,i}, \dots, \omega_{n,i})$$
$$\dots$$

- Gibbs sampling: most of the computational time is spent sampling regions where the probability is higher
- End up with a numerical estimation P(ω_k) marginalized on all the others

(Eriksen et al. 2006, 2008)

Parametric component separation: Commander

Samples t

Recovers

Gibbs Cha

$\beta_s, T_d]$

$_B, a_d, a_s]$

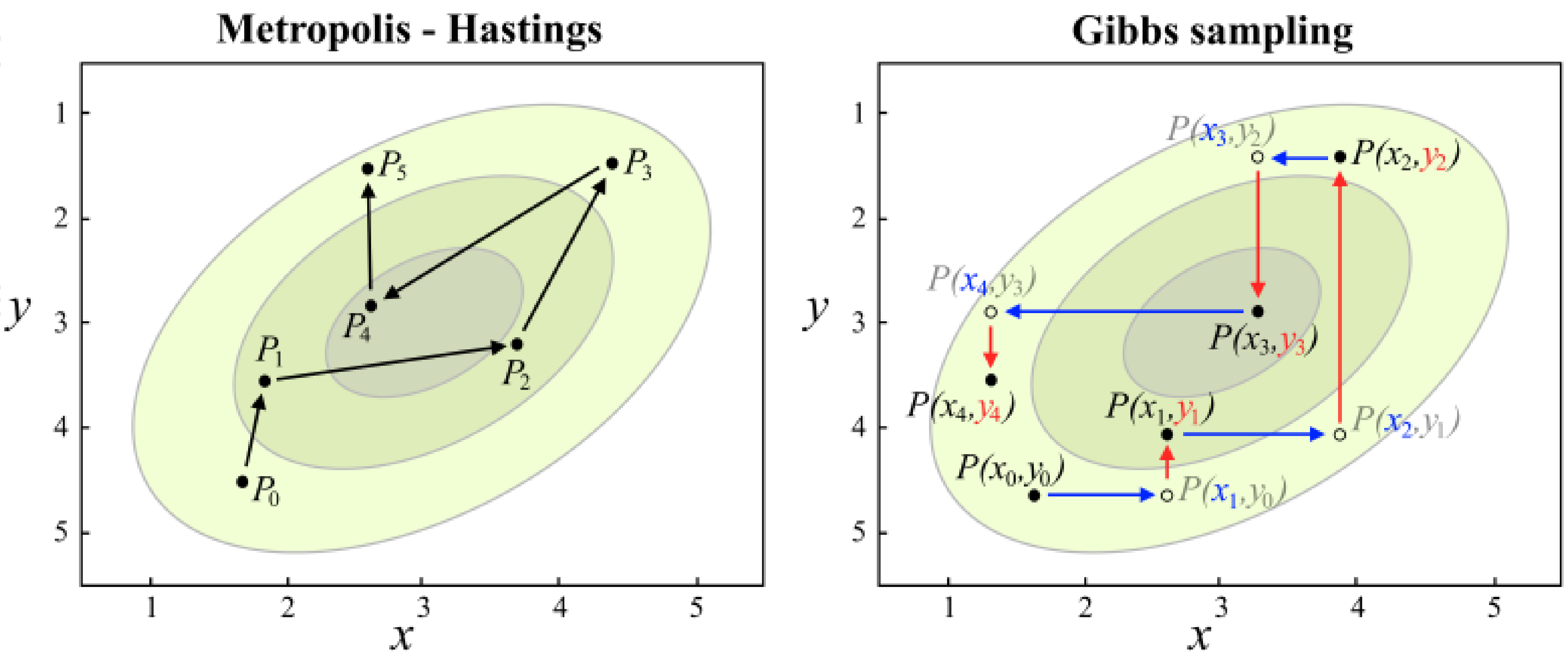

- Gibbs sampling: most of the computational time is spent sampling regions where the probability is higher
- End up with a numerical estimation P(ω_k) marginalized on all the others

(Eriksen et al. 2006, 2008)

Parametric component separation: Commander

Gibbs Chain:

$$\omega_{1,i+1} \leftarrow P(\omega_1 | \vec{d}, \omega_{2,i}, \omega_{3,i}, \dots, \omega_{n,i})$$
$$\omega_{2,i+1} \leftarrow P(\omega_2 | \vec{d}, \omega_{1,i+1}, \omega_{3,i}, \dots, \omega_{n,i})$$
$$\omega_{3,i+1} \leftarrow P(\omega_3 | \vec{d}, \omega_{1,i+1}, \omega_{2,i+1}, \omega_{4,i}, \dots, \omega_{n,i})$$
$$\dots$$

$\vec{s} = [a_{CMB}, a_d, a_s]$ sampled from a Gaussian distribution

$\vec{\omega} = [\beta_d, \beta_s, T_d]$ sampled from a Cumulative distribution

(Eriksen et al. 2006, 2008)

Dust emission complexities

Dust grains ID

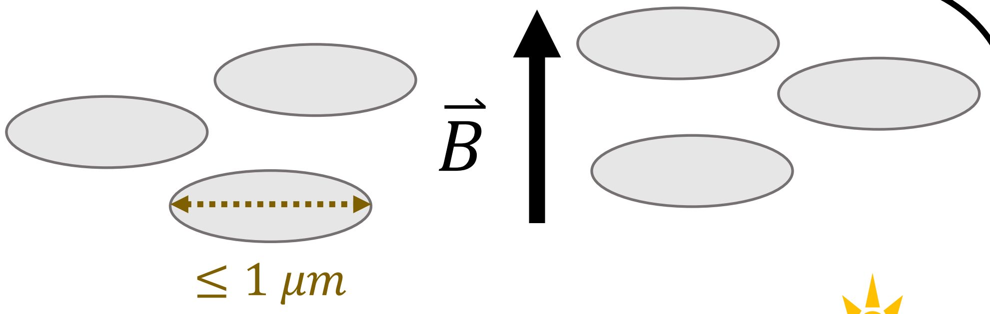

- Sub-μm
- Silicate, carbonaceous, iron
- Asymmetric
- Aligned with magnetic field $\vec{B}$ along short axis
- Absorb nearby star light : $T_d = 10 - 30\ K$
- Thermally emit it with polarization along its major axis -> linear polarization
- Emits at lower frequency (energy) : IR
- Emission : MBB, i.e. $I_d = B_\nu(T_d) \cdot \varepsilon(\nu)$.
  - Emissivity $\varepsilon(\nu) = 1 - \eta(\nu) = 1 - e^{-\tau(\nu)} \rightarrow \tau(\nu) = \tau_0 \left(\frac{\nu}{\nu_0}\right)^{\beta_d}$
  - $\beta_d \approx 1.54$

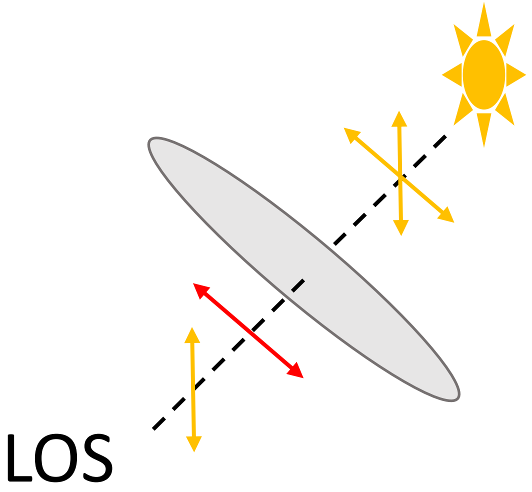

Emission depends on the 3D structure of the InterStellar Medium (ISM) : composition, molecular clouds distribution, temperature and magnetic field

Dust frequency decorrelation

Emission depends on the 3D structure of InterStellar Medium (ISM) : composition, molecular clouds distribution, temperature and magnetic field

LOS (Line of Sight) frequency decorrelation means: the polarization angle $\psi_d = \psi_d(\nu)$

$$Q_d = \frac{p_d \cdot I_d}{\sqrt{1 + \ tan^2(2\psi_d)}}$$
$$U_d = Q_d \cdot \ \tan 2\psi_d$$

- If $\vec{B}$ changes along the (LOS), the grain alignment changes
- If also T_d and/or β_d change along the LOS

Then $\psi_d = \psi_d(\nu)$

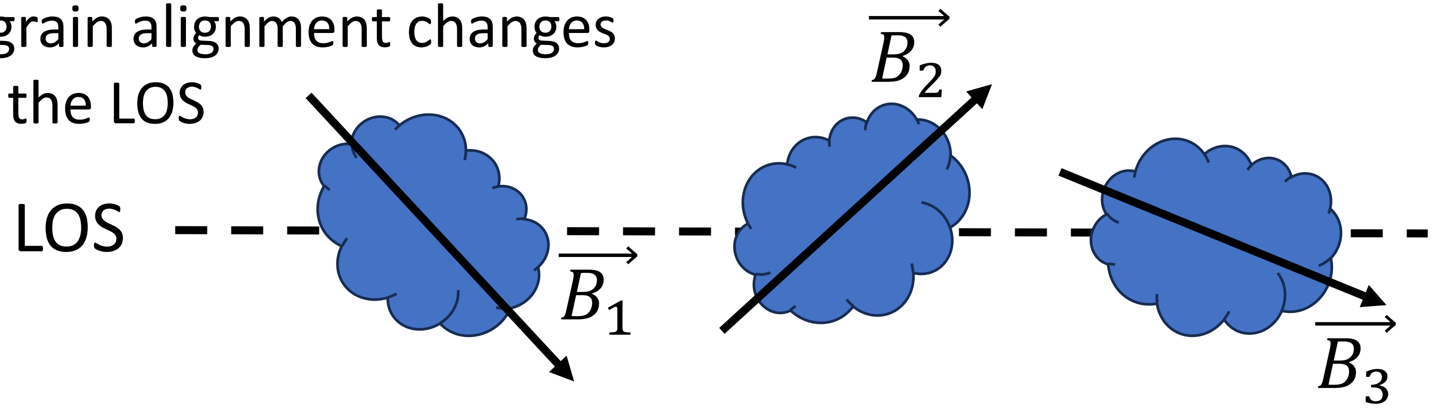

Dust frequency decorrelation

$$M_{353} = M_{d,353} + M_{CMB}$$

$$M_{217} = \alpha \cdot M_{d,353} + M_{CMB}$$

$$R_\ell(\nu_1, \nu_2) = \frac{C_\ell^{\nu_1 \times \nu_2}}{\sqrt{C_\ell^{\nu_1 \times \nu_1} \cdot C_\ell^{\nu_2 \times \nu_2}}}$$

$$= \frac{\alpha \cdot C_{\ell,d} + C_{\ell,CMB}}{\sqrt{\alpha^2 \cdot \left(C_{\ell,d}\right)^2 + \left(C_{\ell,CMB}\right)^2 + (1+\alpha^2) C_{\ell,d} \cdot C_{\ell,CMB}}}$$

Even if α = const. over pixels,

$R_\ell \neq 1$

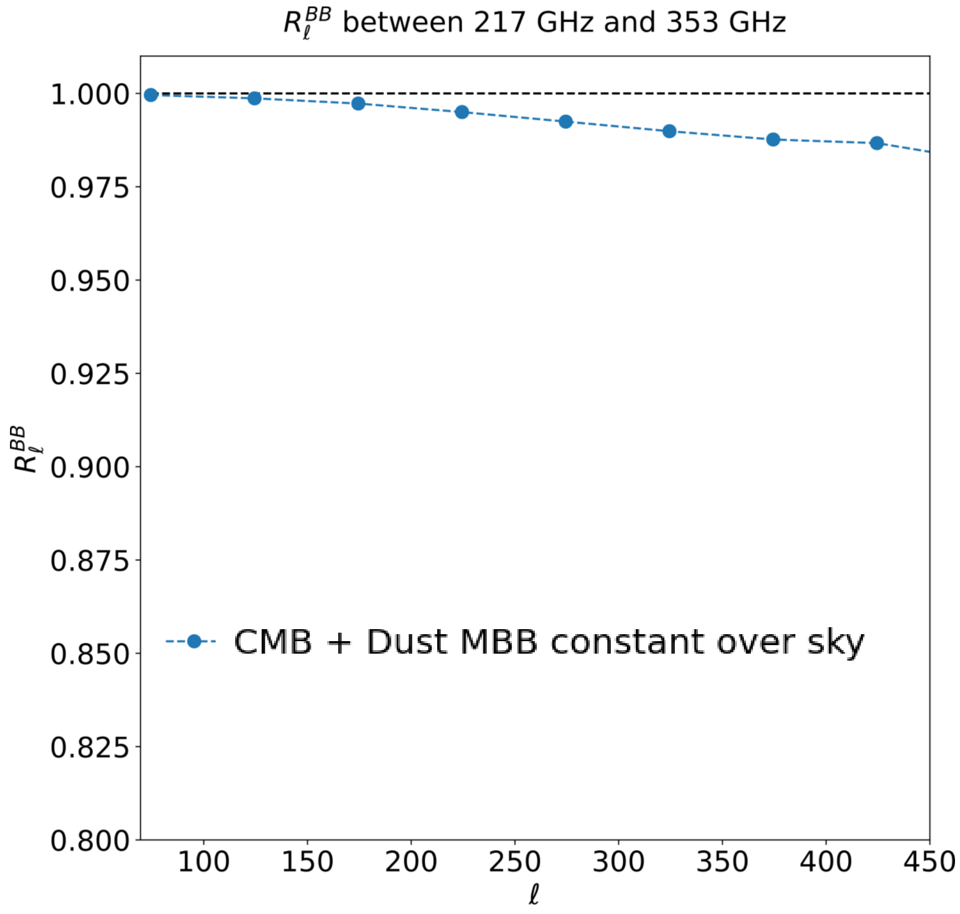

Synchrotron emission models in our study

Conventionally modelled as a Power Law

$$I_s(\hat{n},\nu) = A_{s,\nu_0}(\hat{n})\left(\frac{\nu}{\nu_{0,s}}\right)^{\beta_s + C\ln\left(\frac{\nu}{\nu_{0,s}}\right)}$$

- PySM model **s0**: spatially constant spectral parameter $\beta_s = const$ and no curvature ($C = 0$)

- PySM model **s1**: spatially varying spectral parameter $\beta_s(\hat{n})$ and no curvature ($C = 0$)

https://pysm3.readthedocs.io/en/latest/

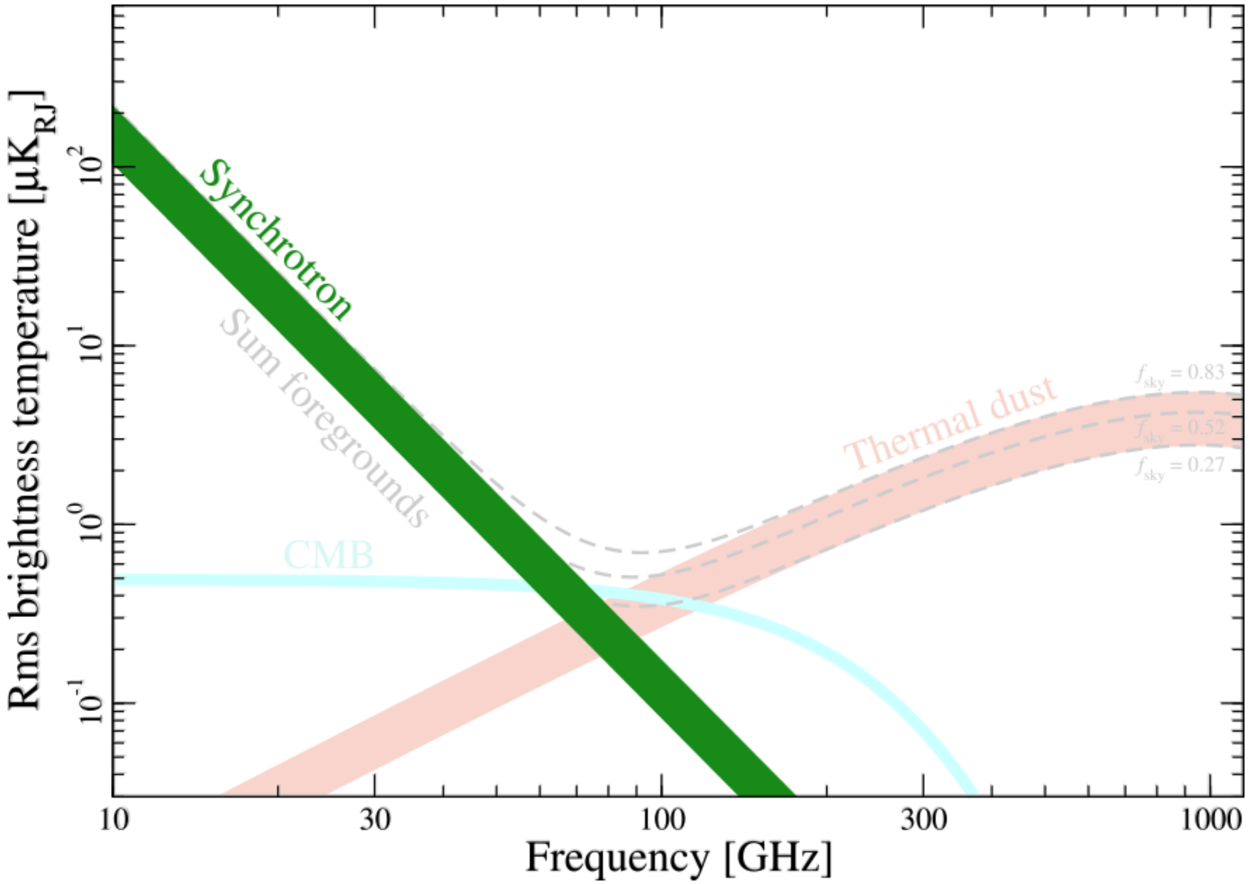

(Planck collaboration et al, 2015, A&A, 594, A10)